Functional Molecular Electronics

AUKE JISK KRONEMEIJER

Functional Molecular Electronics

Auke Jisk Kronemeijer

PhD Thesis

Rijksuniversiteit Groningen

University of Groningen
Zernike Institute
for Advanced Materials

Zernike Institute PhD Thesis Series 2011-11

ISSN: 1570-1530

ISBN: 978-90-367-4844-5 (Print)

ISBN: 978-90-367-4845-2 (Digital)

The work described in this thesis was financially supported by the Zernike Institute for Advanced Materials and NanoNed, a national nanotechnology program coordinated by the Dutch ministry of Economic Affairs. Flagship: Bottom-up Nanoelectronics.

RIJKSUNIVERSITEIT GRONINGEN

FUNCTIONAL MOLECULAR ELECTRONICS

Proefschrift

ter verkrijging van het doctoraat in de
Wiskunde en Natuurwetenschappen
aan de Rijksuniversiteit Groningen
op gezag van de
Rector Magnificus, dr. E. Sterken,
in het openbaar te verdedigen op
maandag 23 mei 2011
om 11.00 uur

door

Auke Jisk Kronemeijer

geboren op 13 december 1982
te Tietjerksteradeel

Promotores:	Prof. dr. P. W. M. Blom
	Prof. dr. D. M. de Leeuw
Beoordelingscommissie:	Prof. dr. B. L. Feringa
	Prof. dr. B. J. van Wees
	Prof. dr. H. J. W. Zandvliet

Dedicated to

My parents
'A house doesn't make a home.'

and

Bert de Boer (1973 – 2009)

Contents

Chapter 1

Scientific Background

1.1 The Building Blocks of Matter

All matter around us consists of small entities called atoms. Classically, atoms are considered as a core consisting of positively charged protons and uncharged neutrons surrounded by a cloud of negatively charged electrons. Various combinations of protons and neutrons in the core yield different chemical elements, in turn surrounded by a number of electrons to ensure charge neutrality. About 100 different chemical elements are known today, although some of these elements have only been synthesized in the laboratory and are only stable for ultra-short periods of time.

While classical mechanics describes the movement of physical entities at the macroscopic scale, the subatomic particles do not conform to these laws. Early in the 20^{th} century quantum mechanics was developed to describe the optoelectronic properties of atoms. The most important propositions of quantum mechanics hold the wave-particle duality and the quantization of energy. In quantum mechanics small particles are described theoretically by waves. The wave-particle duality nevertheless states that particles sometimes behave like waves and at other times behave like particles. The quantization of energy holds that the energy that particles possess is not a continuous variable, but can only exhibit specific values. Electrons inside atoms are thus described by waves and can only possess specific amounts of energy. Consequently, electrons occupy only certain electronic states in an atom called atomic orbitals, described by wavefunctions ψ. Based on their spatial symmetry they are denoted as s, p or d-orbitals. Each atomic orbital can accommodate two electrons with opposite electron angular momentum.

Atoms are the building blocks for larger structures. Atoms can donate or take up electrons yielding charged ions. Crystals with a strictly periodic structure of ions can be formed. The ions are bound to each other by Coulomb attraction. The common sharing of all electrons in a periodic crystal can also connect atoms to each other. Electrons are then delocalized. The energetic states they occupy form bands containing a large number

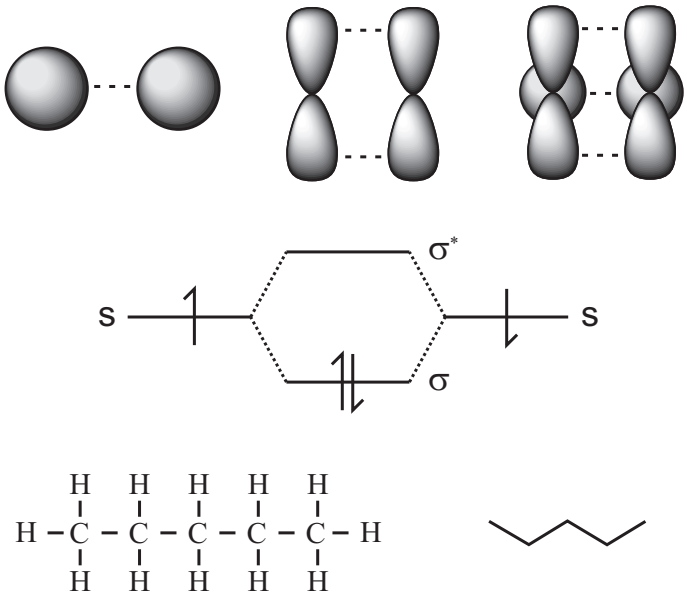

Figure 1.1: Covalent bonding between atoms. The top part depicts the spatial formation of a σ-bond between two s-orbitals, a π-bond between two p-orbitals and the combination of both to form a double bond. The middle part shows the energy diagram of a bond between two s-orbitals resulting in the construction of two σ molecular orbitals. The bottom part demonstrates the common simplification for the representation of the structure of molecules, the bond-line notation. Covalent bonds are represented by straight lines between the symbols of the chemical elements. Further condensation, useful for the representation of larger molecules, shows only the chemical bonds.

of allowed states. The density of electronic bands and the electron occupancy of these bands are imposed by the atoms that constitute the material. Specific filling patterns, in combination with the energy level ordering, lead to metallic or semiconducting properties.

A third option for atoms to bind to each other is to form a covalent bond between pairs of atoms only. In contrast to the delocalized nature of electrons in a crystal, electrons in covalent bonds are localized. Larger structures build up from covalent bonds between atoms are molecules. A great library of molecules exists by virtue of the enormous number of possibilities to couple different chemical elements to each other. Molecules can range in size from nanometers to micrometers.

Covalent bonds can be described starting from the atomic orbitals of the constituent atoms. In the simplest case for a diatomic molecule, two atomic orbitals overlap to form

two molecular orbitals, described by linear combinations of the atomic wavefunctions. The combinations yield a bonding and an anti-bonding orbital. A bonding orbital has a lower energy compared to the constituent atomic orbitals while an anti-bonding orbital has a higher energy. Based on the spatial symmetry molecular orbitals are specified as σ, π and δ-orbitals and covalent bonds as σ, π and δ-bonds. Multiple bonds between two atoms can occur by the coexistence of two types of bonds. Figure 1.1 shows a σ-bond, a π-bond and a combined double bond of both. The energetic representation of a σ-bond between two s-orbitals is depicted as well.

Whether a covalent bond is stable depends on the accommodation of electrons in the molecular orbitals. Each molecular orbital can accommodate two electrons in analogy with atomic orbitals. Orbitals will be filled up from lower to higher energy until all electrons have been accommodated. The total energy of the system after bonding must be lower than before. As shown in the middle part of Figure 1.1, for the case of the two single-occupied

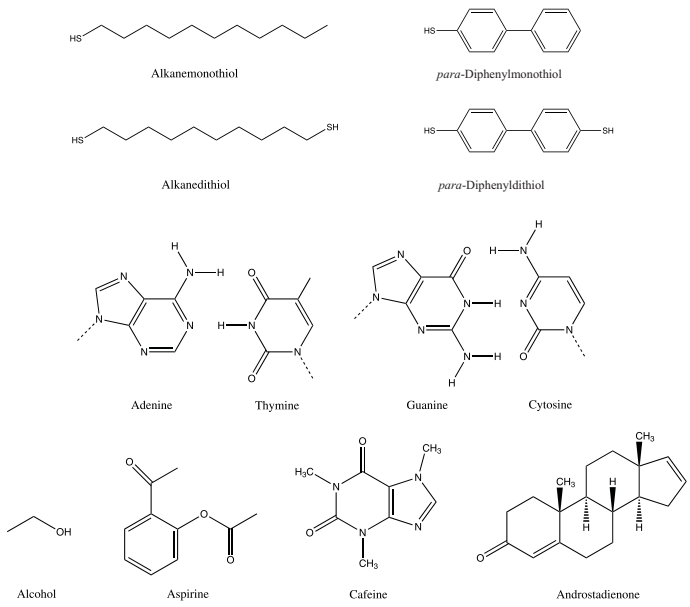

Figure 1.2: Molecular structures of model compounds used in this thesis to study electrical transport of molecules compared to more complex molecules governing various processes in nature. The top compounds are benchmark molecules for saturated and π – conjugated compounds. The lower part of the figure depicts the four bases that code our genetic information in DNA together with a number of compounds with specific functions in our life.

atomic s-orbitals overlapping to form two molecular σ-orbitals, the two electrons can both occupy the bonding molecular orbital. Therefore the total energy of the system is lowered and the bond is stable. For the ease of drawing more complex molecules, the bonding mechanism is represented by straight lines between the chemical elements, as shown in the lower part of Figure 1.1.

The molecular orbital picture of a single chemical bond can be extended to larger molecules. The linear combinations of n atomic orbitals yield n molecular orbitals. The molecular orbitals are filled with electrons from lower to higher energy. Up to a specific molecular orbital all orbitals will contain two electrons while the next orbitals will be empty. The last filled orbital is called the Highest Occupied Molecular Orbital, abbreviated as HOMO, while the next orbital is called the Lowest Unoccupied Molecular Orbital, abbreviated as LUMO. The energetic separation between the two orbitals is called the HOMO – LUMO gap or bandgap, in analogy with the bandgap of crystalline inorganic semiconductors.

Carbon exhibits four valence electrons that form four covalent bonds. All life on the planet relies on carbon, added with predominantly hydrogen, oxygen and nitrogen. The simplest organic molecules are alkanes, linear chains of carbon atoms connected with single bonds and complemented with hydrogen atoms. By the introduction of functional groups, groups with different bonding schemes or other chemical elements, the physical properties and chemical reactivity can be adjusted.

Molecules, both simple and very complex, govern all aspects of our life. Our genetic information is encoded in DNA. Functions in our body are governed by, amongst other, enzymes, hormones, aminoacids and pheromones. Chemistry, the study of the synthesis and properties of molecules, has a rich history and has made significant progress in the last two centuries. Our modern society relies on many synthetic chemical compounds such as fertilizers, drugs and plastics. Figure 1.2 shows a number of model compounds used in this thesis compared to various molecules that perform functions in daily life.

1.2 Organic Electronics

The ability for organic compounds to conduct electricity was discovered in 1977 in doped π – conjugated polyacetylene [1]. Conjugation is defined by the alternation of single and double bonds in a chain of atoms. A double bond consists of a σ-bond together with a π-bond, as shown in Figure 1.1. The σ-bonds are mostly responsible for the bonding of the atoms in the chain. The electrons in these bonds are localized. The π-bonds are formed by the overlap of the π-orbitals. The electrons in these bonds are delocalized due to resonance, *i.e.* two or more alternative bonding patterns of equal energy exist, as shown in Figure 1.3.

The electronic structure of π – conjugated polymers is similar to that of periodic structures of atoms such as crystals. The energetic difference between the bonding and antibonding molecular orbitals decreases due to delocalization, yielding a relatively small HOMO – LUMO gap. Since an electronic gap is still present while electrons are delocalized, π – conjugated molecules can be regarded as the molecular counterpart of wide bandgap inorganic semiconductors.

The electronics industry has severe impact on the worldwide economy. Increasingly more computer power and more compact multifunctional portable devices shape the current way of life. Television technology has had a recent boom bringing flat televisions in most households. Cost reduction is a major driving force. *Organic Electronics* holds the fabrication of electronic components based on π – conjugated materials. The field has promised and is starting to fulfill this new generation. Organic components might be produced in high volume over large areas at lower cost by applying manufacturing techniques such as spincoating and ink-jet printing. Furthermore, organic materials are lightweight and can be mechanically flexible. Synthesis can tailor the properties of π – conjugated materials to suit specific applications. Organic light-emitting diodes (OLEDs) are commercially available. Solar cells (OPVs) are in the development stage and intensively investigated to optimize performance.

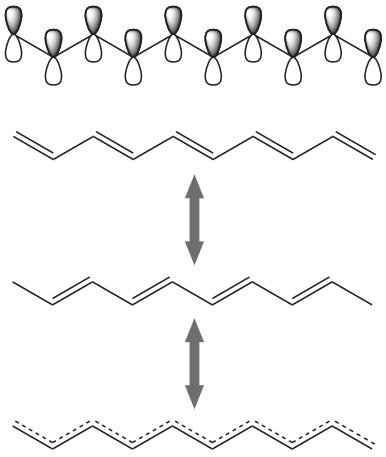

Figure 1.3: Structure of a π – conjugated chain of carbons atoms. Introduction of double bonds, the overlap of two π-orbitals, in saturated alkanes leads eventually to resonance and to delocalization of the electrons over the π – conjugated system. Conjugated molecules are the molecular counterpart of wide bandgap inorganic semiconductors.

1.3 The Rise of Molecular Electronics

The clock frequency of electronic integrated circuits is inversely proportional to the minimum feature size of electronic components. When electronic components are smaller, an integrated circuit contains more of these components in a unit area. More components effectively yield more computation power. An additional advantage is that smaller circuits will consume less energy.

The electronics industry is a well-developed industry with over 50 years of experience in research. Since around 1960, the minimum feature size of electronic components has decreased every two years by a factor of two. Alternatively, the number of components in an integrated circuit has doubled every two years. This observation is known as Moore's Law.

It is expected that miniaturization of electronic components will reach a fundamental limit and Moore's Law will not longer be obeyed. There is ongoing debate about exactly when the limit is reached, but it is clear that in the future current technologies will not be able to create smaller, less energy-consuming and faster electronic components. Solutions for future electronic devices are therefore being investigated, keeping a worldwide multibillion industry on track.

Molecular Electronics was proposed in 1974 as a possible technology capable of solving the miniaturization problem to extend Moore's Law. At that time the minimum feature size was $\sim 5\ \mu$m. The main concept of *Molecular Electronics* is the use of a single molecule as individual electronic component in circuitry. Organic molecules are the size of a couple of nanometers, leading to a minimum feature size in the nanometer range. The initiation of the field started with a theoretical paper in 1974 by A. Aviram and M. A. Ratner describing a single molecule rectifier [2]. Interest was sparked in the substitution of electronic components by functional molecules.

Parallel to developments in *Molecular Electronics*, the silicon industry shrunk single components to sizes comparable to molecules. The minimum feature size in the year 2000 was around 150 nm, while in 2010 already 45 nm was achieved. Therefore, the initial reason to develop *Molecular Electronics* has largely disappeared. The emphasis of the community has therefore shifted from single-molecule electronics towards self-assembly.

Self-assembly is the autonomous organization of components into patterns or structures without human intervention [3]. Self-assembly has developed as part of life to create order from disorder. Ordered structures, such as lipid bilayers, proteins and the helix structure of DNA spontaneously come into existence by virtue of intermolecular interactions. Self-assembly is envisioned as one of the most cost-effective ways to fabricate nanostructures. Without any intervention a small electronic chip could build up from individual components. Molecules can be tailored to assemble into desired hierarchical structures.

Interest in *Molecular Electronics* was thus sparked by the inherent size of molecules and the concept of self-assembly. Progress in the understanding of electronic transport by molecules was, however, severely hampered since the fabrication of an electrical contact to molecules proved not to be an easy task. The first measurements evolved from the ability to create thin molecular films on electrical conducting substrates.

The study of molecular monolayers dates back to Benjamin Franklin when he investigated the 'stilling of waves by means of oil' [4]. Franklin observed during travel at sea in 1757 that waves behind certain ships decreased dramatically. He asked the captain what could be the reason. The captain answered that cooks probably had emptied their greasy water at the back of the ship. Franklin kept being puzzled and set out to investigate the effect. He started experimenting with drops of oil dispensed on top of water. After some time, he found out that the oil spreads into a monolayer of floating oil molecules on top of the water surface. The exact mechanism how the film suppresses the formation of waves is still not known. At the end of the 19^{th} century Agnes Pockels showed in kitchen experiments that the monolayers Franklin had discovered could be compressed [5]. Subsequently, Irving Langmuir and Katharine Blodgett demonstrated that compressed layers could be transferred onto a solid substrate by immersing the substrate in a solvent containing a monomolecular film on top, resulting in so-called Langmuir-Blodgett monolayers [6].

Langmuir-Blodgett monolayers were used in the first experimental studies on the electrical transport through molecular layers. Monolayers were formed on a metallic electrode while a second electrode was evaporated on top. Current-voltage (J–V) characteristics were determined as a function of layer thickness, *i.e.* molecular length. For the first time, an exponential decrease of conductivity on molecular length was observed [7, 8]. The main problem with the experiments was the yield of functioning junctions. Due to penetration of the metallic atoms through the monolayer, most of the fabricated junctions were short-circuited.

In the 1980s a new concept for the fabrication of ordered monolayers of molecules was discovered. Monolayers of organosulfur compounds (alkanethiols) were formed on gold and silver substrates by immersion of the substrate into a solution containing the molecules [9]. The alkanethiols organized spontaneously onto these metals by specific chemical interactions between the so-called 'head group' and the metal [10]. Self-assembled monolayers consist of an ordered layer of molecules. Nowadays a large number of head group – substrate combinations are known from which ordered monolayers are formed. An essential difference with the Langmuir-Blodgett monolayers is the chemical attachment to the surface (chemisorption) of the SAMs in contrast to the physical absorption (physisorption) of the Langmuir-Blodgett layers.

In the early 1990s interest expanded due to the development of the Scanning Tunneling Microscope (STM) and the Atomic Force Microscope (AFM) [11, 12]. The organization of molecular layers was investigated extensively. The improved resolution led to direct observation of single molecules. Hence the properties of single molecules could be addressed. The scanning probe techniques were used to study the electrical properties of single molecules. Single conjugated molecular wires were inserted in an insulating alkanethiol matrix and contacted with an STM tip [13] and STM-based breakjunction techniques were developed [14]. The AFM technique, originally not able to measure electrical signals, was altered with a conducting tip [15]. The small effective tip radii of both STM and AFM ensured that single molecules or a small number of molecules in a layer were contacted.

Micro-fabrication techniques for small electronic structures improved as well. Mechanically controlled breakjunctions were used to electrically contact single molecules [16]. A breakjunction consists of a small free hanging restriction in a metallic wire on a substrate. By bending the substrate the restriction can be stressed and eventually be broken. The distance between the two ends of the broken wire can be tuned. A gap close to the length of a single molecule can be maintained and by introduction of molecules to the system a metal-molecule-metal electronic junction can be created.

Molecular junctions of single molecules are fragile and at the atomic scale not always reproducible. Therefore, a large number of measurements have to be performed to obtain statistical relevant data. The single molecule measurements were therefore complemented by experiments on larger numbers of molecules. Stochastic differences of the conductance of single molecules, due to *e.g.* local environment or electronic coupling to the contacts, are then averaged out.

The main difficulty in the fabrication of larger molecular junctions still remained the yield of the junctions. Renewed attempts on large areas lead to short-circuits by metal penetration through the molecular layers [17, 18], resulting in a very low yield of molecular junctions [19]. Specialized thermal evaporation of metals on monolayers using nanopores was applied [20]. The yield of the electronic junctions nevertheless remained rather low and metal penetration was still the major cause. To alleviate the yield problems, a multitude of different solutions were devised. Contact methods such as nanotransfer printing of metallic contacts [21] and other soft-lamination based techniques [22–24] ensured soft landing of the metallic atoms on the monolayers. The use of liquid electrical conductors was explored by contacting molecules with Hg [25, 26] and eutectic Ga-In [27]. Minimization of the intrusion of metal atoms has also been realized with crossed-wire junctions [28], two-dimensional arrays of quantum dots [29] and surface-diffusion mediated deposition [30]. In summary, a broad range of testbeds has been developed to investigate charge transport through molecules.

1.4 Electrical Transport through Single Molecules

In standard organic electronic devices the electrodes are micrometers apart. This distance is orders of magnitude larger than the size of a single molecule. To conduct electricity, electrons therefore need to jump from molecule to molecule through the material, a transport mechanism called hopping conduction [31–34]. This conduction mechanism in principle does not yield information on intra-molecular transport but on inter-molecular transport. Shrinking down the electrode separation eventually yields a molecular junction. In a molecular junction one single molecular orbital can bridge from one electrode to another. The intra-molecular transport is therefore probed.

Alkanes have been used as benchmark compounds to study intra-molecular transport because of the simplicity of their molecular structure. Figure 1.4 shows a simplified energy diagram of a molecular junction. It consists of a number of molecular energy levels completely bridging two metallic electrodes. Electrical transport will be governed by the energy difference between the Fermi level of the metal and the HOMO and LUMO levels of the molecule. In general, the energy difference is larger than the thermal energy kT. Therefore, according to classical mechanics, electrons cannot pass through the molecular junctions since no energy levels are available.

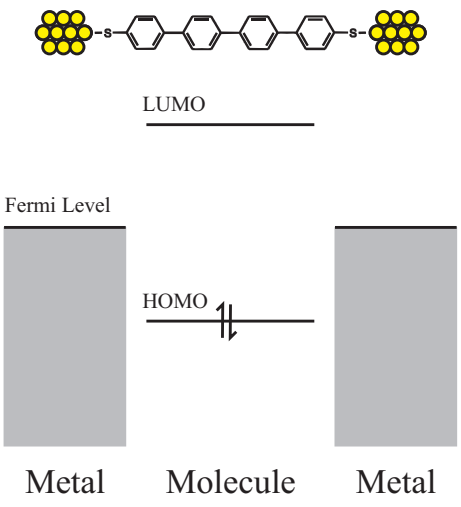

Figure 1.4: Simplified energy diagram of a molecular junction. The metallic electrodes constitute a continuum of electronic states filled with electrons up to the Fermi level. The important molecular orbitals, the HOMO and LUMO, bridge the electrodes.

Quantum mechanically electrons can pass a classically forbidden gap by tunneling. For thin regions the electronic wavefunctions of electrons can have a non-zero amplitude on the opposite side of a potential barrier because the wave is not sufficiently damped in the forbidden region. This leads to a non-zero probability for electrons to pass the potential barrier and current can flow if a potential difference is applied. The tunnel effect is independent of temperature. The dependence of the tunneling current density on potential barrier height ϕ and barrier thickness d can be approximated at low bias as [35]:

$$J \propto exp^{-2\frac{\sqrt{2m\phi}}{\hbar}d} \tag{1.1}$$

Experiments on molecular transport have shown an exponential decreasing current density when increasing the molecular length of alkanes in the junctions [36, 37]:

$$J \propto exp^{-\beta L} \tag{1.2}$$

The tunneling decay parameter β ranges from $0.38 - 0.88$ Å^{-1} [36]. Temperature-dependent measurements have shown that the transport is independent of temperature [19, 38, 39]. Hence electrons pass through short alkanes by non-resonant tunneling. The tunneling decay parameter for vacuum is around 2 Å^{-1} depending on the specific workfunction of the metallic electrodes used. Molecules enhance the transport compared to vacuum due to the smaller energy difference between the metal Fermi level and the available states inside the junction.

Many molecules in molecular junctions are slightly tilted with respect to the surface normal of the electrodes. Therefore, electrons have two possible tunneling pathways to exploit, the shortest perpendicular distance between the electrodes and a longer pathway along the tilted molecular backbone. The processes are called through-space and through-bond tunneling, respectively. It has been shown that the transport in molecular junctions is specifically sensitive to the molecular length instead of the length of the direct pathway, making through-bond tunneling the dominant pathway in short alkanes [40, 41].

A number of issues remain to be solved. First, the literature shows a large range of β coefficients for identical homologue series of molecules [36]. No relation with the number of molecules probed or type of contact is uncovered. Second, the simple relation of Equation 1.1 often yields unphysical values for the barrier height ϕ. The absolute currents differ by orders of magnitude between experiments and theory.

Finally, the electrical contacts to the molecules are crucial. Electrical contacts can be either strongly bound by chemical attachment to the molecules or loosely bound by physisorbed bonding. Chemical binding leads to hybridization of the molecular orbitals with the metal states. Hybridization leads to a shift in the energy positions of the molecular

orbitals and the density of states. A physically bound contact, such as an STM tip, leads to less interaction and minor change of the molecular energy levels.

Comparison of a large number of different experiments lead to the phenomenological observation that the conductance G is factorized. The conductance is generally expressed as a multiplication of transmission and reflection coefficients [36, 37, 42, 43]. For low transmissions, as can be expected for a tunnel barrier, the reflection coefficients are negligible and the conductance can be approximated as:

$$G = \frac{2e^2}{h} \cdot T_{lc} \cdot T_{molecule} \cdot T_{rc} \tag{1.3}$$

where T_{lc}, $T_{molecule}$ and T_{rc} are the transmission coefficients of the left electrical contact, the molecule and the right electrical contact, respectively. The molecular transmission is exponentially dependent on the molecular length by Equation 1.2, *i.e.* $T_{molecule} \propto exp^{-\beta L}$. Contrary to a classical contact resistance in series, which adds to the total resistance, the electrical contacts in molecular junctions exhibit a multiplicative character. The molecules thus determine the length dependence of the transmission. The absolute value of the transmission can be offset by the electrical contacts.

A quantitative relation between the coupling strength and the resulting transmission is still an issue. The coupling strength is benchmarked using alkane molecules. Generally a physisorbed contact leads to lower transmission than a chemisorbed contact [36]. Several chemical anchoring groups are used such as thiols (–SH), amines (–NH_2) and isocyanides (–NC). Commonly used metal electrodes are Au, Ag and Pt. The type of metal influences the current density by the different workfunction. Different chemical anchoring groups modulate the current density while they only have a minor effect on the molecular orbitals. Influence of the anchoring group has been reported for alkanes although they exhibit a very large HOMO – LUMO gap [44, 45]. The origin could be the formation of surface dipoles on the metallic contact and an accompanying shift in workfunction [46]. Finally, it is noted that for a single combination of metal and chemical anchoring group, the detailed geometry and close environment of the metal-molecule bonds is crucial. Multiple transmission values have been observed for identical molecules in single molecule experiments. Thus, multiple geometrical configurations exist with different transmission probabilities [47, 48].

For short π – conjugated molecules tunneling has been determined to be the dominant transport mechanism as well [37, 49–51]. The transport depends exponentially on molecular length yielding a tunneling decay coefficient β. For conjugated molecular compounds β is generally lower than for saturated compounds. The lower β is the result of a smaller HOMO – LUMO gap. The electrical contacts complicate the measurements on conjugated compounds as well. A spread in β coefficients is observed for identical molecules as well.

The spread is influenced by the conformation of identical conjugated molecules in different junctions. The conformation determines the effective conjugation length in the molecules.

For longer saturated compounds no current is observed. For longer π – conjugated molecules a transition in the length-dependence accompanied by a transition of the temperature-dependence has been observed [52–54]. The transport becomes temperature-activated and exhibits a lower length-dependence. The transition has been interpreted as a change in transport mechanism from tunneling to hopping conduction. For the compounds studied, the transition occurs around molecular lengths of 3 nm.

1.5 Molecular Functionality

The target of *Molecular Electronics* is to arrive at functional molecular components. Integrated circuits are based on a number of functional components such as transistors and diodes. A transistor is a three-terminal device in which one contact controls the current between the two other contacts. A diode is a rectifying component, meaning that current can only flow through the diode in one bias polarity. Promising for non-volatile data storage are two-terminal resistive switches, basically resistors with two different stable resistive states. The field of *Molecular Electronics* searches for molecular equivalents for all of these functionalities. Figure 1.5 depicts a number of investigated molecules as examples.

The original Aviram and Ratner ansatz of unipolar rectification is based on an asymmetry of orbitals over a single molecule [2]. It assumes perfect symmetric coupling to the metallic electrodes. The rectification is solely based on the molecule. In the strong coupling regime, (modified) tunneling is the dominant transport mechanism. Tunneling only leads to small rectification ratios on the order of unity [55]. Rectification, however, has been observed for a number of molecular electronic junctions [56, 57]. The larger rectification ratios are due to hopping as dominant transport mechanism. Asymmetric coupling with the electrodes, in energy and space, is responsible for rectification. The rectification ratio can be tuned [58]. Symmetric molecules inside an asymmetric junction can then also lead to rectification. Considering the hopping conduction observed for longer π – conjugated molecules, the use of asymmetric metallic electrodes in theory can yield high rectification ratios. Asymmetric injection of carriers in organic electronic devices to fabricate diodes is well established and might have been already observed in ferrocene molecular diodes [57]. Molecular junctions are then still the size of a single molecule but the function would be governed by the electrical contacts, giving rise to the question whether 'true' molecular rectification exists.

The fabrication of molecular field-effect transistors is a huge challenge. A field-effect transistor is based on the modulation of the charge carrier density in a semiconductor

channel between source and drain electrodes by an electric gate field. The channel of a transistor is positioned at the interface of a semiconductor and an insulator. By capacitive coupling of a third electrode with the semiconductor over the insulator the amount of charge carriers in the channel is modulated. The first dimension to shrink down is the thickness of the semiconductor. Self-assembled monolayer field-effect transistors have been fabricated. The semiconductor is only a monolayer thick [59]. Next the source-drain spacing of the transistors needs to be reduced. The feature sizes that can be reached by electron-beam lithography are in the order of tens of nanometers. This means that still tens of molecules constitute the channel of the transistor. Only using breakjunctions in combination with a relatively large back gate, single molecule transistors were fabricated [60–62]. The challenge is the capacitive coupling of the gate electrode to the molecule. For adequate transistor performance the thickness of the insulator should be around half of the channel length, *i.e.* half the size of the molecule of which the channel consists.

Therefore, the incorporation of a gate dielectric in a single molecule has been theoretically investigated. The transistor then consists of a single molecule covalently bound to three electrodes. Single molecule based logic is investigated. Several switching mechanisms within a single molecule are proposed [63]. Multi-terminal molecules have been devised

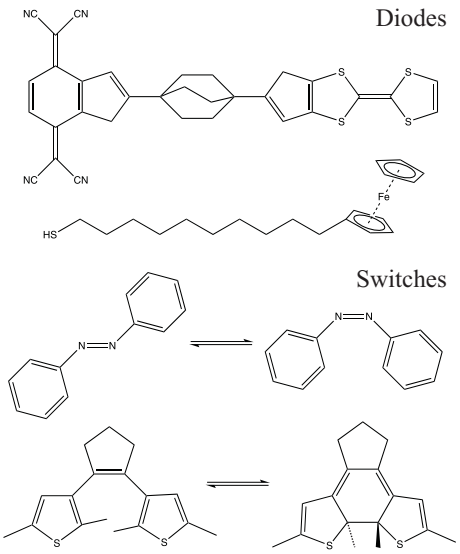

Figure 1.5: Molecules that have been investigated for the realization of functional molecular junctions. The original Aviram and Ratner molecule [2] and a ferrocene compound used by Whitesides *et. al.* [57] are depicted as examples of diodes. As examples of resistive switches azobenzene and diarylethene photochromic cores are shown [65, 66].

to act as complete logic gates such as AND or NOR gates [64]. Although theoretically attractive and well described, experimental verification of the mechanisms for molecular based logic has not been reported.

For memory applications, two-terminal molecular diodes exhibiting bistable switching have been investigated. A broad range of organic compounds has been synthesized. The compounds exhibit two or more stable states which can be interchanged by external stimuli [65]. The states can differ by electronic energy levels, redox states or conformation. External stimuli that can be used to interchange the states can be light, voltage or heat. Different types of molecular switches have been incorporated in molecular junctions [66]. Voltage-based switching in junctions has been reported. However, the switching might be due to extrinsic effects, such a metal-filament formation [67]. The geometry of the molecular junctions is of importance. Molecules can loose switching properties by the fabrication of the electrical contacts to the molecules or the lack of conformational freedom.

Molecules might accomplish other functionalities as well. A resonant tunneling diode that exhibits negative differential resistance (NDR) has been reported [44]. More work on the exclusion of external effects on the observed effect is, however, necessary.

In summary, molecules can perform a multitude of different functions in molecular junctions. The performance depends on the molecular structure, the electronic coupling to the electrode and the geometry of the molecular junction. Chemical synthesis can deliver many compounds and even yield molecules with completely unexpected and new functionalities.

1.6 Upcoming Themes

This thesis describes an understanding of the charge transport in large-area molecular junctions. The influence of molecular structure and electrical contacts will be described and finally molecular functionality will be covered. Large-area molecular junctions are based on a conducting polymer top electrode consisting of PEDOT:PSS. The fabrication and first characterization of the junctions will be reviewed in Chapter 2. The electrical transport of PEDOT:PSS is investigated in Chapter 3. The influence of molecular structure on the β tunneling decay coefficient will be covered in Chapter 4. The effect of the polymer top contact on the electrical transport is described in Chapter 5. Finally, Chapter 6 covers the introduction of functionality in large-area molecular junctions. Chapter 7 concludes this thesis to summarize the key findings.

References

[1] H. Shirakawa, E. J. Lewis, A. G. McDiarmid, C. K. Chiang and A. J. Heeger. J. Chem. Soc., Chem. Commun. 578–580 (1977).

[2] A. Aviram and M. A. Ratner. Chem. Phys. Lett. **29**, 277–283 (1974).

[3] G. M. Whitesides and B. Grzybowski. Science **295**, 2418–2421 (2002).

[4] B. Franklin. Philos. Trans. R. Soc. London **64**, 445–460 (1774).

[5] A. Pockels. Nature **43**, 437–439 (1891).

[6] K. B. Blodgett. J. Am. Chem. Soc. **57**, 1007–1022 (1935).

[7] B. Mann and H. Kuhn. J. Appl. Phys. **42**, 4398–4405 (1971).

[8] E. E. Polymeropoulos. J. Appl. Phys. **48**, 2404–2407 (1977).

[9] R. G. Nuzzo and D. L. Allara. J. Am. Chem. Soc. **105**, 4481–4483 (1983).

[10] J. C. Love, L. A. Estroff, J. K. Kriebel, R. G. Nuzzo and G. M. Whitesides. Chem. Rev. **105**, 1103–1169 (2005).

[11] G. Binnig, H. Rohrer, Ch. Gerber and E. Wiebel. Phys. Rev. Lett. **49**, 57–61 (1982).

[12] G. Binnig, C. F. Quate and Ch. Gerber. Phys. Rev. Lett. **56**, 930–933 (1986).

[13] L. A. Bumm, J. J. Arnold, M. T. Cygan, T. D. Dunbar, T. P. Burgin, L. Jones II, D. L. Allara, J. M. Tour and P. S. Weiss. Science **271**, 1705–1707 (1996).

[14] B. Xu and N. Tao. Science **301**, 1221–1223 (2003).

[15] D. J. Wold and C. D. Frisbie. J. Am. Chem. Soc. **122**, 2970–2971 (2000).

[16] M. A. Reed, C. Zhou, C. J. Muller, T. P. Burgin and J. M. Tour. Science **278**, 252–254 (1997).

[17] B. de Boer, M. M. Frank, Y. J. Chabal, W. Jiang, E. Garfunkel and Z. Bao. Langmuir **20**, 1539–142 (2004).

[18] H. Haick, J. Ghabboun and D. Cahen. Appl. Phys. Lett. **86**, 042113 (2005).

[19] T. W. Kim, G. Wang and T. Lee. Nanotechnology **18**, 315204 (2007).

[20] C. Zhou, M. R. Deshpande, M. A. Reed, L. Jones II and J. M. Tour. Appl. Phys. Lett. **71**, 611–613 (1997).

[21] Y.-L. Loo, D. V. Lang, J. A. Rogers and J. W. P. Hsu. Nano Lett. **3**, 913–917 (2003).

[22] A. Vilan and D. Cahen. Adv. Funct. Mat. **12**, 795–807 (2002).

[23] K. T. Shimizu, J. D. Fabbri, J. J. Jelincic and N. A. Melosh. Adv. Mat. **18**, 1499–1504 (2006).

[24] N. Stein, R. Korobko, O. Yaffe, R. Har Lavan, H. Shpaisman, E. Tirosh, A. Vilan and D. Cahen. J. Phys. Chem. C **114**, 12769–12776 (2010).

[25] R. E. Holmlin, R. Haag, M. L. Chabinyc, R. F. Ismagilov, A. E. Cohen, A. Terfort, M. A. Rampi and G. M. Whitesides. J. Am. Chem. Soc. **123**, 5075–5085 (2001).

[26] M. A. Rampi and G. M. Whitesides. Chem. Phys. **281**, 373–391 (2002).

[27] R. C. Chieci, E. A. Weiss, M. D. Dickey and G. M. Whitesides. Angew. Chem. Int. Ed. **47**, 142–144 (2008).

[28] J. G. Kushmerick, D. B. Holt, J. C. Yang, J. Naciri, M. H. Moore and R. Shashidhar. Phys. Rev. Lett. **89**, 086802 (2002).

[29] J. Liao, L. Bernard, M. Langer, C. Schönenberger and M. Calame. Adv. Mat. **18**, 2444–2447 (2006).

[30] A. P. Bonifas and R. L. McCreery. Nature Nanotechnology **5**, 612–617 (2010).

[31] A. B. Kaiser. Rep. Prog. Phys. **64**, 1–49 (2001).

[32] V. Coropceanu, J. Cornil, D. A. da Silva Filho, Y. Olivier, R. Silbey and J.-L. Brédas. Chem. Rev. **107**, 926–952 (2007).

[33] N. Mott and E. A. Davis. *Electronic Processes in Non-Crystalline Materials* (Clarendon, Oxford, 1979).

[34] A. Miller and E. Abrahams. Phys. Rev. **120**, 745–755 (1960).

[35] J. G. Simmons. J. Appl. Phys. **34**, 1793–1803 (1963).

[36] H. B. Akkerman and B. de Boer. J. Phys. Condens. Matter **20**, 013001 (2008).

[37] A. Salomon, D. Cahen, S. Lindsay, J. Tomfohr, V. B. Engelkes and C. D. Frisbie. Adv. Mat. **15**, 1881–1890 (2003).

[38] W. Wang, T. Lee and M. A. Reed. Phys. Rev. B **68**, 035416 (2003).

[39] H. Song, Y. Kim, Y. H. Jang, H. Jeong and M. A. Reed. Nature **462**, 1039–1043 (2009).

[40] K. Slowinski, R. V. Chamberlain II, R. Bilewicz and M. Majda. J. Am. Chem. Soc. **118**, 4709–4710 (1996).

[41] K. Slowinski, R. V. Chamberlain, C. J. Miller and M. Majda. J. Am. Chem. Soc. **119**, 11910–11919 (1997).

[42] J. M. Seminario and L. Yan. J. Quant. Chem **102**, 711–723 (2005).

[43] Y. Imry and R. Landauer. Rev. Mod. Phys. **71**, 306–312 (1999).

[44] F. Chen, X. Li, J. Hihath, Z. Huang and N. Tao. J. Am. Chem. Soc. **128**, 15874–15881 (2006).

[45] J. M. Beebe, V. B. Engelkes, L. L. Miller and C. D. Frisbie. J. Am. Chem. Soc. **124**, 11268–11269 (2002).

[46] C. D. Frisbie. Presentation Technical University Eindhoven (2010).

[47] C. Li, I. Pobelov, T. Wandlowski, A. Bagrets, A. Arnold and F. Evers. J. Am. Chem. Soc. **130**, 318–326 (2008).

[48] X. Li, J. He, J. Hihath, B. Xu, S. M. Lindsay and N. Tao. J. Am. Chem. Soc. **128**, 2135–2141 (2006).

[49] S. M. Lindsay and M. A. Ratner. Adv. Mat. **19**, 23–31 (2007).

[50] R. L. McCreery and A. J. Bergren. Adv. Mat. **21**, 4303–4322 (2009).

[51] N. Tao. Nature Nanotechnology **1**, 173–181 (2006).

[52] S. H. Choi, B. Kim and C. D. Frisbie. Science **320**, 1482–1486 (2008).

[53] Q. Lu, K. Liu, H. Zhang, Z. Du, X. Wang and F. Wang. ACS Nano **3**, 3861–3868 (2009).

[54] S. H. Choi, C. Risko, M. C. Ruiz Delgado, B. Kim, J.-L. Bredas and C. D. Frisbie. J. Am. Chem. Soc. **132**, 4358–4368 (2010).

[55] R. Stadler, V. Geskin and J. Cornil. Adv. Funct. Mat. **18**, 1119–1130 (2008).

[56] M. Elbing, R. Ochs, M. Koentopp, M. Fisher, C. von Hanisch, F. Weigend, F. Evers, H. B. Weber and M. Mayor. Proc. Natl. Acad. Sci. USA **102**, 8815–8820 (2005).

[57] C. A. Nijhuis, W. F. Reus and G. M. Whitesides. J. Am. Chem. Soc. **131**, 17814–17827 (2009).

[58] J. G. Kushmerick, C. M. Whitaker, S. K. Pollack, T. L. Schull and R. Shashidhar. Nanotechnology **15**, 489–493 (2004).

[59] E. C. P. Smits, S. G. J. Mathijssen, P. A. van Hal, S. Setayesh, T. C. T. Geuns, K. A. H. A. Mutsaers, E. Cantatore, H. J. Wondergem, O. Werzer, R. Resel, M. Kemerink, S. Kirchmeyer, A. M. Muzafarov, S. Ponomarenko, B. de Boer, P. W. M. Blom and D. M. de Leeuw. Nature **455**, 956–959 (2008).

[60] J. Park, A. Pasupathy, J. I. Goldsmith, C. Chang, Y. Yaish, J. R. Petta, M. Rinkoski, J. P. Sethra, H. D. Abruna, P. L. McEuen and D. C. Ralph. Nature **417**, 722–725 (2005).

[61] W. Liang, M. P. Shores, M. Bockrath, J. R. Long and H. Park. Nature **417**, 725–729 (2002).

[62] H. Song, Y. Kim, Y. H. Jang, H. Jeong, M. A. Reed and T. Lee. Nature **462**, 1039–1043 (2009).

[63] J. M. Tour, M. Kozaki and J. M. Seminario. J. Am. Chem. Soc. **120**, 8486–8493 (1998).

[64] M. van der Veen. *Pi Logic*. PhD Thesis, University of Groningen (2006).

[65] B. L. Feringa (Editor). *Molecular Switches*. Wiley-VCH (2001).

[66] S. J. van der Molen and P. Liljeroth. J. Phys. Condens. Matter **22**, 133001 (2010).

[67] C. N. Lau, D. R. Stewart, R. S. Williams and M. Bockrath. Nano Lett. **4**, 569–572 (2004).

Chapter 2

Large-Area Molecular Junctions

2.1 History

In this thesis the electrical transport of molecules is measured in large-area molecular junctions. The name of the junctions originates from the large number of ~ 10^{12} molecules that are probed simultaneously. The junctions were developed at the University of Groningen and at Philips Research Eindhoven [1–3]. The technological breakthrough is the use of a conducting polymer electrode. Direct thermal evaporation of metals on molecules to fabricate an electrical contact results in short-circuit formation. The conducting polymer on top of the molecules prevents short-circuit formation. The junctions are reliable and the yield is almost unity. The reproducibility of the junctions facilitates straightforward acquisition of statistical relevant electrical data.

2.2 Fabrication

The success of the technology is based on the process flow chart, as shown in Figure 2.1. The fabrication starts out with a 4" or 6" silicon wafer as substrate. The wafer is covered with 500 nm thermally grown oxide passivated with hexamethyldisilazane (HMDS). A first layer of gold bottom contacts and interconnects is defined by standard photolithography and subsequent etching. The thickness of the bottom electrode is 50 nm and the surface roughness 0.7 nm. Circular vertical interconnects (*vias*) are defined in insulating photoresist (MA1400 or L6000.5) on top of the gold bottom electrodes. The diameters of the circular *vias* range from 1 μm to 50 μm. The photoresist is annealed at 200 °C to render it insoluble in common organic solvents such as ethanol, toluene and THF. The *vias* expose the bottom gold electrode where molecules can be self-assembled. The exposed gold is cleaned in a low-power plasma etcher. Subsequently the wafer is immersed in a solution of thiolated molecules that spontaneously chemically attach to the gold bottom electrode forming a self-assembled monolayer (SAM) of one molecule thick. The concentration of molecules, the solvent and the time of immersion depend on the specific molecules used. After taking

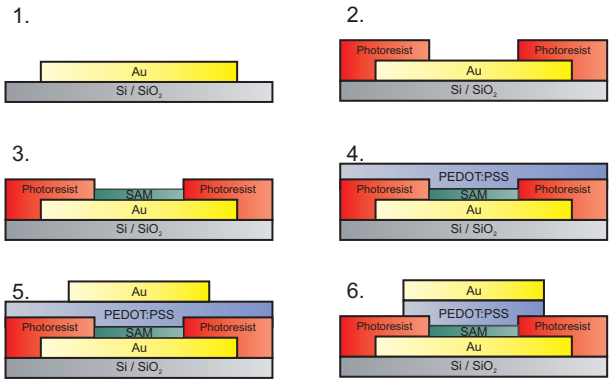

Figure 2.1: Schematic process flow chart for the fabrication of large-area molecular junctions. 1. Deposition bottom electrode. 2. *Via* definition. 3. SAM formation. 4. Spincoating of PEDOT:PSS. 5. Deposition top electrode. 6. Etching of redundant PEDOT:PSS.

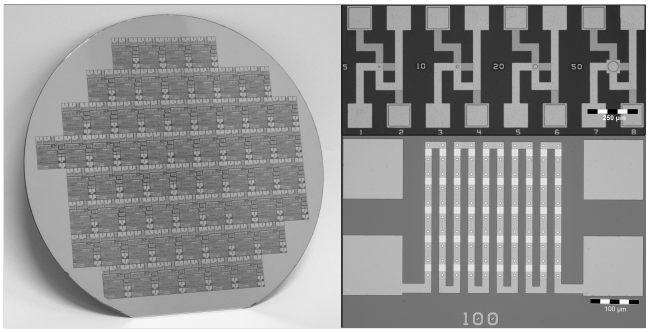

Figure 2.2: Photograph of a finished 6" wafer with 62 identical dies containing discrete large-area molecular junctions of diameters of 1 – 50 μm and strings of molecular junctions. The micrographs show discrete junctions of diameter 5 – 50 μm and a string of 5 μm junctions.

the wafer out of the solution, generally after 2-3 days, the wafer is washed with ethanol, toluene and propanol to wash away extra unbound molecules. The conducting polymer PEDOT:PSS is spincoated on top of the SAM to make electrical contact to the top surface of the monolayer. The thickness of the PEDOT:PSS layer is 90 nm. The layer is dried in a dynamic vacuum at room temperature to remove excess water. Drying of PEDOT:PSS is performed in vacuum at room temperature because at elevated temperatures molecules may desorb. A gold top electrode of 150 nm is evaporated and structured on top of the PEDOT:PSS. Finally, using reactive ion etching the exposed PEDOT:PSS is etched away to

electrically isolate discrete molecular junctions. Because both top and bottom electrodes are patterned, diodes can be serially connected in strings. Figure 2.2 shows micrographs of finished discrete molecular junctions and a string of diodes. Large 6" wafers consist of 62 identical dies containing discrete molecular junction of 1 – 50 μm and strings of devices of 5 μm, resulting in the simultaneous fabrication of over 20.000 molecular junctions with a yield of devices of nearly 100 %.

2.3 Self-Assembled Monolayers

Large-area molecular junctions are based on self-assembled monolayers (SAMs). Self-assembly is the autonomous organization of components into patterns or ordered structures without human intervention [4]. Self-assembly is a key aspect of nature. Many processes are dominated by self-assembly such as the three-dimensional folding of proteins or the formation of lipid bilayers. SAMs are spontaneously ordered monomolecular layers chemically attached to a substrate. SAMs are a specific subset of self-assembled structures. SAMs grow on a variety of different substrates due to specific molecular headgroups that attach to the substrate.

The first SAM reported is an alkanethiol monolayer on gold [5]. This combination has become the model system for monolayers [6–9]. Alkanethiol SAMs exhibit a $(\sqrt{3} \times \sqrt{3})R30°$ reconstructed surface, resulting in a packing density of $\sim 4.6 \times 10^{14}$ molecules / cm^{-2}. The carbon chains are tilted 30° from the surface normal. The length of the molecules determines the thickness.

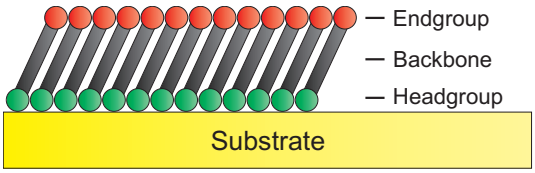

Headgroup	Substrates
–SH	Au, Ag, Pt, Hg, Cu
–CN	Au, Ag
–$SiCl_3$	SiO_x

Figure 2.3: Schematic representation of a self-assembled monolayer (SAM) on a substrate and common examples of headgroup - substrate combinations from which SAMs can be grown.

Nowadays many different substrate – headgroup combinations are known to produce ordered SAMs [6, 7]. Therefore, SAMs can be formed from a large variety of molecular compounds differing in headgroup, length, chemical backbone and endgroup. The structure of the SAMs and the physical properties of the monolayers can be tuned to engineer interfaces. Pioneers in the field have used SAMs to tailor properties such as the wettability of surfaces [10] and the workfunction of metals [11]. The use of mixed SAMs leads to even more fine-tuned control over the engineered surface [12, 13].

2.4 PEDOT:PSS

The key ingredient of large-area molecular junctions is the conducting polymer used to fabricate the top electrode, *i.e.* poly(3,4-ethylenedioxythiophene) stabilized with poly(4-styrenesulphonic acid), PEDOT:PSS. It is the most successful conducting polymer material up to date. Originally PEDOT was designed as a polythiophene variant with less steric hindrance between monomers to promote backbone planarity. Substitution at the 3,4-positions of the thiophene rings increased stability. PEDOT exhibits high conductivity, optical transparency and high stability [14–16].

However, the polymer is insoluble. PSS is a water-soluble polymer. PEDOT:PSS is a complex in which the PSS stabilizes oxidized PEDOT while simultaneously increasing the solubility, resulting in a water-based colloidal lattice [17]. The suspension can be used to yield stable coatings with high conductivity and optical transparency [18]. Different commercial formulations are nowadays available with conductivities upto 1000 S/cm. Thin films of PEDOT:PSS have found its way into numerous applications [19, 20]. In this thesis commercial formulations PHCV4 and PH500 from H. C. Starck and ICPnewtype from Agfa are used.

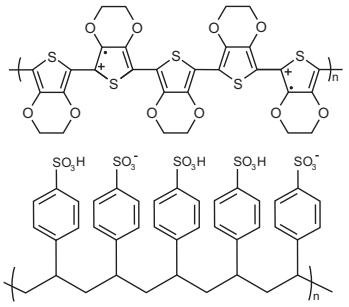

Figure 2.4: Molecular structures of PEDOT (top) and PSS (bottom). PSS simultaneously stabilizes doped PEDOT, while increasing the solubility of the complex.

Thin films of PEDOT:PSS consist of spherical grains of PEDOT-rich cores surrounded by PSS-rich shells. The microstructure has been resolved using scanning tunneling microscopy [21] and electron microscopy studies [22]. Elongated pancake-like grains have also been reported [23]. The electrical transport in PEDOT:PSS is dominated by hopping of charge carriers from grain to grain. The workfunction of PEDOT:PSS is ~ 5 eV, close to the workfunction of gold.

2.5 Electrical Characterization

Large-area molecular junctions are two-terminal diodes. The characterization therefore comprises the determination of the absolute value of the current density ($|J|$), the dependence of current density on applied bias voltage (J–V characteristics) and the dependence of the current density on temperature (J–T characteristics).

Electrical measurements were performed in commercial and home-built probe stations under both ambient conditions and under vacuum. PEDOT:PSS is hygroscopic, a small amount of water is constantly present. The water can be removed under vacuum or at elevated temperatures. However, upon re-exposure to ambient the water immediately re-absorbs. The presence of water slightly influences the absolute value of the current density [2].

The current was measured by either a Keithley 4200 Semiconductor Characterization System or a Keithly 2400 Sourcemeter controlled by a labview program. Direct-current (DC) measurements were generally performed within a range of 0.5 V – 1 V. The maximum voltage window of the molecular junctions is set by the water content since electrolysis of water causes breakdown of the junctions [24]. Formation of H_2 gas in the photoresist-enclosed junctions leads to blow up of the junctions and delamination of PEDOT:PSS from the bottom contact. The electrolysis is not destructive for biases < 1 V, but does lead to small hysteresis in the J–V characteristics. At higher biases the junctions break down.

In order to investigate the transport characteristics at higher biases, pulsed measurements were performed. Short millisecond pulses of the required bias were applied with a Keithley 2602 System Sourcemeter while in between the pulses the connections were grounded. Reduction of the effective ON-time of the voltage bias to the molecular junctions decreases the amount of H_2 formed and leads to an increased stable bias window up to at least 5 V. A direct correlation between the duty cycle, ON-time pulse width and breakdown voltage has been obtained [25].

Temperature-dependent measurements, both pulsed and DC, were performed in a Cryogenic Probestation (Janis Research Co.) equipped with a closed-cycle Helium refrigerator. The sample table can be cooled down to 8 K. On top of the table the silicon wafer with

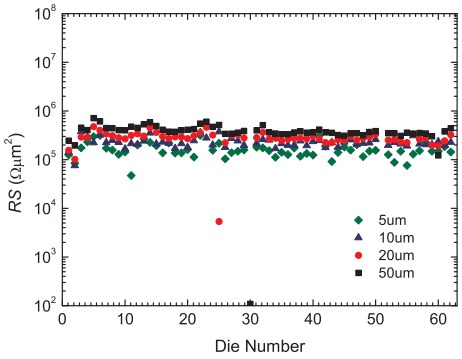

Figure 2.5: Normalized resistance (RS) of ~ 240 molecular junctions with diameter 5 – 50 μm based on a C18 monothiol SAM. The high yield of working devices in combination with the reproducibility of the junctions leads to statistical relevant electrical transport data.

molecular junctions was mounted. For increased thermal contact Apiezon N thermal grease was used. The temperature of the junctions was calibrated with a temperature-dependent resistor on top of the junctions. The lowest achievable temperature was 25 K. Any temperature in the range 25 K – 300 K was achieved by the combination of cooling and appropriate heating of the sample table.

The measured currents as a function of bias voltage and temperature were generally averaged over a large number of junctions. As a reminder, large 6" wafers consist of 62 identical dies containing molecular junctions. Figure 2.5 shows the normalized resistance of C18 monothiol molecular junctions of different diameters as a function of die number. The electrical characteristics are reproducible from junction to junction. Because of the large number of simultaneously fabricated junctions and their reproducibility, large-area molecular junctions yield statistical relevant electronic transport data.

2.6 Electrical Properties of Alkanedithiols

The first junctions were based on alkanedithiols [1, 2]. Because of the –SH terminated endgroups, SAMs of dithiols yield a hydrophilic top surface. The initial hypothesis for using dithiols was that this hydrophilicity would lead to an increased wetting of the water-based PEDOT:PSS colloidal suspension as compared to more hydrophobic surfaces. Molecules with 8, 10, 12 and 14 carbon atoms and the PHCV4 type of PEDOT:PSS were used. The SAMs were grown from 3 mM ethanol solutions and the electrical characteristics of junctions of 10 – 100 μm in diameter were measured. Reproducible junctions were fabricated with a yield of > 95 %. The junctions were stable, both versus repeated voltage

cycling and upon storage. Figure 2.6a shows average current density versus voltage (J–V) characteristics of the junctions. The current scales linearly with the area of the junctions. The current densities are identical. For all junctions the low voltage transport is Ohmic while at higher voltages the current increases superlinear with voltage. The J–V behavior is consistent with tunneling through a metal-molecule-metal junction with a high barrier height of a few eV. Temperature-dependent measurements were performed from 293 K – 199 K. No change in the electronic properties was observed. Figure 2.6b displays the dependence of the current density as a function of molecular length, at different voltages of 0.1, 0.3 and 0.5 V for the C8, C10, C12 and C14 alkanedithiols. The current density depends exponentially on the molecular length $J \propto exp^{-\beta L}$. The value of β changes with voltage resulting in 0.66 $Å^{-1}$ at 0.1 V, 0.61 $Å^{-1}$ at 0.3 V and 0.57 $Å^{-1}$ at 0.5 V. The transport characteristics, *i.e.* the voltage- and temperature-dependence, and the exponential length-dependence lead to the conclusion that non-resonant tunneling is the dominant transport mechanism in large-area molecular junctions. Furthermore, in the original paper it was argued that PEDOT:PSS could be regarded as a non-interacting metallic electrode [1].

Further effort in understanding the transport resulted in an adequate description of the J–V characteristics at low bias using the Simmons tunneling model [2, 26, 27]. The dielectric constant of the monolayers was determined by impedance spectroscopy and used to incorporate the image potential of the metallic electrodes into the model. A good agreement was obtained. However, the obtained tunnel barrier heights were not realistic.

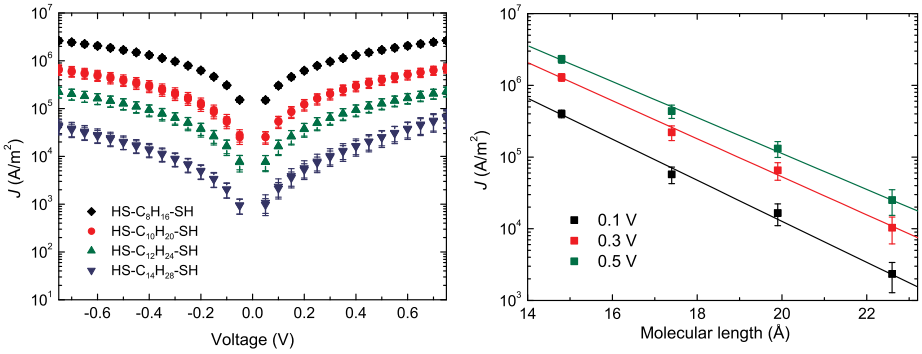

(a) (b)

Figure 2.6: (a) Current density versus voltage (J–V) characteristics of alkanedithiols in large-area molecular junctions. (b) Exponential dependence of the current density versus molecular length. The tunneling decay coefficient β depends on the applied voltage. Figure reproduced from [1].

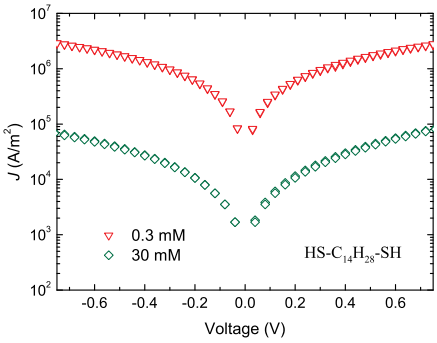

Figure 2.7: Dependence of the *J*–*V* characteristics of junctions with C14 dithiol on the concentration of molecules in solution. High concentrations result in a full standing-up phase while low concentrations yield a looped-phase with both –SH groups attached to Au. The looped-phase effectively constitutes a thinner monolayer and results in higher current densities. Figure reproduced from [28].

The barrier heights decreased with molecular length while the electronic orbitals, especially the HOMO and LUMO, do not change in energy as a function of length.

The orientation of the molecules in the SAMs was shown to have a profound effect on the electronic properties [2, 28]. Alkanedithiol molecules contain two terminal –SH groups. For long molecules both groups can attach to the Au bottom contact, forming a looped-phase. X-ray Photoelectron Spectroscopy (XPS) showed that the formation of the looped-phase depends on the concentration of molecules in the SAM-solution [28]. At high concentration, rapid absorption of a second molecule next to a first one will prevent the first molecule to loop back to the surface since no free absorption site is available. Therefore a higher dithiol concentration will lead to a smaller fraction of the looped-phase. Figure 2.7 shows the dependence of the *J*–*V* characteristics for HS-$C_{14}H_{28}$-SH assembled from ethanol solutions containing different concentrations of molecules. High concentrations of 30 mM, yielding almost exclusively the standing-up phase of C14-dithiol, result in low current density. Very low concentrations of 0.3 mM lead to the looped-phase that effectively constitute a thinner SAM, resulting in a significantly higher current density.

The concentration dependence in principle opens the possibility for a continuous variation of the current density of large-area molecular junctions based on identical molecules. Continuous variation of the microstructure of the SAM yields accordingly different resistance values. Surprisingly, the yield of the junctions remained > 95 %. The looped-phase of alkanedithiols does not expose the –SH endgroup on the SAM surface but a canted –CH_2– group, leading to a more hydrophobic SAM surface.

2.7 Electrical Properties of Alkanemonothiols

Since the looped-phase of alkanedithiols, exhibiting a hydrophobic top SAM surface, could be successfully characterized, the next logical choice was the characterization of alkanemonothiols. For the first characterization of alkanemonothiols, molecules with 8 – 22 even carbon atoms and the ICPnewtype formulation of PEDOT:PSS were used [3]. The reproducibility, stability, area-scaling and yield of the molecular junctions were identical to the junctions based on alkanedithiols. The *J*–*V* characteristics were non-linear as well. The red diamonds in Figure 2.8 show the normalized resistance RS as a function of molecular length. RS of molecules with 8 – 12 carbon atoms were indistinguishable from PEDOT:PSS only, while for longer molecules RS increases exponentially with molecular length. A slope of 0.9 per carbon atom is found, resulting in 0.73 $Å^{-1}$. This value corresponds well with the value of 0.66 $Å^{-1}$ found for alkanedithiols.

The absolute value of the resistance of the alkanemonothiol junctions was lower than that found for the corresponding dithiols. The length dependence of both molecular series was practically identical. Extrapolation of the dependence to zero molecular length showed

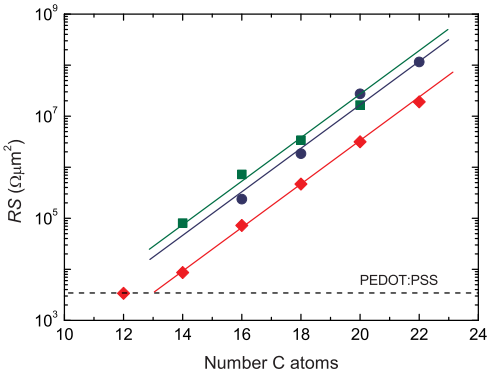

Figure 2.8: The influence of process parameters on the absolute value of the normalized resistance RS of alkanemonothiols in large-area molecular junctions. RS is plotted as a function of molecular length. The different datasets represent junctions that were fabricated using different process parameters. The dependence on molecular length is constant, while the absolute value is determined by the specific combination of photoresist and type of PEDOT:PSS. The red diamonds represent junctions fabricated with L6000.5 photoresist and the ICPnewtype formulation of PEDOT:PSS, the blue circles using L6000.5 and PH500 with 5 % DMSO and the green squares using MA1400 and ICPnewtype. Figure reproduced from [3].

a lower $RS_{L=0}$ for monothiols than for dithiols. The difference was argued to stem from a lower contact resistance. A lower contact resistance for alkanemonothiols was counterintuitive since water-based PEDOT:PSS is expected to exhibit less adhesion with the monothiol SAM surface, resulting in less intimate contact. In order to investigate the differences in absolute resistance, the influence of process parameters on the device characteristics was determined.

2.8 Influence of Process Parameters

The technology of large-area molecular junctions is based on PEDOT:PSS as a top electrode. Numerous commercial formulations are available. Formulations differ in *e.g.* electrical conductivity, PEDOT-to-PSS ratio and added surfactants. Alkanemonothiols were used as constant SAMs to investigate the influence of process parameters such as the formulation of PEDOT:PSS on the electrical transport. The blue circles in Figure 2.8 represent the resistance of molecular junctions fabricated using the PH500 formulation of PEDOT:PSS with 5 % dimethylsulfoxide (DMSO) added. The conductivity of the PH500 formulation is typically ~ 0.1 S/cm while the addition of DMSO results in a conductivity of ~ 300 S/cm. This value is comparable to the conductivity of the ICPnewtype formulation. The resistance of the molecular junctions fabricated with the PH500 formulation was higher than the junctions fabricated with the ICPnewtype formulation. The dependence on molecular length was nevertheless identical. The comparison showed that the resistance of the molecular junctions depends on the type of PEDOT:PSS used. The conductivity of the PEDOT:PSS layer is reflected in the molecular junctions. This implies that molecular junctions can be fabricated with identical molecules using different process parameters that results in a range of different resistance values.

The second adjustable process parameter is the type of photoresist used in which the molecular junctions are embedded. The green squares in Figure 2.8 represent data of molecular junctions fabricated with MA1407 negative photoresist instead of the L6000.5. The type of PEDOT:PSS is the ICPnewtype formulation. Figure 2.8 shows that the absolute value of the resistance of the junctions depends on the type of photoresist as well while the length-dependence remains constant. Apparently not only the conductivity of PEDOT:PSS is crucial but also how it is applied on top of the SAM. In first order approximation the type of photoresist does not influence the interface between the SAM and PEDOT:PSS. The influence of the photoresist is tentatively explained by the different surface energies. The morphology of PEDOT:PSS will depend on the surface energy of the photoresist. It remains a second order effect however.

The absolute value of the resistance of the molecular junctions thus depends on the PEDOT:PSS and the type of photoresist used. A single measurement can yield various resistance values based on process parameters and wetting parameters of the SAM. Therefore, length series of molecules are necessary to investigate charge transport in large-area molecular junctions. Furthermore, a default fabrication process needs to be defined since measurements depend critically on the process. In this thesis, the default photoresist is MA1400 and the default PEDOT:PSS formulation is ICPnewtype.

2.9 Conclusions

Stable and reproducible large-area molecular junctions can be fabricated using a conducting polymer interlayer between a SAM and a gold top electrode. Molecular junctions yield statistical relevant and reliable transport characteristics of benchmark self-assembled monolayers of alkanedithiols and alkanemonothiols. The influence of the molecular monolayer is observed in an exponential dependence of the resistance on molecular length, $RS \propto exp^{\beta L}$, with β = 0.66 Å^{-1} for alkanedithiols and β = 0.73 Å^{-1} for alkanemonothiols. Furthermore, variations in structure of the monolayers are reflected in changes of the electrical characteristics of the molecular junctions. The absolute value of the resistance, nevertheless, depends crucially on the type of PEDOT:PSS and type of photoresist used to fabricate the junctions.

References

[1] H. B. Akkerman, P. W. M. Blom, D. M. de Leeuw and B. de Boer. Nature **441**, 69–72 (2006).

[2] H. B. Akkerman. *Large-Area Molecular Junctions*. PhD Thesis, University of Groningen (2008).

[3] P. A. van Hal, E. C. P. Smits, T. C. T. Geuns, H. B. Akkerman, B. C. de Brito, S. Perissinotto, G. Lanzani, A. J. Kronemeijer, V. Geskin, J. Cornil, P. W. M. Blom, B. de Boer and D. M. de Leeuw. Nature Nanotechnology **3**, 749–754 (2008).

[4] G. M. Whitesides and B. Grzybowski. Science **295**, 2418–2421 (2002).

[5] R. G. Nuzzo and D. L. Allara. J. Am. Chem. Soc. **105**, 4481–4483 (1983).

[6] A. Ulman. Chem. Rev. **96**, 1533–1554 (1996).

[7] J. C. Love, L. A. Estroff, J. K. Kriebel, R. G. Nuzzo and G. M. Whitesides. Chem. Rev. **105**, 1103–1169 (2005).

[8] F. Schreiber. Prog. Surf. Sci. **65**, 151–256 (2000).

[9] C. Vericat, M. E. Vela, G. Benitez, P. Carro and R. C. Salvarezza. Chem. Soc. Rev. **39**, 1805–1834 (2010).

[10] G. M. Whitesides and P. E. Laibinis. Langmuir **6**, 87–96 (1990).

[11] I. H. Campbell, S. Rubin, T. A. Zawodzinski, J. D. Kress, R. L. Martin and D. L. Smith. Phys. Rev. B **54**, 14321–14324 (1996).

[12] U. Zschieschang, F. Ante, M. Schlörholz, M. Schmidt, K. Kern and H. Klauk. Adv. Mat. **20**, 4489–4493 (2010).

[13] K.-Y Wu, S.-Y. Yu and Y.-T. Tao. Langmuir **25**, 6232–6238 (2009).

[14] F. Jonas and L. Schrader. Synth. Met. **41-43**, 831–836 (1991).

[15] G. Heywang and F. Jonas. Adv. Mat. **4**, 116–118 (1992).

[16] M. Dietrich, J. Heinze, G. Heywang and F. Jonas. J. Electroanal. Chem. **369**, 87–92 (1994).

[17] F. Jonas and W. Krafft. Macromol. Symp. **100**, 169–173 (1995).

[18] F. Jonas and J. T. Morisson. Synth. Met. **85**, 1397–1398 (1997).

[19] L. Groenendaal, F. Jonas, D. Freitag, H. Pielartzik and J. R. Reynolds. Adv. Mat. **12**, 481–494 (2000).

[20] S. Kirchmeyer and K. Reuter. J. Mat. Chem. **15**, 2077–2088 (2005).

[21] M. Kemerink, S. Timparano, M. M. de Kok, E. A. Meulenkamp and F. J. Touwslager. J. Phys. Chem. B **108**, 18820–18825 (2004).

[22] U. Lang, E. Müller, N. Naujoks and J. Dual. Adv. Funct. Mat. **19**, 1215–1220 (2009).

[23] A.M. Nardes, M. Kemerink, R. A. J. Janssen, J. A. M. Bastiaansen, N. M. M. Kiggen, B. M. W. Langeveld, A. J. J. M. van Breemen and M. M. de Kok. Adv. Mat. **19**, 1196–1200 (2007).

[24] B. C. de Brito, E. C. P. Smits, P. A. van Hal, T. C. T. Geuns, B. de Boer, C. J. M. Lasance, H. L. Gomez and D. M. de Leeuw. Adv. Mat. **20**, 3750–3753 (2008).

[25] I. Katsouras et al. To be published.

[26] H. B. Akkerman, R. C. G. Naber, B. Jongbloed, P. A. van Hal, P. W. M. Blom, D. M. de Leeuw and B. de Boer. Proc. Natl. Acad. Sci. USA **104**, 11161–11166 (2007).

[27] J. G. Simmons. J. Appl. Phys. **34**, 1793–1803 (1963).

[28] H. B. Akkerman, A. J. Kronemeijer, P. A. van Hal, D. M. de Leeuw, P. W. M. Blom and B. de Boer. Small **4**, 100–104 (2008).

Chapter 3

Electrical Transport of PEDOT:PSS

3.1 Introduction: Transport in Polymers

The first highly conducting organic polymer, chemically doped polyacetylene, was reported in 1977 [1]. A fundamental and still unresolved question is the nature of the charge transport in conjugated polymers. Since interactions between monomers are covalent, leading to strong orbital overlap and delocalization over the π – conjugated system, conjugated polymers can be regarded as one-dimensional semiconductors. On the other hand, disorder due to kinks, cross-links and impurities will disrupt the π – system and transport will be governed by hopping between conjugated parts of one polymer chain or neighboring chains, resembling a three-dimensional semiconductor. To describe the properties of standard three-dimensional conductors, Fermi Liquid theory is widely used. Introducing disorder in a Fermi Liquid induces localization and consequently electrical transport occurs by hopping of charge carriers at the Fermi level. For many doped, disordered organic polymers the conductivity was reported to follow a stretched exponential temperature dependence, $\sigma \propto exp\ (-(1/T)^{\nu})$ [2]. The reported values for the exponent ν suggest so-called variable range hopping in one to three dimensions, $\nu = 1/(D+1)$ where D, the number of dimensions, varies between 1 and 3 [3]. In one-dimensional systems however, quantum confinement amplifies Coulomb interactions between electrons and Luttinger Liquid theory needs to be applied [4]. Typical for Luttinger Liquid theory is that the dispersion relation near the Fermi energy is approximated as both linear and continuous. This assumption is valid when high-energy excitations can be disregarded and when the one-dimensional lattice is semi-infinite. The combination of a linear dispersion and Coulomb interaction results in a power-law density of states that vanishes at the Fermi level. Hence, tunneling into a Luttinger Liquid yields power-law relations with both temperature and voltage, more exactly, $J \propto T^{\alpha}$ at low voltages ($kT \gg eV$) and $J \propto V^{\beta}$ at low temperatures ($eV \gg kT$), with

* This chapter has been previously published as: A. J. Kronemeijer, E. H. Huisman, I. Katsouras, P. A. van Hal, T. C. T. Geuns, P. W. M. Blom, S. J. van der Molen and D. M. de Leeuw. Phys. Rev. Lett. **105**, 156604 (2010).

$\beta = \alpha + 1$. Furthermore, when the scaled current density $J/T^{1+\alpha}$ is plotted as a function of eV/kT, a universal curve is obtained described by [5–7]:

$$J = J_0 \cdot T^{1+\alpha} \cdot sinh\left(\gamma \frac{eV}{kT}\right) \cdot \left|\Gamma\left(1 + \frac{\alpha}{2} + i\gamma \frac{eV}{\pi kT}\right)\right|^2 \tag{3.1}$$

where the parameter α is derived from the measurements, J_0 and γ are two fit parameters, e is the elementary charge, k is the Boltzmann constant and Γ is the Gamma function. The fit parameter γ^{-1} has been related to the number of tunnel barriers between the contacts, and determines a cross over from Ohmic behavior to a power-law dependence.

It has recently been reported that Equation 3.1 describes the charge transport of the conjugated polymer poly(2,5-bis-(3-tetradecylthiophen-2-yl)thieno[3,2-b] thiophene) (PBTTT) in high carrier density field-effect transistors and in electrochemically doped films [8]. Density functional theory calculations have classified PBTTT as a quasi one-dimensional system [9]. Supported by the fit of Equation 3.1 and the calculated electrical anisotropy, the scaling of the electrical transport has been interpreted as a fingerprint of Luttinger Liquid behavior originating from one-dimensional transport in conjugated polymers [8, 10].

To address whether one-dimensionality is a prerequisite for the power-law scaling the charge transport in PEDOT:PSS is studied. This complex is a mixture of doped PEDOT stabilized with PSS. Thin films can be spin coated from waterborne lattices and exhibit conductivities upto about 1000 S/cm. Scanning tunneling and electron microscopy studies have shown that the microstructure consists of spherical grains in the order of 20 – 50 nm [11, 12]. The individual grains have a PEDOT rich core and a PSS rich shell [12]. Therefore, PEDOT:PSS is a three-dimensional disordered electronic system and a model compound for highly doped conducting polymers. Previously, the conductivity of PEDOT:PSS was reported to follow a stretched exponential temperature dependence [13–16]. However, contrary to the stretched exponential temperature dependence, a few reports have also shown a power-law dependence [14, 17, 18]. The bias dependence of these measurements has not been reported. Here a detailed analysis of the electrical transport is presented as a function of both bias and temperature.

3.2 Electrical Characteristics: Universal Scaling

To test the validity of Equation 3.1, a crossover from Ohmic transport to a power-law dependence has to be observed. This implies a relatively large value of γ that can only be realized with small electrode spacing, in the order of 100 nm. To this end the transport is measured transversal through PEDOT:PSS thin films fabricated in large-area molecular

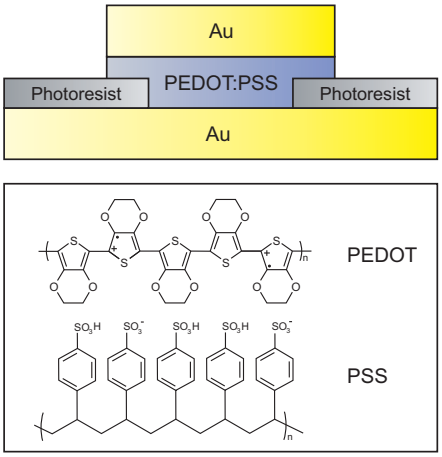

Figure 3.1: Schematic representation of the junctions and the chemical structure of PEDOT:PSS.

junctions, as shown in Figure 3.1. The current through the junctions scaled with the lateral dimensions with a small standard deviation [19–21].

The current density versus voltage (J–V) characteristics averaged over 8 PEDOT:PSS junctions are presented as a function of temperature in Figure 3.2. The bias was varied between 0 V and 0.5 V and the temperature was varied between 25 K and 300 K. The transport characteristics are symmetric for negative and positive bias. At room temperature the transport is Ohmic up to the applied bias of 0.5 V. At lower temperatures, the current density decreases and the transport deviates from Ohmic behavior. To magnify the non-linearity, measurements at higher bias are required. However, at room temperatures the junctions break down at higher bias due to electrolysis of remaining water in the PEDOT:PSS layer [21]. To circumvent the breakdown, pulse measurements were applied. At low temperature and with a low duty cycle the transport could be measured up to high biases of 3 V, while at higher temperatures electrolysis still hampered the measurements. The current density versus voltage (J–V) characteristics up to 3 V are presented in Figure 3.3 as a function of temperature between 25 K and 100 K. At low bias the current density decreases with decreasing temperature. At higher biases the temperature dependence disappears.

To analyze the electrical transport, the current density as a function of temperature is plotted on a double logarithmic scale. The inset of Figure 3.3 shows that straight lines are obtained, indicating a power-law dependence of the current density on temperature. The slope depends on the applied bias. Extrapolating the value of the slope to 0 V bias, where

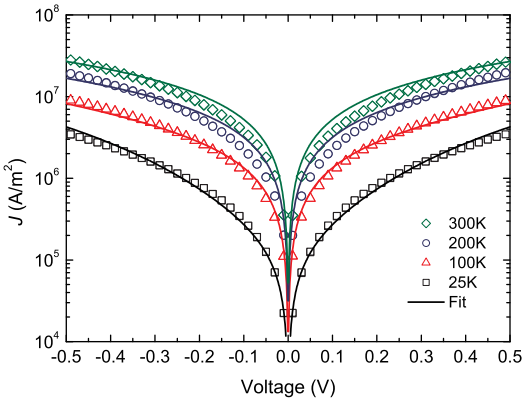

Figure 3.2: *J*–*V* characteristics of the PEDOT:PSS junctions up to 0.5 V bias at temperatures between 25 K and 300 K. The current density is averaged over 8 devices with device diameter between 5 and 50 μm. The solid curves stem from the universal curve calculated using Equation 3.1.

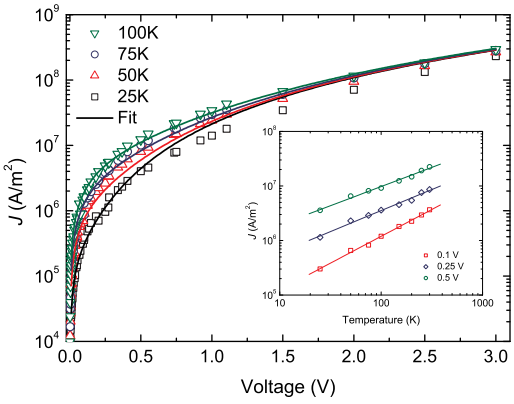

Figure 3.3: *J*–*V* characteristics of the PEDOT:PSS junctions up to 3 V bias at temperatures between 25 K and 100 K. The current density is averaged over 6 devices with device diameter of 4 and 5 μm. The solid curves stem from the same universal curve calculated using Equation 3.1. The inset shows the *J*–*T* characteristics on a double logarithmic scale.

$kT \gg eV$, yields $J \propto T^{\alpha}$ with $\alpha = 1.25$. With this fixed value of α the scaled current density, $J/T^{1+\alpha}$, is calculated at each temperature. Figure 3.4 shows the scaled current density as a function of the dimensionless parameter eV/kT. Both DC measurements at low bias and pulse measurements at high applied bias are included. Varying the temperature between 25 K and 300 K and the bias between 0 V and 3 V, leads to a change in the parameter eV/kT over four orders of magnitude. The corresponding scaled current density then varies over six orders of magnitude. Figure 3.4 nevertheless shows that even over this wide parameter space a universal dependence is obtained. The solid curve in Figure 3.4 is calculated using Equation 3.1. A perfect agreement is obtained using the fit parameters γ of 0.025 and J_0 of 200 (A/m^2). The quality of the fit is illustrated by recalculating the discrete *J(V,T)* characteristics. The solid curves in Figures 3.2 and 3.3 are computed and demonstrate that with only two parameters the complete *J(V,T)* curves can be described.

Figure 3.4 shows that for small values of eV/kT the slope of the scaled current density is unity. This Ohmic behavior implies that at a fixed, low bias the current density follows a power-law dependence on temperature as $J \propto T^{\alpha}$ with $\alpha = 1.25$. For values of eV/kT much larger than unity the slope of the scaled current density becomes about 2.25. This implies that at a fixed, low temperature the current density follows a power-law dependence on bias

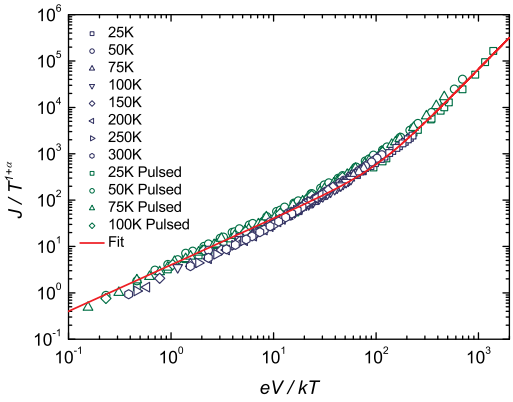

Figure 3.4: Scaled current density as a function of the dimensionless parameter eV/kT. Both DC measurements at low bias, Figure 3.2, and pulse measurements at high applied bias, Figure 3.3, are included. The solid curve is calculated using Equation 3.1 with fit constants $\gamma = 0.025$ and $J_0 = 200$ A/m^2. The solid curves of Figures 3.2 and 3.3 are generated from this fit.

as $J \propto V^{\beta}$ with $\beta = 2.25$. The crossover from linear to superlinear behavior is dominated by the value of the parameter γ. The parameter J_0 is a multiplication constant.

Equation 3.1, which completely describes the *J(V,T)* characteristics, has been shown to hold for a Luttinger Liquid. However, the reverse is not necessarily true, *i.e.* if the *J(V,T)* characteristics can be described by Equation 3.1, this does not automatically imply that one is dealing with a Luttinger Liquid. In fact, Equation 3.1 was originally derived for dissipative tunneling in a biased double-well quantum system where the electron tunnels between the two wells [6, 7]. Dissipative coupling was provided by an (unspecified) external heat bath. Although Luttinger Liquid behavior is not a necessary condition for Equation 3.1, this equation has since been used as a direct proof of Luttinger Liquid behavior [5]. Given this background, it is noted again that PEDOT:PSS is a disordered conducting polymer; the microstructure of thin films consists of spherical amorphous grains [11, 12]. Furthermore, the conjugation of PEDOT chains is too short to form a semi-infinite one-dimensional lattice needed for a Luttinger Liquid. Hence, PEDOT:PSS is effectively a three-dimensional electronic system and can therefore not be regarded as a Luttinger Liquid. Nevertheless, the scaling behavior is observed.

Another physical origin related to three-dimensional electronic systems is thus responsible for the scaling. In general, the tunneling rate at an energy E is determined by a convolution of the tunnel probability $P(E)$ and the density of states $\rho(E)$. The observed scaling can thus originate from power-law scaling of either $P(E)$ or $\rho(E)$ [22]. Power-law scaling of $\rho(E)$ arises naturally in a Luttinger Liquid because of the linear dispersion relation. Scaling of $P(E)$ arises in the general dissipative tunneling models due to coupling of the system with an (unspecified) environment [6, 7]. Additional effort to specify dissipation has resulted in the theoretical description of systems where unconventional Coulomb Blockade mechanisms yield power-law behavior. The most prominent is so-called environmental Coulomb blockade in ultra-small tunnel junctions [23, 24], while also arrays of quantum dots [25, 26] and non-conventional tunneling between disordered conductors [27–29] produce similar results. The specific models yield power-law behavior that can hardly be distinguished from Luttinger Liquid behavior [22, 30, 31].

Weak Coulomb Blockade is a viable option in PEDOT:PSS to explain the observed scaling behavior [26], since thin films consist of relatively strongly coupled grains of PEDOT [32]. Coulomb Blockade is, however, not immediately expected for PBTTT because of the semi-crystalline microstructure of the films. Therefore a general origin of the universal scaling cannot be unambiguously determined from the present experimental efforts.

3.3 Conclusions

It has been shown that the electrical transport of PEDOT:PSS junctions as a function of both temperature and bias can be described over a wide parameter space by a single equation with only two fit parameters. A similar scaling with temperature and bias has previously been reported for the highly doped conducting polymer PBTTT and has been interpreted as a signature of one-dimensional Luttinger Liquid behavior. PEDOT:PSS, however, cannot be regarded as one-dimensional electronic system. The scaling can be due to dissipative tunneling such as environmental Coulomb blockade but the origin cannot unambiguously be assigned. Scaling nevertheless appears to be general for highly doped polymer systems and opens new opportunities for understanding the charge transport in these materials.

References

[1] H. Shirakawa, E. J. Lewis, A. G. McDiarmid, C. K. Chiang and A. J. Heeger. J. Chem. Soc., Chem. Commun. 578–580 (1977).

[2] A. B. Kaiser. Rep. Prog. Phys. **64**, 1–49 (2001).

[3] N. Mott and E. A. Davis. *Electronic Processes in Non-Crystalline Materials* (Clarendon, Oxford, 1979).

[4] J. Voit. Rep. Prog. Phys. **58**, 977–1116 (1995).

[5] M. Bockrath, D. H. Cobden, J. Lu, A. G. Rinzler, R. E. Smalley, L. Balents and P. L. McEuen. Nature **397**, 598–601 (1999).

[6] H. Grabert and U. Weiss. Phys. Rev. Lett. **54**, 1605–1608 (1985).

[7] M. P. A. Fisher and A. T. Dorsey. Phys. Rev. Lett. **54**, 1609–1612 (1985).

[8] J. D. Yuen, R. Menon, N. E. Coates, S. Cho E. B. Namdas, S. T. Hannahs, D. Moses and A. J. Heeger. Nat. Mater. **8**, 572–575 (2009).

[9] J. E. Northrup. Phys. Rev. B **76**, 245202 (2007).

[10] J. H. Worne, J. E. Anthony and D. Natelson. Appl. Phys. Lett. **96**, 053308 (2010).

[11] M. Kemerink, S. Timparano, M. M. de Kok, E. A. Meulenkamp and F. J. Touwslager. J. Phys. Chem. B **108**, 18820–18825 (2004).

[12] U. Lang, E. Müller, N. Naujoks and J. Dual. Adv. Funct. Mat. **19**, 1215–1220 (2009).

[13] A. N. Aleshin, S. J. Williams and A. J. Heeger. Synth. Met. **94**, 173–177 (1998).

[14] J. Y. Kim, J. H. Jung, D. E. Lee and J. Loo. Synth. Met. **126**, 311–316 (2002).

[15] S. Ashizawa, R. Horikawa and H. Okuzaki. Synth. Met. **153**, 5–8 (2005).

[16] A. M. Nardes, M. Kemerink and R. A. J. Janssen. Phys. Rev. B **76**, 085208 (2007).

[17] A. Aleshin, R. Kiebooms, R. Menon and A. J. Heeger. Synth. Met. **90**(61-68) (1997).

[18] C. S. Sangeeth, M. Jaiswal and R. Menon. J. Phys. Condens. Matter **21**, 072101 (2009).

[19] H. B. Akkerman, P. W. M. Blom, D. M. de Leeuw and B. de Boer. Nature **441**, 69–72 (2006).

[20] P. A. van Hal, E. C. P. Smits, T. C. T. Geuns, H. B. Akkerman, B. C. de Brito, S. Perissinotto, G. Lanzani, A. J. Kronemeijer, V. Geskin, J. Cornil, P. W. M. Blom, B. de Boer and D. M. de Leeuw. Nature Nanotechnology **3**, 749–754 (2008).

[21] B. C. de Brito, E. C. P. Smits, P. A. van Hal, T. C. T. Geuns, B. de Boer, C. J. M. Lasance, H. L. Gomez and D. M. de Leeuw. Adv. Mat. **20**, 3750–3753 (2008).

[22] E. B. Sonin. Physica E **18**, 331–332 (2003).

[23] M. H. Devoret, D. Esteve, H. Grabert, G. L. Ingold, H. Pothier and C. Urbina. Phys. Rev. Lett. **64**, 1824–1827 (1990).

[24] S. M. Girvin, L. I. Glazman, M. Jonson, D. R. Penn and M. D. Stiles. Phys. Rev. Lett. **64**, 3183–3186 (1990).

[25] Sh. Farfangfar, R. S. Poikolainen, J. P. Pekola, D. S. Gobulev and A. D. Zaikin. Phys. Rev. B **63**, 075309 (2001).

[26] J. F. Dayen, T. L. Wade, G. Rizza, D. S. Gobulev, C. S. Cojocaru, D. Pribat, X. Jehl, M. Sanquer and J. E. Wegrowe. Eur. Phys. J. Appl. Phys. **48**, 10604 (2009).

[27] R. Egger and A. O. Gogolin. Phys. Rev. Lett. **87**, 066401 (2001).

[28] J. Rollbühler and H. Grabert. Phys. Rev. Lett. **87**, 126804 (2001).

[29] E. G. Mishchenko, A. V. Andreev and L. I. Glazman. Phys. Rev. Lett. **87**, 246801 (2001).

[30] K. A. Matveev and L. I. Glazman. Phys. Rev. Lett. **70**, 990–993 (1993).

[31] A. Bachtold, M. de Jonge, K. Grove-Rasmussen, P. L. McEuen, M. Buitelaar and C. Schönenberger. Phys. Rev. Lett. **87**, 166801 (2001).

[32] The size of the PEDOT grains is consistent with the weak Coulomb Blockade regime at elevated temperatures. For this regime, it is required that the grain–to–grain resistance $R \ll h/2e^2$ (relatively strongly coupled islands) and that $kT \lesssim \hbar/RC = e^2/2C \times R_0/R$ with $R_0 = 2\hbar/e^2$. Note that $R_0/R \gg 1$ via the first requirement. The estimated total capacitance of a 30 nm PEDOT grain is $10\,aF$, resulting in a charging energy $E_c = e^2/2C = 8\,meV$. Hence for moderate values of R_0/R the weak Coulomb Blockade regime is still valid at room temperature.

Chapter 4

Electrical Properties of Conjugated Self-Assembled Monolayers

4.1 Introduction: Transport vs. Structure

Establishing structure-property relations is vital for the envisioned applications of *Molecular Electronics*. The relationship can be derived from scaling of the resistance with molecular length, yielding information on the transport mechanism as well as on the molecular orbitals involved in the transport. Length dependent transport through molecules has been investigated in various test beds such as breakjunctions and scanning probe techniques [1,2]. For alkanes, molecules with sp^3 hybridized carbon atoms, it is well-established that off-resonant tunneling is the dominant charge transport mechanism. The resistance (R) increases exponentially with molecular length (L), $R \propto exp^{\beta L}$ with β ranging from 0.38 – 0.88 A^{-1} [2].

Studies on various π – conjugated molecules have been performed [3–20]. Table 4.1 shows the chemical structures of various compounds that have been investigated and the resulting tunneling decay coefficients. The molecules, with delocalized electrons due to sp^2 hybridized carbon atoms, exhibit a smaller energy gap between the HOMO and LUMO. For π – conjugated molecules longer than ~ 3 nm hopping conduction was observed [12, 19, 20]. For molecules shorter than ~ 3 nm the transport is by tunneling and an exponential dependence of the resistance on molecular length was observed. Values for β range from 0.04 – 0.61 $Å^{-1}$ and are significantly lower than derived for alkanes. Given this large range of β, a further discussion on the relation with molecular geometry is desired. This chapter deals with systematic length-dependent measurements of π – conjugated *para*-phenylene oligomers. Junctions were fabricated using *para*-phenylene dithiols and monothiols with

* This chapter has been previously published as: A. J. Kronemeijer, E. H. Huisman, H. B. Akkerman, A. M. Goossens, I. Katsouras, P. A. van Hal, T. C. T. Geuns, S. J. van der Molen, P. W. M. Blom and D. M. de Leeuw. Appl. Phys. Lett. **97**, 173302 (2010).

increasing number of phenylene rings (abbreviated as P1DT, P2DT, P3DT, P4DT, P1MT, P2MT, P3MT). The chemical structures are presented in Table 4.2. Because large-area molecular junctions combine near 100 % yield with high reproducibility and device stability, reliable values for the decay coefficients can be determined.

Structure	β (Å^{-1})	Reference
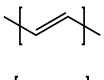	0.22	[9]
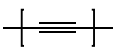	0.06	[17]
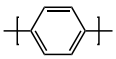	0.35 – 0.61	[3, 5–8, 10]
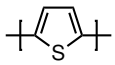	0.1 – 0.41	[4, 13, 18]
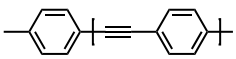	0.2 – 0.21	[15, 19]
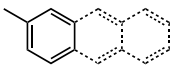	0.45 – 0.51	[11]
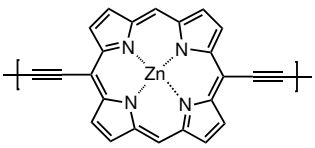	0.04	[14]
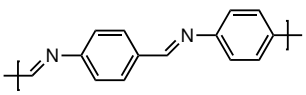	0.3	[12]
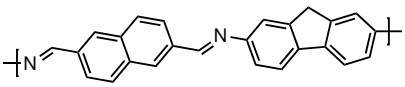	0.25	[20]
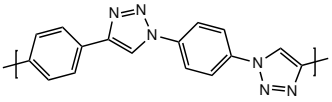	0.22	[21]

Table 4.1: Chemical structures and tunneling decay coefficients β of various π – conjugated oligomers in molecular junctions.

4.2 Monolayer Formation

Synthesis of the molecules was performed via a prescribed procedure [22]. Monolayers of P1DT – P4DT and P1MT – P3MT (Table 4.2) were grown from 300μM SureSeal THF solution in a N_2 glovebox for 36 hours. For P3DT and P4DT the acetyl-protected compounds were used which were deprotected during assembly by the addition of 2 drops of ammonia to 90 ml of SAM solution. SAM formation was checked by variable angle spectroscopic ellipsometry in the spectral range 300 – 500 nm at angles of incidence 65°, 70° and 75°. Monolayer thicknesses were determined by modeling the measured Ψ and Δ at all angles and wavelengths using an isotropic refractive index of 1.55, neglecting absorption of the monolayers.

Table 4.2 presents monolayer thicknesses of P1DT – P4DT and P1MT – P3MT as determined from ellipsometry. These thicknesses are to be compared to the length of the molecules, which fixes the maximal layer thickness of the monolayer assuming alignment with the surface normal. The molecular end-to-end distance is calculated with ACD Labs 11.0 software and 2.3 Å is added for the Au–S bond. For both series, the determined layer thicknesses are consistently below the length of a single molecule. This deviation arises from a non-zero tilt angle of the molecules in the layer. The tilt angle decreases with increasing molecular length which is expected for close-packed monolayers. A smaller tilt is favorable to minimize free energy of long molecules because of increased $\pi - \pi$ interactions between the phenyl rings. The ellipsometry data of Table 4.2 are in agreement with previously published results [22–25] and establish the formation of close-packed monolayers.

Molecule	Structure	Molecular Length (Å)	Monolayer Thickness (Å)	Tilt Angle (Deg.)
P1DT		8.9	5.8	49
P2DT		13.3	9.8	43
P3DT		17.6	14.7	33
P4DT		21.8	20.6	17
P1MT		7.9	2.4	72
P2MT	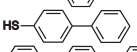	12.3	9.6	38
P3MT	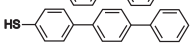	16.6	15.7	17

Table 4.2: Thicknesses of self-assembled monolayers of *para*-phenylenedithiol and *para*-phenylenemonothiol oligomers as determined from ellipsometry measurements.

4.3 Electrical Characteristics: Length Dependence

Large-area molecular junctions of the *para*-phenylene oligomers were characterized as described before. Complete current density versus voltage (J–V) scans were performed on a subset of junctions. Figure 4.1a shows the average J–V characteristics of P4DT. The characteristics are symmetric with respect to bias and are non-linear; the normalized resistance RS is constant at low bias and decreases for higher biases as shown in the inset. Figure 4.1b shows the RS values at 0.5 V of P1MT as a function of device area and die number. For each oligomer, 62 identical dies with 4 molecular junctions of diameter 5, 10, 20 and 50 μm were characterized. The data demonstrate scaling of the resistance with junctions area, as well as the yield and reproducibility of the large-area molecular junctions. Figure 4.1 is representative for all fabricated molecular junctions.

Figure 4.2 presents RS at 0.5 V bias as a function of molecular length for the conjugated series P1DT – P4DT, P1MT – P3MT and for junctions containing only PEDOT:PSS. Every data point is an average of > 240 devices with diameters ranging from 5 – 50 μm. For both series RS increases exponentially with molecular length in agreement with previous reports. The tunneling decay coefficient β equals 0.26 ± 0.04 Å^{-1} for *para*-phenylenedithiols (P1DT – P4DT) and 0.20 ± 0.06 Å^{-1} for *para*-phenylenemonothiols (P1MT – P3MT).

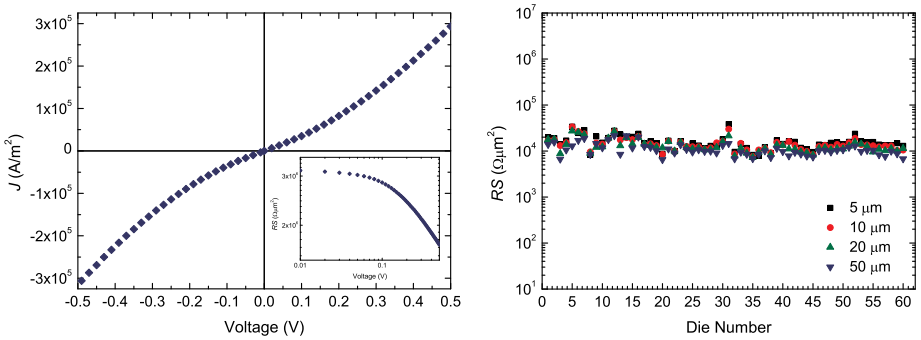

Figure 4.1: (a) Current density versus voltage (J–V) characteristics of P4DT in large-area molecular junctions. Averaged data from devices with diameter 5 – 50 μm. Inset: Replotted RS–V characteristics with a logarithmic voltage axis. (b) Statistics of the measured normalized resistance, RS, of P1MT in large-area molecular junctions. The normalized resistance of 240 molecular junctions is shown from 60 dies each containing 4 junctions with diameter 5, 10, 20 and 50 μm.

By extrapolation of the fit to zero length a contact resistance of 3.5×10^3 $\Omega\mu m^2$ is found. This value coincides with the resistance of junctions without a self-assembled monolayer, *i.e.* with only PEDOT:PSS in the vertical interconnects. A remarkable feature of the dataset is that the RS value for large-area molecular junctions with phenylenes is higher than for similar large-area molecular junctions with alkanes. A possible explanation is a smaller fraction of contacted molecules. However, this effect can probably only explain part of the difference. Understanding of the details of the contact resistance will be discussed in the next chapter. Note that measuring the length dependence of the molecular conductance represents the most consistent technique to investigate and compare different molecular species.

In fact, the decay coefficients for alkanes have been determined using large-area molecular junctions. They were found to be 0.66 $Å^{-1}$ and 0.73 $Å^{-1}$ for alkanedithiols and alkanemonothiols, respectively [26, 27]. Smaller values for β are expected for π – conjugated molecules due to their smaller HOMO – LUMO gap, as indeed observed in the current measurements. In other words, the set of values for β shows consistency within the large-area molecular junction geometry. Nevertheless, the values for β found for the phenylenes are lower than what has been reported in literature using single molecules as well as self-assembled monolayers, *i.e.* $\beta = 0.35 - 0.61$ $Å^{-1}$ [3, 5–8, 10].

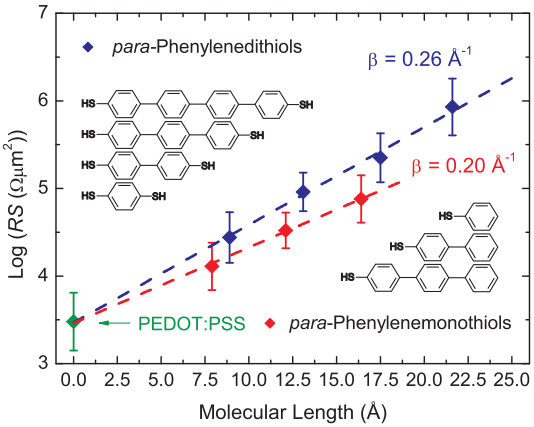

Figure 4.2: Normalized resistance, RS, as a function of molecular length for P1DT – P4DT and P1MT – P3MT in large-area molecular junctions on a semi-logarithmic scale. Every data point is an average of at least 240 junctions of 5 – 50 μm in diameter. Error bars by standard deviation.

To address the relative low value of the decay coefficients, it is interesting to make a comparison with reported theoretical predictions. Calculations using different formalisms resulted in a length dependence with $\beta = 0.17 - 0.51$ Å^{-1} [28–36]. Kondo *et al.* [30] and Liu *et al.* [34] have studied the influence of the ring torsion angle between the phenyl rings and found β coefficients as low as 0.17 Å^{-1} and 0.24 Å^{-1} for planar *para*-phenylene systems, *i.e.* no torsion angle between adjacent phenyl rings. The experimentally determined coefficients in large-area molecular junctions match closely to these values. The small torsion angle can arise from the closed packing of molecules in the SAM. To reduce intermolecular repulsion and maximize $\pi - \pi$ interactions the phenyl rings are forced planar. Increased delocalization over the planar π – conjugated molecule lowers the HOMO – LUMO gap and enhances molecular level broadening, resulting in smaller decay coefficients [10, 37]. The low coefficients are therefore tentatively explained by the influence of the monolayer on the molecular geometry. Single, free molecules are expected to exhibit a non-planar geometry because of freedom of rotation around the chemical bonds. Therefore smaller coefficients can be expected for monolayer junctions compared to single molecule measurements. The described effect of packing is of minor importance for self-assembled monolayers of alkanes.

Additional parallel transport levels as well as enhanced level broadening can further reduce β. Furthermore, possible cooperative effects can account for changes in the electronic structure of the molecules. [38, 39]. Specifically, delocalization in the plane of the monolayer by virtue of the $\pi - \pi$ interactions between molecules can reduce the HOMO – LUMO gap of molecules.

4.4 Conclusions

Large-area molecular junctions have been fabricated containing *para*-phenylene oligomers with an increasing number of phenyl rings. An exponential increasing resistance as function of molecular length is observed, indicating that tunneling through the molecular layer is the dominant transport mechanism in the molecular junctions. The tunneling decay coefficient β is determined for both series, resulting in 0.26 ± 0.04 Å^{-1} and 0.20 ± 0.06 Å^{-1} for dithiols and monothiols respectively. The tunneling decay coefficients are lower than reported for π – conjugated molecules but match closely with theoretical calculations assuming a planar molecular geometry. The low torsion angle can arise from self-assembly of the molecules in a close-packed monolayer. The current results possibly show cooperative effects on the charge transport of single molecules in SAMs.

References

[1] A. Salomon, D. Cahen, S. Lindsay, J. Tomfohr, V. B. Engelkes and C. D. Frisbie. Adv. Mat. **15**, 1881–1890 (2003).

[2] H. B. Akkerman and B. de Boer. J. Phys.: Condens. Matter **20**, 013001 (2008).

[3] R. E. Holmlin, R. Haag, M. L. Chabinyc, R. F. Ismagilov, A. E. Cohen, A. Terfort, M. A. Rampi and G. M. Whitesides. J. Am. Chem. Soc. **123**, 5075–5085 (2001).

[4] H. Sakaguchi, A. Hirai, F. Iwata, A. Sasaki, T. Nagamura, E. Kawata and S. Nakabayashi. Appl. Phys. Lett. **79**, 3708–3710 (2001).

[5] D. J. Wold, R. Haag, M. A. Rampi and C. D. Frisbie. J. Phys. Chem. B **106**, 2813–2816 (2002).

[6] T. Ishida, W. Mizutani, Y. Aya, H. Ogiso, S. Sasaki and H. Tokumoto. J. Phys. Chem. B **106**, 5886–5892 (2002).

[7] S. Wakamatsu, U. Akiba and M. Fujihira. Jpn. J. Appl. Phys. **41**, 4998–5002 (2002).

[8] S. Wakamatsu, S. Fujii, U. Akiba and M. Fujihira. Ultramicroscopy **97**, 19–26 (2003).

[9] J. He, F. Chen, J. Li, O. F. Sankey, Y. Terazono, C. Herrero, D. Gust, T. A. Moore, A. L. Moore and S. M. Lindsay. J. Am. Chem. Soc. **127**, 1384–1385 (2005).

[10] L. Venkataraman, J. E. Klare, C. Nuckolls, M. S. Hybertsen and M. L. Steigerwald. Nature **442**, 904–907 (2006).

[11] B. Kim, J. M. Beebe, Y. Jun, X.-Y. Zhu and C. D. Frisbie. J. Am. Chem. Soc. **128**, 4970–4971 (2006).

[12] S. H. Choi, B. Kim and C. D. Frisbie. Science **320**, 1482–1486 (2008).

[13] R. Yamada, H. Kumazawa, T. Noutoshi, S. Tanaka and H. Tada. Nano Lett. **8**, 1237–1240 (2008).

[14] G. Sedghi, K. Sawada, L. J. Esdaile, M. Hoffmann, H. L. Anderson, D. Bethell, D. Haiss, S. J. Higgins and R. J. Nichols. J. Am. Chem. Soc. **130**, 8582–8583 (2008).

[15] K. Liu, G. Li, X. Wang and F. Wang. J. Phys. Chem. C **112**, 4342–4349 (2008).

[16] L. Lafferentz, F. Ample, H. Yu, S. Hecht, C. Joachim and L. Grill. Science **323**, 1193–1197 (2009).

[17] C. Wang, A. S. Batsanov, M. R. Bryce, S. Martin, R. J. Nichols, S. J. Higgins, V. M. Garcia-Suarez and C. J. Lambert. J. Am. Chem. Soc. **131**, 15647–15654 (2009).

[18] R. Yamada, H. Kumazawa, S. Tanaka and H. Tada. Appl. Phys. Expr. **2**, 025002 (2009).

[19] Q. Lu, K. Liu, H. Zhang, Z. Du, X. Wang and F. Wang. ACS Nano **3**, 3861–3868 (2009).

[20] S. H. Choi, C. Risko, M. C. Ruiz Delgado, B. Kim, J.-L. Bredas and C. D. Frisbie. J. Am. Chem. Soc. **132**, 4358–4368 (2010).

[21] L. Luo and C. D. Frisbie. J. Am. Chem. Soc. **132**, 8854–8855 (2010).

[22] B. de Boer, H. Meng, D. F. Perepichka, J. Zheng, M. M. Frank, Y. J. Chabal and Z. Bao. Langmuir **19**, 4272–4284 (2003).

[23] E. Sabatani, J. Cohen-Boulakia, M. Bruening and I. Rubinstein. Langmuir **9**, 2974–2981 (1993).

[24] Y.-T. Tao, C.-C. Wu, J.-Y Eu and W.-L. Lin. Langmuir **13**, 4018–4023 (1997).

[25] J. M. Tour, L. Jones II, D. L. Pearson, J. J. S. Lamba, T. P Burgin, G. M. Whitesides, D. L. Allara, A. N. Parikh and S. V. Atre. J. Am. Chem. Soc. **117**, 9529–9534 (1995).

[26] H. B. Akkerman, P. W. M. Blom, D. M. de Leeuw and B. de Boer. Nature **441**, 69–72 (2006).

[27] P. A. van Hal, E. C. P. Smits, T. C. T. Geuns, H. B. Akkerman, B. C. de Brito, S. Perissinotto, G. Lanzani, A. J. Kronemeijer, V. Geskin, J. Cornil, P. W. M. Blom, B. de Boer and D. M. de Leeuw. Nature Nanotechnology **3**, 749–754 (2008).

[28] M. Magoga and C. Joachim. Phys. Rev. B **56**, 4722–4729 (1997).

[29] C.-C. Kaun, B. Larade and H. Guo. Phys. Rev. B **67**, 121411 (2003).

[30] M. Kondo, T. Tada and K. Yoshizawa. J. Phys. Chem. A **108**, 9143–9149 (2004).

[31] T. Tada, D. Nozaki, M. Kondo, S. Hamayama and K. Yoshizawa. J. Am. Chem. Soc. **126**, 14182–14189 (2004).

[32] W. Su, J. Jiang and Y. Luo. Chem. Phys. Lett **412**, 406–410 (2005).

[33] R. Cohen, K. Stokbro, J. M. L. Martin and M. A. Ratner. J. Phys. Chem. C **111**, 14893–14902 (2007).

[34] H. Liu, N. Wang, J. Zhao, Y. Guo, X. Yin, F. Y. C. Boey and H. Zhang. Chem. Phys. Chem. **9**, 1416–1424 (2008).

[35] S. Y. Quek, H. J. Choi, S. G. Louie and J. B. Neaton. Nano Lett. **9**, 3949–3963 (2009).

[36] G. Peng, M. Strange, K. S. Thygesen and M. Mavrikakis. J. Phys. Chem. C **113**, 20967–20973 (2009).

[37] A. Mishchenko, D. Vonlanthen, V. Meded, M. Bürkle, C. Li, I. V. Pobelov, A. Bagrets, J. K. Viljas, F. Pauly, F. Evers, M. Mayor and T. Wandlowski. Nano Lett. **10**, 156–163 (2010).

[38] A. Landau, L. Kronik and A. Nitzan. J. Comput. Theor. Nanosci. **5**, 535–544 (2008).

[39] Y. Selzer, L. Cai, M. Cabassi, Y. Yao, J. M. Tour, T. S. Mayer and D. L. Allara. Nano Lett. **5**, 61–65 (2005).

Chapter 5

Transport Mechanism in Large-Area Molecular Junctions

5.1 Introduction: The Influence of Electrical Contacts

Understanding of the charge transport in molecular devices is essential for the progress in the field of *Molecular Electronics*. The two main fundamental problems to resolve are the dependence of conductance on molecular length and the origin of the absolute value of the conductance. Charge transport through single molecules has been determined in break junctions and in scanning probe geometries. For short alkanes and π – conjugated molecules an increase in the molecular length, L, results in an exponential increase in resistance, $R \propto exp^{\beta L}$. The tunneling decay coefficient β depends on the energy gap between the Highest Occupied Molecular Orbital (HOMO) and the Lowest Unoccupied Molecular Orbital (LUMO) [1, 2]. The resistance is temperature-independent, pointing to tunneling as the dominant transport mechanism [3]. For longer π – conjugated molecules (> 3 nm), a transition to temperature-dependent hopping conduction has been reported [4].

The absolute value of the resistance is ideally only determined by the molecular structure. However, in reality, the electrical contacts to the molecule strongly influence the measured resistance [1, 2, 5–7]. Firstly, strongly-coupled chemisorbed contacts yield lower resistances than weakly-coupled physisorbed contacts [2, 8, 9]. Secondly, the metal work function and the composition of the chemical anchoring group change the resistance [9–12]. Finally, differences in the coordination geometry of the chemical anchoring group at the metallic contact affect the resistance by virtue of a different electronic coupling [13, 14]. Scanning probe geometries and break junctions [2, 15] exhibit different coupling strengths to the contacts and therefore lead to dissimilar resistances for identical molecules. Hence an understanding of the contacts is necessary to compare conductance measurements.

* This chapter will be published as: A. J. Kronemeijer, I. Katsouras, E. H. Huisman, P. A. van Hal, T. C. T. Geuns, P. W. M. Blom and D. M. de Leeuw. Small, Accepted (2011).

In large-area molecular junctions, the current density versus voltage (J–V) characteristics show clear molecular features as concluded from the exponential dependence of the junction resistance on molecular length. Tunneling decay coefficients have been determined as 0.26 Å^{-1} and 0.20 Å^{-1} for conjugated *para*-phenylene oligomers and as 0.66 Å^{-1} and 0.73 Å^{-1} for saturated alkanes, for dithiol and monothiol derivatives respectively [16–18].

The origin of the absolute value of the resistance nevertheless remains unclear. The resistance of the junctions is influenced by the composition of the PEDOT:PSS formulation and by the type of photoresist used. The molecular length dependence, however, remains unaffected. The charge transport, therefore, has been described with a multi-barrier tunneling model yielding a factorized resistance:

$$R = \frac{h}{2e^2} \cdot T^{-1} = 12.9k\Omega \cdot T_{Au\text{-}S}^{-1} \cdot T_{Molecule}^{-1} \cdot T_{SAM\text{-}PEDOT}^{-1} \tag{5.1}$$

where T is the overall transmission probability and $T_{Molecule}$, $T_{Au\text{-}S}$, and $T_{SAM\text{-}PEDOT}$ are the transmission probabilities of the molecule, the Au-S bond and the SAM/PEDOT contact, respectively [17]. The molecular transmission is exponentially dependent on molecular length, $T_{Molecule} \propto exp^{-\beta L}$. However, a detailed understanding of the physics of $T_{Au\text{-}S}$ and, especially, of $T_{SAM\text{-}PEDOT}$ is missing. The SAM/PEDOT contact is difficult to study experimentally since the interface is buried inside the junction.

To analyze the electrical transport, Chapter 3 has first focused on large-area junctions without molecules, or so-called PEDOT:PSS only diodes as a reference. The electrical transport was shown to exhibit a power-law dependence on both temperature and voltage, *viz.* $J \propto T^{\alpha}$ at low voltage ($eV \ll kT$) and $J \propto V^{\beta}$ at low temperature ($eV \gg kT$), with $\beta = \alpha + 1$. Furthermore, all J–V curves at different temperatures can be normalized onto a single universal curve by plotting $J/T^{1+\alpha}$ versus eV/kT. The universal curve is described by:

$$J = J_0 \cdot T^{1+\alpha} \cdot sinh\left(\gamma \frac{eV}{kT}\right) \cdot \left|\Gamma\left(1 + \frac{\alpha}{2} + i\gamma \frac{eV}{\pi kT}\right)\right|^2 \tag{5.2}$$

The parameter α is derived from the measurements, J_0 and γ are fit parameters, e is the elementary charge, k is the Boltzmann constant and Γ is the Gamma function. Equation 5.2 has been derived for dissipative tunneling in a biased double-quantum well [19, 20]. The electron tunnels between the two wells while coupled to an external heat bath of harmonic oscillators. The coupling can be due to, for instance, Coulomb interactions or polaronic effects. The origin of the scaling in the PEDOT:PSS only diodes, however, remains elusive.

In this chapter the current – voltage characteristics of molecular junctions based on saturated alkanes and π – conjugated *para*-phenylene oligomers are analyzed in the

same way as PEDOT:PSS. The combined voltage and temperature dependences have been measured. All junctions exhibit universal scaling of the *J(V,T)* characteristics as described by Equation 5.2. The values of the derived parameters α, J_0 and γ are compared with those of the PEDOT:PSS only diodes. The comparison shows that the resistance of the molecular junctions is factorized with the resistance of PEDOT:PSS. The additional factorization is verified by deliberately varying the PEDOT:PSS conductance. Previously unresolved and poor understood issues regarding large-area molecular junctions will be discussed.

5.2 Electrical Characteristics: Universal Scaling

As described in previous chapters, for each series of molecules the resistance increases exponentially with molecular length (Figures 2.8 and 4.2). In order to understand the origin of the absolute value of the resistance, a combined temperature and voltage dependent analysis of the measured electrical transport is performed. Figure 5.1a shows as a representative example the temperature- dependent *J–V* measurements of a benzenedithiol (P1DT) junction from 300 K down to 25 K. The current density is symmetric versus bias voltage and non-linear; the resistance decreases with increasing bias. Furthermore, the current density decreases when lowering the temperature. The current density at 0.1 V, 0.3 V and 0.5 V bias is presented as a function of temperature in Figure 5.1b on a double logarithmic scale. The straight lines obtained indicate a clear power-law dependence on temperature. The slope decreases with increasing bias voltage.

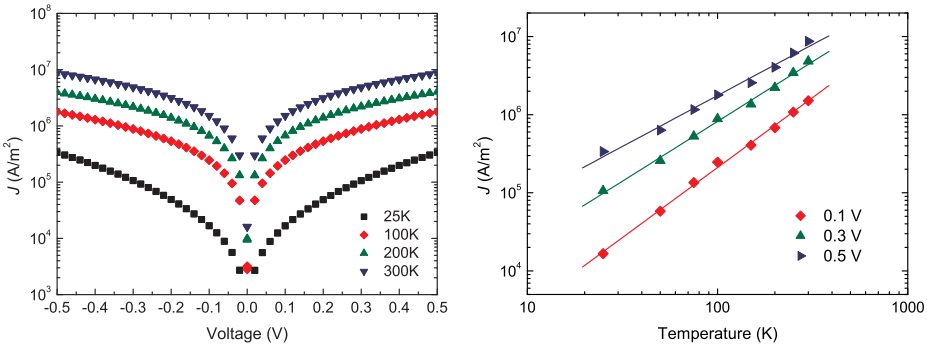

(a) (b)

Figure 5.1: (a) Current density as a function of bias for a benzenedithiol (P1DT) based junction as measured at temperatures between 25 K and 300 K. (b) Current density of the P1DT junction at 0.1 V, 0.3 V and 0.5 V as a function of temperature on a double logarithmic scale.

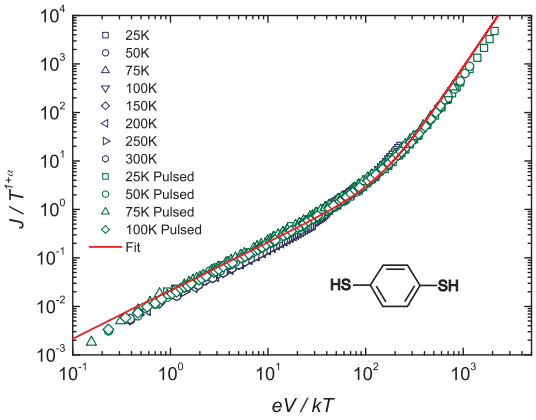

Figure 5.2: Scaled current density of a benzenedithiol (P1DT) junction presented on a double logarithmic scale as a function of eV/kT. Both DC measurements up to 0.5 V bias and pulse measurements up to 5 V are included. The solid curve is calculated with Equation 5.2 using $\alpha = 2.0$, $\gamma = 2.0 \times 10^{-2}$ and $J_0 = 1.1$ (A/m^2).

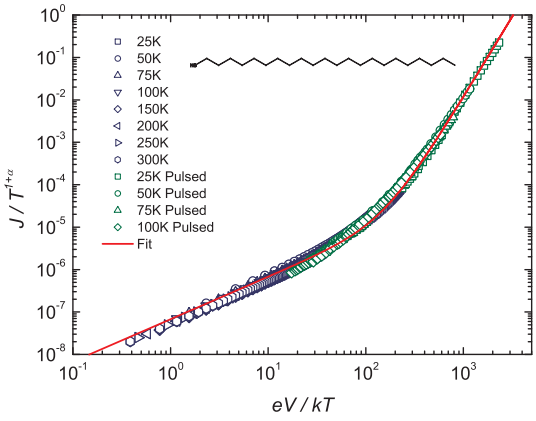

Figure 5.3: Scaled current density of a docosanethiol (C22MT) junction presented on a double logarithmic scale as a function of eV/kT. Both DC measurements up to 0.5 V bias and pulse measurements up to 5 V are included. The solid curve is calculated with Equation 5.2 using $\alpha = 2.8$, $\gamma = 2.3 \times 10^{-2}$ and $J_0 = 1.9 \times 10^{-6}$ (A/m^2).

Extrapolation of the value of the slope to 0 V bias where $kT \gg eV$ yields the value of the parameter α. A value for α of 2.0 is obtained. The experimental data of Figure 5.1 can now be replotted as $J/T^{1+\alpha}$ versus eV/kT. Figure 5.2 shows that a single, smooth curve is obtained, with eV/kT spanning 4 orders of magnitude and the scaled current density spanning 7 orders of magnitude. The solid line is calculated with Equation 5.2. A good agreement is obtained. There are only two fit parameters J_0 and γ. The value of $\gamma = 2.0 \times 10^{-2}$ determines the position of the knee in the curve while $J_0 = 1.1$ (A/m^2) fixes the absolute value. The other π – conjugated molecules (P2DT – P4DT, P1MT – P3MT) show a similar scaling of the normalized current density versus eV/kT.

Similar scaling was observed for the alkanemonothiol (C18MT – C22MT) junctions as well. As a typical example Figure 5.3 shows the scaled current density as function of eV/kT for docosanemonothiol (C22MT). A single, smooth curve is found. The solid line is calculated by Equation 5.2 with $\alpha = 2.8$ and using fit constants $\gamma = 2.3 \times 10^{-2}$ and $J_0 = 1.9 \times 10^{-6}$ (A/m^2). A good agreement is obtained. The observation of temperature dependence is in contrast with previous reports where, from measurements down to 200 K, temperature-independent transport was claimed [16]. Note that a decisive statement can only be made when measurements to lower temperatures are performed. The power-law dependence results in only minor changes in the electrical characteristics down to 200 K. For lower temperatures however, the temperature-dependence progressively increases.

The complete *J(V,T)* characteristics of all large-area molecular junctions can be described using only three parameters, *viz.* α, γ and J_0. Table 5.1 summarizes the values for all molecular junctions and for the corresponding PEDOT:PSS only diode. Table 5.1 shows that the values of γ for the molecular junctions are nearly constant. Furthermore they are identical to that of the PEDOT:PSS only diode from which it is concluded that the value of γ in the molecular junctions is determined by PEDOT:PSS. The normalized resistance for the junctions varies over 4 orders of magnitude while α varies only between 2 and 3. The value of α determines the temperature dependence at low bias. Table 5.1 shows that the values of α and γ are essentially constant and the main difference between the junctions is the value of the prefactor J_0. When α is exactly the same for all junctions, the prefactor should scale linearly with RS at low bias. When compensated for the small differences in α, a one-to-one correspondence is indeed found. When variations in α can be disregarded J_0 depends exponentially on the molecular length. Therefore J_0 contains the molecular contribution.

The similarity between the molecular junctions and the PEDOT:PSS only diode implies that the temperature and voltage dependence originates from PEDOT:PSS. The molecular contribution is only a length-dependent prefactor. Furthermore, the similarity suggests that the prefactor J_0 scales with the PEDOT:PSS resistance. To verify this factorization the

Junction	RS ($\Omega\mu m^2$)	α	γ ($\times 10^{-2}$)	$\pi\gamma^{-1}$	J_0
PEDOT:PSS	3.0×10^3	1.3	2.5	126	2.0×10^2
P1DT	2.8×10^4	2.0	2.0	157	1.1
P2DT	9.1×10^4	2.1	1.9	165	1.3×10^{-1}
P3DT	2.2×10^5	2.3	2.3	137	7.7×10^{-3}
P4DT	8.5×10^5	2.4	3.3	95	1.3×10^{-3}
P1MT	1.3×10^4	2.4	2.4	131	7.0×10^{-2}
P2MT	3.3×10^4	2.2	2.2	143	2.2×10^{-1}
P3MT	7.6×10^4	1.9	2.1	150	5.8×10^{-1}
C18MT	2.7×10^5	1.6	2.5	126	1.8×10^{-1}
C20MT	8.4×10^6	3.0	2.2	143	4.0×10^{-6}
C22MT	1.9×10^7	2.8	2.3	137	1.9×10^{-6}

Table 5.1: Parameters derived from the analysis of the electrical transport in large-area molecular junctions using Equations 5.2. The table shows the normalized resistance (RS), the power-law coefficient α and the fit parameters γ and J_0. Furthermore, the value of $\pi\gamma^{-1}$, related to the number of microscopic tunneling events, is presented.

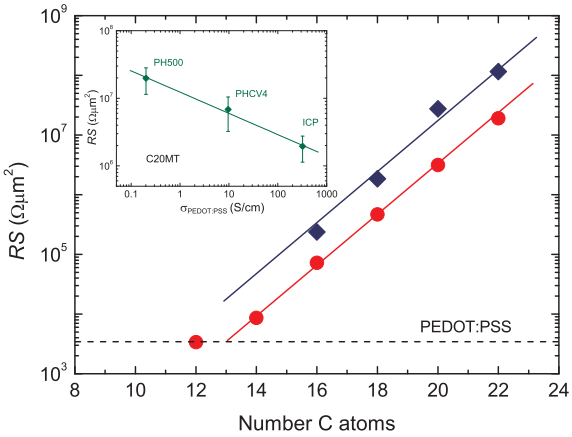

Figure 5.4: Normalized resistance versus molecular length of alkanemonothiol based junctions fabricated with different PEDOT:PSS formulations. Data are reproduced from Ref. [17]. The inset shows the normalized resistance of icosanemonothiol (C20MT) junctions versus the (four-point probe) bulk conductivity of the PEDOT:PSS formulation used to fabricate the junctions.

conductivity of PEDOT:PSS is varied between 0.2 and 300 S/cm. Figure 5.4 presents the normalized resistance of alkanemonothiols as a function of molecular length for junctions containing two PEDOT:PSS formulations. For both series an identical length dependence is obtained. The difference is about an order of magnitude in the absolute value of the resistance. The inset of Figure 5.4 shows the dependence of the resistance of icosanemonothiol (C20MT) junctions on the bulk PEDOT:PSS conductivity. The correlation implies that J_0 depends not only on the molecular length but on the conductivity of PEDOT:PSS as well.

Consequently, in the multi-barrier tunneling model for the large-area junctions the factorization with the PEDOT:PSS resistance has to be explicitly included:

$$R = 12.9k\Omega \cdot T_{Au\text{-}S}^{-1} \cdot exp^{\beta L} \cdot T_{SAM\text{-}PEDOT}^{-1} \cdot T_{PEDOT:PSS}^{-1} \tag{5.3}$$

A relation with the bulk conductivity of PEDOT:PSS has previously been suggested [17]. The current analysis unambiguously demonstrates this factorization.

Previously, the Simmons model was used to interpret the electrical transport in large-area molecular junctions [21]. A good description for the normalized resistance at low bias was obtained. At higher bias, however, the model underestimated the resistance. The discrepancy is due to the fact that the Simmons model is derived for an insulator sandwiched between two metallic electrodes. The electrical transport is by tunneling and depends exponentially on the applied bias. The transport in large-area molecular junctions, however, is factorized with the PEDOT:PSS resistance. This polymer is a highly doped semiconductor and yields a power-law dependence on both bias and temperature.

5.3 Relation to Processing

Factorization of the resistance of molecular junctions with PEDOT:PSS accounts for a number of previously poorly understood processing issues. The resistance of the junctions was shown to depend on the type of PEDOT:PSS used as contact and on the type of photoresist used to define the *vias* [17]. It has now been demonstrated that the influence stemming from PEDOT:PSS is actually the conductivity of the film. The dependence on the type of photoresist might be explained by differences in surface tension, leading to a modified morphology of the PEDOT:PSS film, effectively modifying $T_{SAM\text{-}PEDOT}$.

For large-area junctions the current density is constant, *i.e.* the current scales with device area. For *vias* with a diameter smaller than 5 μm deviations can occur. The wetting of PEDOT:PSS on the SAM is different than on the photoresist. The electrical contact at the perimeter of the *vias* can be different from that in the middle. The non-homogeneity increases with smaller *via* diameters. Hence the larger the *via*, the better is the scaling.

The yield of junctions is in first order approximation "digital", either 100 % or 0 %. A junction is called shorted when the resistance coincides with the PEDOT:PSS only resistance. The resistance of the junction is given by Equation 5.3. The inverse transmission prefactors of the molecule and the contacts can not be smaller than unity. Hence, the resistance can not be smaller than that of a PEDOT:PSS only diode. Any higher value is counted as a functioning junction. The quality of a wafer is therefore not assessed by the yield but by the parameter spread.

The establishment of factorization and the dominant role of PEDOT:PSS on the transport in molecular junctions demonstrates that PEDOT:PSS cannot be regarded as a simple metallic electrode. Any change in the processing can yield different transmission factors and hence, differences in the absolute value of the resistance. However, if the fabrication technology is strictly kept constant a clear signature of the molecular structure is observed. Consequently, large-area molecular junctions can yield valuable information on transport through functional molecules.

5.4 Conclusions

The temperature and voltage dependence of the charge transport through monolayers of alkanethiols and *para*-phenylene oligomers in large-area molecular junctions has been investigated. The current density exhibits a power-law dependence on both temperature and bias, *viz.* $J \propto T^{\alpha}$ at low voltage ($eV \ll kT$) and $J \propto V^{\beta}$ at low temperature ($eV \gg kT$), with $\beta = \alpha + 1$. The value of α is unambiguously determined from the temperature dependence at low bias. For all investigated molecules replotting the scaled current density $J/T^{1+\alpha}$ as a function of eV/kT yields a single smooth curve spanning over orders of magnitude. With only two fit parameters, γ and J_0, the complete *J(V,T)* characteristics can quantitatively be described. The prefactor J_0 depends on the molecular length. The values of α and γ are essentially constant for the molecular junctions and, furthermore, identical to those of the corresponding PEDOT:PSS only diode. This similarity implies that the temperature and voltage dependence originates from PEDOT:PSS. The molecular contribution is only a length-dependent prefactor. Furthermore, by varying the type of PEDOT:PSS it was shown that J_0 depends on the bulk conductivity of PEDOT:PSS as well. Consequently, in a multi-barrier tunneling model the factorization with the PEDOT:PSS resistance has to be explicitly included. The dominant role of the PEDOT:PSS contact explains the absolute value of the junction resistance and its relation to processing conditions.

References

[1] A. Salomon, D. Cahen, S. Lindsay, J. Tomfohr, V. B. Engelkes and C. D. Frisbie. Adv. Mat. **15**, 1881–1890 (2003).

[2] H. B. Akkerman and B. de Boer. J. Phys. Condens. Matter **20**, 013001 (2008).

[3] W. Wang, T. Lee and M. A. Reed. Phys. Rev. B **68**, 035416 (2003).

[4] S. H. Choi, B. Kim and C. D. Frisbie. Science **320**, 1482–1486 (2008).

[5] K. W. Hipps. Science **294**, 536–537 (2001).

[6] J. G. Kushmerick. Mater. Today **8**(7), 26–30 (2005).

[7] D. Vuillaume and S. Lenfant. Microelectron. Eng. **70**, 539–550 (2003).

[8] X. D. Cui, A. Primak, X. Zarate, J. Tomfohr, O. F. Sankey, A. L. Moore, T. A. Moore, D. A. Gust, G. Harris and S. M. Lindsay. Science **294**, 571–574 (2001).

[9] V. B. Engelkes, J. M. Beebe and C. D. Frisbie. J. Am. Chem. Soc. **126**, 14287–14296 (2004).

[10] F. Chen, X. Li, J. Hihath, Z. Huang and N. Tao. J. Am. Chem. Soc. **128**, 15874–15881 (2006).

[11] J. M. Beebe, V. B. Engelkes, L. L. Miller and C. D. Frisbie. J. Am. Chem. Soc. **124**, 11268–11269 (2002).

[12] Y. S. Park, A. C. Whalley, M. Kamenetska, M. L. Steigerwald, M. S. Hybertsen, C. Nuckolls and L. Venkataraman. J. Am. Chem. Soc. **129**, 15768–15769 (2007).

[13] X. Li, J. He, J. Hihath, B. Xu, S. M. Lindsay and N. Tao. J. Am. Chem. Soc. **128**, 2135–2141 (2006).

[14] C. Li, I. Pobelov, T. Wandlowski, A. Bagrets, A. Arnold and F. Evers. J. Am. Chem. Soc. **130**, 318–326 (2008).

[15] B. A. Mantooth and P. S. Weiss. Proc. IEEE **91**, 1785–1802 (2003).

[16] H. B. Akkerman, P. W. M. Blom, D. M. de Leeuw and B. de Boer. Nature **441**, 69–72 (2006).

[17] P. A. van Hal, E. C. P. Smits, T. C. T. Geuns, H. B. Akkerman, B. C. de Brito, S. Perissinotto, G. Lanzani, A. J. Kronemeijer, V. Geskin, J. Cornil, P. W. M. Blom, B. de Boer and D. M. de Leeuw. Nature Nanotechnology **3**, 749–754 (2008).

[18] A. J. Kronemeijer, E. H. Huisman, H. B. Akkerman, A. M. Goossens, I. Katsouras, P. A. van Hal, T. C. T. Geuns, S. J. van der Molen, P. W. M. Blom and D. M. de Leeuw. Appl. Phys. Lett. **97**, 173302 (2010).

[19] H. Grabert and U. Weiss. Phys. Rev. Lett. **54**, 1605–1608 (1985).

[20] M. P. A. Fisher and A. T. Dorsey. Phys. Rev. Lett. **54**, 1609–1612 (1985).

[21] H. B. Akkerman, R. C. G. Naber, B. Jongbloed, P. A. van Hal, P. W. M. Blom, D. M. de Leeuw and B. de Boer. Proc. Natl. Acad. Sci. USA **104**, 11161–11166 (2007).

Chapter 6

Reversible Conductance Switching in Molecular Devices

6.1 Introduction: Functionality

In the last decades, the use of organic molecules as active elements in electronic devices has attracted considerable attention following the theoretical studies of Aviram and Ratner [1], predicting that a single molecule can operate as a diode. Electronic transport through molecules has been investigated experimentally in many different device geometries including scanning probes, break-junctions and metallic crossbars [2, 3]. These studies showed that producing good electrical contacts to molecules is very challenging, but of great significance to measure the molecular properties, the interface at the molecular level, and to achieve functional active devices [4–6]. To realize a molecular electronic circuit, crossbar junctions are required with functional molecules sandwiched between two electrodes. To introduce functionalities in the molecular junctions, molecules should be designed to deliver a specific property to the electronic device like rectification [1, 7] or switching [8, 9]. However, the difficulty of making proper electric contacts to molecules has strongly hindered the successful realization of devices with the incorporated functions solely attributed to addressable organic molecules [10]. Diode-like characteristics can often be explained by instable or unreliable contacts [11]. Metal filament growth through molecular monolayers is also common [12] and is, instead of molecular functionalities, an explanation for switching behavior observed in molecular junctions [13].

A fundamental problem with electrical molecular switches is that the conductance of the ON and OFF state is not a priori known. As a result, extrinsic effects such as filament formation can easily mask molecular switching properties. In this chapter a reliable and reproducible approach is presented that measures the intrinsic conductance switching of a

* Part of this chapter has been previously published as: A. J. Kronemeijer, H. B. Akkerman, T. Kudernac, B. J. van Wees, B. L. Feringa, P. W. M. Blom and B. de Boer. Adv. Mat. **20**, 1467 – 1473 (2008).

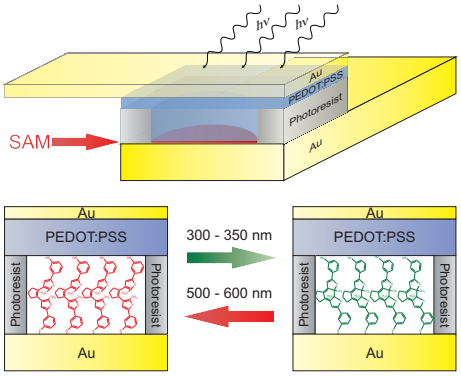

Figure 6.1: Schematic cross-section of the device layout of a large-area molecular junction in which the diarylethene is sandwiched between Au and PEDOT:PSS/Au. Using UV (312 nm) illumination the open, non-conjugated isomer (in red) can be converted to the closed, conjugated isomer (in green). Visible irradiation of 532 nm reverses the photoisomerization process.

functional molecular monolayer based on photochromic diarylethenes shown in Figure 6.1 and the inset of Figure 6.2. These molecular switches have two distinct isomers of which the ring-closed form is conjugated and the ring-open form non-conjugated. It is expected that both isomers show different conductances since the conjugation is changed [14, 15]. Theoretical studies have shown a change in conductance of 1–2 orders of magnitude, being subject to the specific chemical substitution pattern around the basic diarylethene photochromic core [16, 17].

To realize a solid-state molecular switch, the large-area molecular junction geometry is applied for producing stable and reliable molecular junctions. The diarylethene monolayer is self-assembled in the individual interconnects. Then, upon irradiation with a specific wavelength range, the conductance of these devices can be optically switched. The major advantage of this approach is that the two distinct isomers of the diarylethene can be individually synthesized and, therefore, separately assembled in a device. Consequently, the ON and OFF state can be independently measured in the as-assembled devices, without any involvement of a switching event. Optically induced switching of the conductance of the devices in between these two states then provides a direct proof of the molecular origin of the switching events.

In solution [18], mesoscopic [19], and crystalline phases [20], these compounds demonstrate photochromic behavior and the conjugated and non-conjugated states of the diarylethene can be interconverted, in a fully reversible manner, by exposure to different specific wavelength ranges. In the dark, these switches show low fatigue and high thermal

stability [18]. Ring closure, the transformation to the conjugated state, is achieved upon irradiation of 300 – 350 nm and ring opening to the non-conjugated state is realized with 500 – 600 nm irradiation. The particular molecular switch used in this chapter was designed with the thiolate group at the *meta*-position of the phenyl ring [21] to avoid direct conjugation of the diarylethene switching unit with the contacts [22].

In a molecular junction, when tunneling is the dominant conduction mechanism, the tunneling current through the closed state is expected to be higher than through the open state. Due to the lowering of the HOMO – LUMO gap when the π–conjugation is extended, the tunnel barrier for electrons to flow is effectively lowered. Indeed, this is supported by break-junction experiments [14, 23], STM measurements [15], experiments with carbon nanotube electrodes [24] and data from Au nanoparticle networks [25, 26]. However, reversible switching behavior solely based on molecular characteristics still has to be demonstrated in solid-state electronic devices in which the ON and OFF states can be independently assembled and characterized.

Large-area molecular junctions containing diarylethenes were processed according to the previously reported method. The PHCV4 formulation of PEDOT:PSS was used. For the monolayer formation the wafer was immersed in a 1 mM ethanol solution of molecular switches for at least 36 hours. The thioacetyl end-group spontaneously dissociates to form a gold surface-bound thiolate during the self-assembly process [27]. Instead of a thick electrode a semi-transparent 20 nm top gold contact was thermally evaporated on the junctions to ensure transmission of light onto the molecular monolayer.

6.2 Monolayer Formation

The formation of the SAM on identically prepared Au samples was investigated by X-ray Photoelectron Spectroscopy (XPS). Angular dependent measurements were performed with an angle of 10°, 45° and 90° between the sample surface and the detector. These angles give rise to an information depth of approximately 2, 7 and 10 nm, respectively. The elements present at the surface were first identified while the atomic concentrations of these elements were determined from narrow-scan measurements. For all samples, measurements were obtained in duplicate. The raw data of the measurements at 45° is listed in Table 6.1, while the data for the different angles are similar and in good agreement with each other, indicating that a homogeneous layer is present on the Au surface. As reference, a cleaned gold substrate was used which was prepared in the same vapor deposition batch as the substrates used for the monolayers of both the open and the closed isomer.

To extract more useful parameters, the results from Table 6.1 have been analyzed by means of a model calculation [28], assuming the following three layers: the Au substrate,

Sample	Au 4f	C 1s					O 1s	S 2p		
		C_xH_y	C-O	C=O	O-C=O	Shake		SO_x	C-S^H	Au-S
Reference	71.4	20.3	3.5	1.1	1.5	-	2.2	-	-	-
Reference	71.6	20.8	2.2	1.4	1.7	-	2.3	-	-	-
Closed-1	37.5	46.0	4.6	2.1	0.7	-	2.5	0.3	4.2	2.0
Closed-2	37.8	46.4	4.2	1.4	1.8	-	2.1	0.2	4.2	2.0
Open-1	32.1	48.2	5.9	1.2	1.3	-	3.4	0.3	5.5	2.1
Open-2	32.3	48.0	6.0	1.6	0.9	-	3.2	0.3	5.4	2.3

Table 6.1: Raw atomic concentrations (at%) on the surface of the XPS samples measured directly from peak areas at 45° angle.

Sample	d (nm)	N_S (cm^{-2})	C 1s		O 1s	S 2p		
			C_xH_y	CO_x		SO_x	C-S^H	Au-S
Reference	0.6	-	71.6	21.3	6.7	-	-	-
Reference	0.6	-	73.7	19.0	6.9	-	-	-
Closed-1	2.0	4.4×10^{14}	72.3	11.7	3.4	0.6	7.0	5.0
Closed-2	2.0	4.3×10^{14}	73.2	11.7	2.9	0.3	7.0	5.0
Open-1	2.4	5.4×10^{14}	69.4	12.2	4.4	0.4	8.3	5.2
Open-2	2.4	5.7×10^{14}	69.3	12.3	4.2	0.4	8.1	5.6

Table 6.2: Results of the standard model calculations: thickness (d), coverage of sulfur (N_S) and composition of the organic top layer.

the Au-thiol bonds and all other components of the organic layer. The results are shown in Table 6.2. The theoretically calculated length of the molecules, and thus the layer thicknesses for a 0° tilt angle along the surface normal, are 2.0 and 1.9 nm for the closed and open switches, respectively. The terminal S–H bond length was substracted from the end-to-end distance and the Au–S distance of 2.3 Å was added. The correspondence between the calculated and measured layer thickness of the SAMs indicate, together with the similarity of data obtained for the various angles, that a homogeneous monolayer of molecular switches is present on the Au surface.

For further analysis of the electronic data obtained on these molecular switches, as discussed later in this chapter, it is interesting to emphasize the fact that the planar closed switch has a lower grafting density than the open switch. Furthermore, the calculated

layer thickness for the closed switch (2.0 nm) is higher than calculated for the open switch (1.9 nm), whereas the measured layer thicknesses show the opposite effect namely that the closed switch (2.0 nm) forms a thinner layer than the open switch (2.4 nm). This effect can be explained by a difference in tilt angle in correlation with the packing density, similar to alkanethiols on Au and Ag [29]. The grafting of the sulfur head group on the underlying Au surface (with a Au-Au spacing of 2.88 Å) and the mutual interactions (π–π stacking, van der Waals interaction) of the molecular switches determine the energetically most favorable packing density and tilt angle. Since the grafting density of the closed switch is lower according to the XPS measurements (most likely the closed, conjugated isomer will form a herringbone-like packing [30]), the molecules have to increase their off-normal tilt angle to optimize the interactions with neighboring molecules and to minimize their free energy. In this manner the molecules will adopt conformations that allow high degrees of interactions with their neighboring molecules and, therefore, a closer packing of the molecular backbone. Consequently, the effective layer thickness is smaller than anticipated from the calculated end-to-end distance. Vice versa, the bulky and non-coplanar open isomer occupies more conformational space (free volume) and interacts with its neighboring molecules even without any tilting. The free energy is minimized by using its internal rotational freedom to optimize the interactions with the neighboring open isomers.

6.3 Device Characteristics

After the verification of the SAM formation, as a first step in the electronic characterization of the molecular switches, separate current density versus voltage (J–V) characteristics were measured of large-area molecular junctions in which molecules exclusively in the open or closed states are self-assembled between the electrodes. The as-assembled open (OFF) and closed (ON) switches determine the lower and higher limits, respectively, and thus the maximum possible current density ratio between the OFF and ON state. Figure 6.2a shows the obtained J–V characteristics. During all J–V measurements up and down sweeps were performed. No hysteresis was observed for any of the devices. Average current densities are calculated from at least 35 devices for both isomers with device diameters ranging from 10 – 100 μm.

The values obtained for the current density through the open, insulating state are in good agreement with measurements on alkanedithiols with comparable layer thickness (20 Å, HS-$C_{14}H_{28}$-SH) in the junctions. At low bias the current increases linearly with applied voltage while at higher bias an superlinear increase is observed. The conductance through the closed, more conducting state of the switch is shown to be 16 times higher at 0.75 V bias. These reference measurements demonstrate that the resistance of this

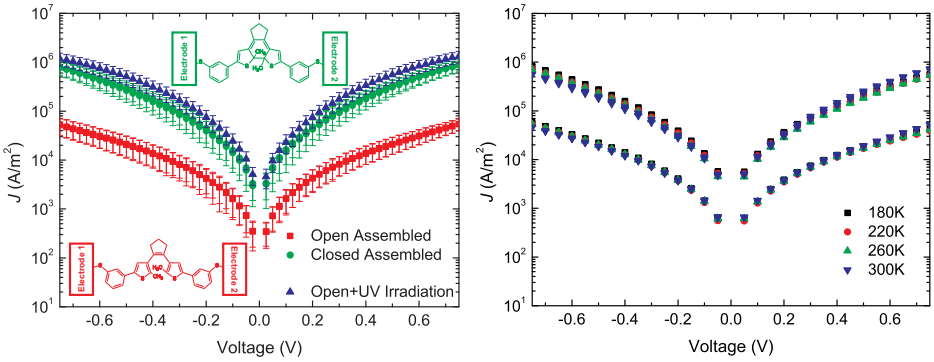

Figure 6.2: (a) *J*–*V* characteristics of the closed (green) and open (red) isomers as self-assembled in the molecular junctions, and the *J*–*V* characteristics of the junctions with the open isomer self-assembled and subsequently photoisomerized to the closed isomer with UV irradiation (blue). Averaged data (at least 35 devices) from devices with diameters of 10 – 100 μm. Error bars by standard deviation. (b) Temperature dependence of the *J*–*V* characteristics of the open (lower curves) and closed isomeric state (upper curves). Averaged data for each temperature of at least 35 devices with diameters of 10 – 100 μm.

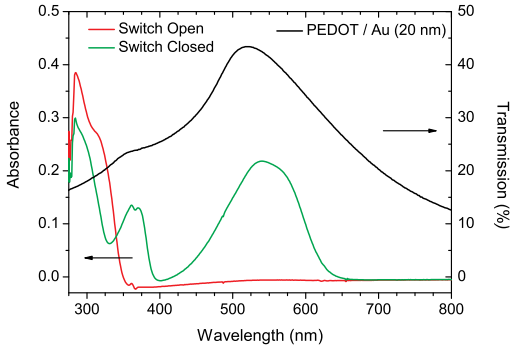

Figure 6.3: Absorbance of the open (red) and closed (green) isomers obtained in toluene compared with the transmission (black) of the top electrode stack PEDOT:PSS (90 nm) / Au (20 nm).

specific switch can be varied more than an order of magnitude by changing the isomeric (or conjugated) state of the molecules. Furthermore, Figure 6.2b shows that the current densities through both open and closed switches shows no significant temperature dependence in the range 180 – 300 K. Temperature dependence of large-area molecular junctions has been extensively discussed in Chapter 5 of this thesis. For the present junctions the temperature-independent transport in this temperature range infers that minor heating of the devices while irradiating will not influence the conductance of the molecular devices and eliminates the assignment of current changes to small temperature fluctuations.

The absorption spectra in Figure 6.3 of the open and closed switch demonstrate the possibility to utilize distinctly different wavelengths for switching from the open to the closed state (300 – 350 nm) and vice versa (500 – 600 nm). The ability to optically access the molecules in the junctions imposes restraints on the thickness of the top contact. Figure 6.3 shows that the 20 nm thickness of the gold top electrode ensures sufficient optical transmission through the layers of PEDOT:PSS (90 nm) and Au (20 nm), namely 19 % and 43 % in the 300 – 350 nm and 500 – 600 nm regimes, respectively. This ensures proper illumination of the molecules inside the devices.

Wafers with the open isomer of the switch self-assembled in the devices were illuminated for 15 min with 312 nm UV irradiation, to convert the molecular switches in the devices to the closed isomer. As shown in Figure 6.2a, the J–V characteristics of the converted open state isomer after UV irradiation show an increase of the conductance through the monolayer as expected from the as-assembled devices with closed isomers. Following upon the UV irradiation and consecutive measurements, these devices were illuminated with 532 nm irradiation (visible light). The quantum efficiency for ring opening of these switches is known to be appreciably lower than for ring closure [18]. Therefore, an illumination time of 45 minutes was chosen for visible light to achieve ring opening of the switches in the SAM. The observed J–V characteristics showed a significant decrease (by a factor 3) of the conductance upon visible light irradiation, but the conductance of the as-assembled open state isomer was not fully recovered. This might be a consequence of the ring opening kinetics, molecular conformation, packing of the self-assembled monolayer or perhaps the inherent energetic structure of the electrode – molecule system is such that not all molecular switches can be switched back after ring closure.

Conversely, no change in conductance upon visible illumination is observed when the starting point of the experiments is the as-assembled closed isomer. An explanation can possibly be found in a partial conversion of the monolayers. When partially converting the monolayer from the open state to the closed state, the conductance will quickly be dominated by the smaller fraction of closed isomer. In the conversion from closed to open a larger fraction of the monolayer should be switched before the open isomers start to dominate the

conductance. However, since the devices with the UV irradiated open assembled isomers so uniquely reproduce the *J*–*V* characteristics of the closed assembled devices, it is more probable that the observed phenomenon stems from a different packing of the molecules in the SAM [31]. In the monolayer, this packing is imposed by the underlying gold surface, in contrast to packing in crystals. While the closed state isomer is conjugated, less flexible and more planar, the open state is non-conjugated and preferably both halves adopt a non-planar (strongly twisted out of plane) conformation. The planarity and rigidity of the closed state results in a denser packing of the molecular backbone in the monolayer on the gold surface, even though the grafting density is lower, as explained before in the discussion of the XPS data. Consequently, no sufficient conformational freedom is present for the out of plane bending during the conrotatory ring-opening process due to steric hindrance of surrounding molecules. As the open state isomer requires more space, a less dense monolayer is formed, which allows for conformational and rotational freedom (more free volume), and as a consequence a reversible switching process is possible. This reversible process is in accordance with reversible optical switching of diarylethenes in solution and a variety of condensed phases [15, 18–20, 22, 25, 26].

To confirm that the observed changes in current density through the junctions are intrinsically due to the molecular switching events in the devices, illumination of reference devices without switchable moieties is mandatory. First, devices were processed omitting the self-assembly of switches, resulting in Au/PEDOT:PSS/Au junctions in the vertical interconnects. As expected for these devices, the current densities are orders of magnitude higher. Figure 6.4a shows that UV irradiation and subsequent measurements show no change of the electrical characteristics. This implies that nor the PEDOT:PSS layer, nor the interface PEDOT:PSS/Au is responsible for any increase in conductance upon illumination. To eliminate the possibility of switching caused by the bottom S–Au bond, the top thiol/PEDOT:PSS interface or some other characteristic general to molecules, devices with 1,12-dodecanedithiol (HS-$C_{12}H_{24}$-SH) were processed and irradiated. Again, as shown in Figure 6.4b, no change of conductance is observed. As a final check, to rule out that a general conjugated system in a monolayer connected to Au electrodes can cause switching behavior, devices were fabricated with *para*-quaterphenylenedithiol (P4DT, HS-$(C_6H_4)_4$-SH). As Figure 6.4c shows, after UV illumination these devices show a slightly decreased conductance contrary to the increased conductance of the molecular switches. The absorption of P4DT is shown in Figure 6.4d. The P4DT molecule was chosen because it absorbs the 312 nm UV wavelength similar to the molecular switch. The complete set of reference measurements – no molecules, saturated molecules and conjugated molecules – demonstrates that the isomerization of the diarylethenes is the origin for the observed conductance switching.

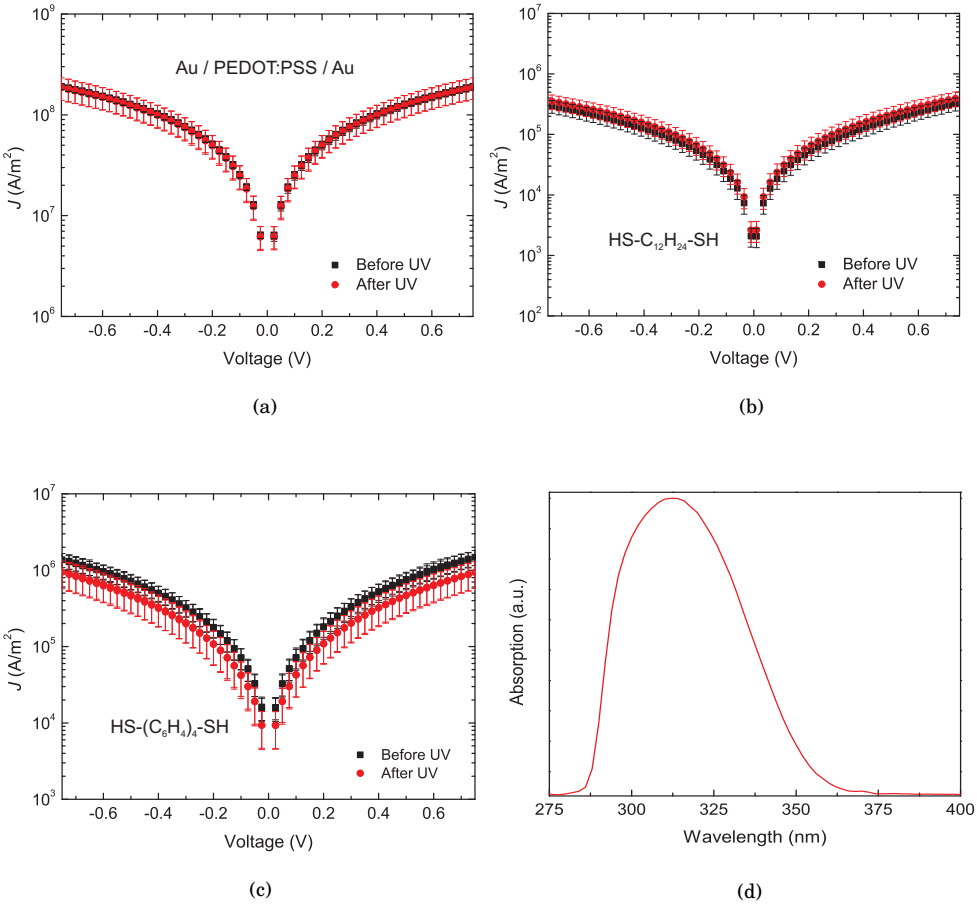

Figure 6.4: (a) Ohmic Au/PEDOT:PSS/Au short-circuited devices show no change of the *J*–*V* characteristics upon UV irradiation. (b) No switching is observed in the *J*–*V* characteristics of devices with a SAM of 1,12-dodecanedithiol in the large-area molecular junctions. (c) Illumination of *para*-quaterphenylenedithiol results in no switching. (d) Absorption spectrum of quaterphenylenedithiol, demonstrating that the molecules absorb at the UV wavelength used (312 nm).

As for the visible irradiation, large-area molecular junctions with alkanedithiols and thin top contact can be stored for at least 75 days in ambient (light) conditions, identical to the standard alkanedithiol junctions with thicker top contacts [32]. The junctions with thin top contacts have been measured in ambient light conditions, implying that visible light has no effect on the conduction in these junctions. Clearly, the decrease of the current upon visible irradiation, as observed through devices with incorporated switches, is of true molecular nature and due to the presence of the molecular monolayer of switches.

To further elucidate the bidirectional switching, multiple in situ illumination cycles were performed as shown in Figure 6.5. The modulation of the current density through the devices by multiple irradiation sequences is a compelling demonstration of molecular switching. Figure 6.5a demonstrates that when the assembled monolayer of the open isomer is irradiated with 312 nm for 4 minutes a rapid increase of the current density by a factor 7 is observed, due to the photoisomerization to the closed conjugated state. After 4 minutes a current density of 1.5×10^5 A m^{-2} is achieved. Then the light source is removed for 60 seconds and subsequently the switches in the molecular junction are irradiated with 532 nm for 4 minutes. Immediately, the current density through the monolayer of switches decreases, since the photoisomerization reverses the closed state to the open isomeric state. A current density of 4×10^4 A m^{-2} is achieved, which is only a factor of 2 higher than the value obtained for the as-assembled open switch. The observed profiles suggest that the majority of the molecules is switched relatively easily and fast, while upon prolonged exposure the current more slowly changes. Prolonged illumination with both 312 nm and 532 nm will enhance the ON/OFF ratio, since saturation of the current density has not been reached after 4 minutes, but will approach its maximum asymptotically. As Figure 6.5c shows, in total 25 irradiation cycles were performed, the alternation of 13 UV cycles of 2 minutes and 12 visible illumination cycles for 4 minutes, while measuring the current densities at 0.5 V to demonstrate the stability and reversibility of the isomeric switches under ambient conditions. A distinct ON/OFF ratio is maintained throughout the 25 cycles.

It is noted that complete switching to the OFF state is difficult to achieve as mentioned above. Furthermore, these measurements establish that the conductance of the high conducting state is slowly decreasing after switching off the UV light, in contrast to devices with the assembled closed state. This arises from the presence of a constant voltage bias stress of 0.5 V for almost one hour over the samples during these in situ measurements. It has been previously shown that under electrochemically-controlled conditions an applied voltage induces switching [33]. Charging of the molecules during bias stress is a possibility although tunneling is the main transport mechanism. Charged species of the closed isomer, depending on the specific substitution of the photochromic core, can destabilize this isomer, resulting in a complicated ring opening process [33]. Without any or only shortly applied

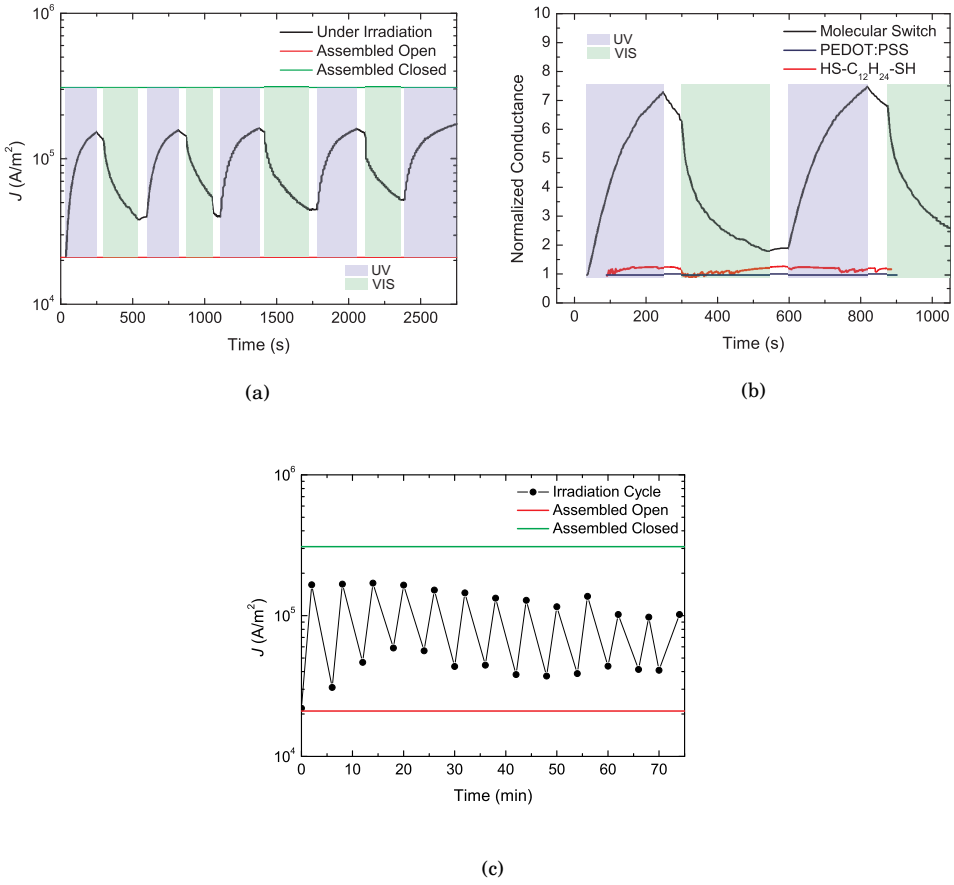

Figure 6.5: In situ optical switching of a monolayer of diarylethenes at 0.5 V bias results in a direct current modulation of the molecular junctions. (a) Comparison of the current densities of the as-assembled devices based on the open (red) and closed (green) isomer with in situ irradiated molecular junctions (black). (b) Comparison of the normalized conductance data from the molecular diarylethene switches with in situ measurements on junctions with non-switchable 1,12-dodecanedithiol and with PEDOT:PSS only. Identical measurements on quaterphenylenedithiol resulted in short-circuit of the junctions. (c) Current density (at 0.5 V) versus time for the in situ optical switching of a monolayer of diarylethenes. Alternation of UV (2 minutes) and visible (4 minutes) illumination results in a direct current modulation through the molecular junctions.

bias during the illumination, instead of prolonged stress, a complete switching from the OFF to the ON state is observed (Figure 6.2a).

As a further reference experiment, Figure 6.5b shows in situ measurements on devices without any monolayer (Au/PEDOT:PSS/Au in blue) and with 1,12-dodecanedithiol (red) as the SAM. No substantial effect is observed upon irradiation of these devices, which enforces the previously stated conclusion that the observed switching is of molecular origin and that any form of photoconduction in these devices is absent. It should be noted that in situ illumination of the conjugated *para*-phenylenedithiol, as performed before without sample bias, resulted in short-circuit of the devices.

To summarize, junctions with a self-assembled monolayer of photochromic diarylethene-based molecular switches demonstrate clearly an ON/OFF ratio of 16 at 0.75 V bias upon irradiation. No switching is observed for devices without a molecular monolayer, with a monolayer of alkanedithiol molecules and with a monolayer of *para*-phenylenedithiol molecules. Therefore, the bidirectional switching and the accompanying modulation of the conductance are truly a manifestation of the structural and electronic changes of the molecular monolayer of photochromic switches inside the junctions. The macroscopic alteration of the current in these solid-state molecular electronic devices originates from photoisomerization of the molecular monolayer of diarylethenes.

6.4 Dynamics of Switching

As observed in Figure 6.5, the switching time of the molecular devices is still very long. To convert the photochromic monolayer from one state completely into the other, illumination times of minutes are needed. To make a comparison with literature, it is necessary to analyze the time dependence such that more useful parameters can be extracted. A characteristic of the molecules that can readily be compared with other experiments is the internal quantum yield of ring opening and ring closure.

To determine this quantum yield, a simple model is used to calculate the rate of conversion from one state to the other. The rate constants for the ring-closure and ring-opening reactions are k_{UV} and k_{VIS}, respectively. A first-order differential equation is solved to calculate the rate at which the molecules are interconverted. It is assumed that the monolayer acts as a total effective medium in time and therefore that the time dependence of the current density through the monolayer follows the kinetics of the conversion of molecules in the monolayer. This assumption is substantiated by the observation that ring-closure and ring-opening in the molecular junctions have similar time-dependent characteristics. Other models for conduction through monolayers, *e.g.* assuming a parallel resistor model, would show a different overall envelope for UV and visible illumination.

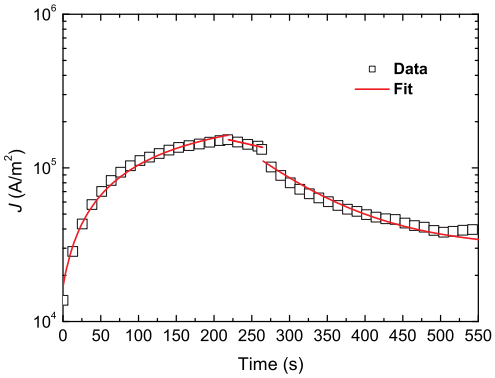

Figure 6.6: Fits of Equations 6.1 – 6.3 to the time dependent current density characteristics of diarylethenes in large-area molecular junctions under UV and visible illumination.

A rate constant k_I is introduced to account for the decrease of the conductance during the interval between UV and visible irradiation. Both this decay process and the ring-opening reaction are assumed to occur simultaneously during the visible illumination. The resulting equations describing the time dependence of the current density under both types of illumination and during the voltage interval are:

$$J_{UV} = J_{Closed} + (J_{Open} - J_{Closed}) \cdot e^{-k_{UV} \cdot t} \tag{6.1}$$

$$J_{Interval} = J_{Open} + (J_{Closed} - J_{Open}) \cdot e^{-k_I \cdot t} \tag{6.2}$$

$$J_{VIS} = J_{Open} + (J_{Closed} - J_{Open}) \cdot e^{-k_I \cdot t} \cdot e^{-k_{VIS} \cdot t} \tag{6.3}$$

Equations 6.1 – 6.3 can be fitted to the experimental data to extract the values of the rate constants. Figure 6.6 shows the fits for the first illumination cycle of Figure 6.5a. The crude model outlined above adequately describes the time-dependent current density of the molecular junctions. The data of the other illumination cycles result in similar fits and values for the rate constants. In order to convert the rate constants into a quantum yield of the underlying process, the incident photon flux per molecule is determined. The intensity of illumination on the junctions is measured by a power meter and converted in a photon flux per molecule, using the approximation that the irradiation is monochromatic. From the flux and the rate constant the quantum yield for the processes can be calculated. Table 6.3 summarizes the obtained results.

Process	Intensity (mW / cm^{-2})	Assumed Wavelength (nm)	Photon Flux (Photons / $cm^2 \cdot$ s)	Transmission Top Contact (%)	Photon Flux per Molecule (Photons / s)	Rate Constants k_{UV} and k_{VIS} (s^{-1})	Quantum Efficiency
UV	~ 4.5	312	7.1×10^{15}	19	3	4×10^{-3}	$\sim 2\times10^{-3}$
VIS	~ 58	532	1.6×10^{17}	43	150	2×10^{-2}	$\sim 1\times10^{-4}$

Table 6.3: Results of the simple model calculations determining the quantum yield of ring-closure and ring-opening of the diarylethenes in large-area molecular junctions.

To determine the origin of the switching dynamics in the large-area molecular junctions the quantum yields are compared to quantum yields of similar diarylethenes attached to gold nanoparticles, measured in solution. The quantum yield of ring-closure has been directly measured while the value for ring-opening can be estimated from the average ratio of both processes for diarylethene molecular switches [18, 22]. The quantum yield for ring-closure in the nanoparticle geometry is 7×10^{-2}, which yields a value for ring-opening of $\sim 2\times10^{-3}$. Table 6.3 shows that the determined quantum yields in the molecular junctions are about an order of magnitude smaller. Quenching of the photoexcited state has been observed when diarylethene molecular switches are connected to gold. The second PEDOT:PSS electrode possible results in even more quenching. Furthermore the packing in a monolayer can result in steric hindrance between molecules inhibiting the switching process.

Although the values for the quantum yields are lower, only part of the slow dynamics inside the molecular junctions can be accounted for by quenching. Other factors therefore also should influence the switching dynamics. Probably the most important is the amount of photons that can be absorbed by the molecules. The monolayer itself is very thin. Furthermore, the absorption cross-section of the molecules is non-ideal. The cross-section is largest perpendicular to the π – conjugated system. This molecular plane, however, is positioned perpendicular to the surface as determined from the XPS thickness measurements.

6.5 Integration in Strings

For any use in applications, mass production of electronic components based on molecules and the integration with standard processing techniques is required. Most of the techniques used for the measurements on molecules do not comply with these demands, since the number of fabricated devices is too low or the reproducibility of the fabrication process limits the amount of properly working devices. Moderate progress has been made in

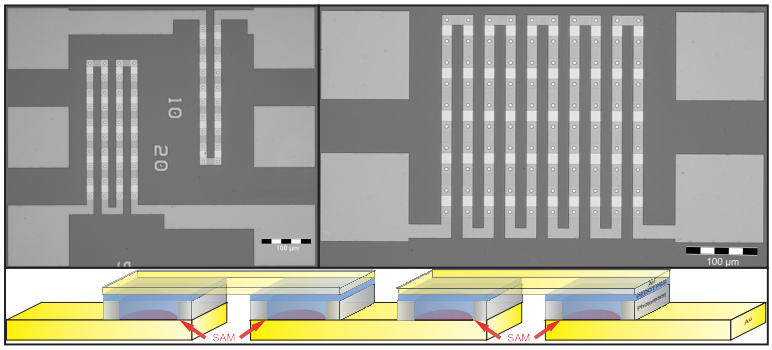

Figure 6.7: Vertical interconnects of 5 μm are connected in series to yield strings of devices. Top: Micrographs of strings of 10, 20 and 100 devices. Bottom: Schematic representation of the strings. Every interconnect is comprised of a monolayer of the photochromic diarylethenes as active component.

fabrication processes to create large amounts of devices simultaneously as needed for integration. Direct evaporation of top metal electrodes on micrometer scale areas covered with SAMs resulted in a yield of working devices of 1.2% [34]. This yield can be increased when nanometer scale device areas are used [35–37]. However, creating these holes with *e.g.* e-beam lithography is too expensive and too slow for any applicational device fabrication. Contacting the molecules that constitute the SAM by means of soft methods is a promising candidate to approach high yields [10, 38–40]. Inherently, these soft methods utilize processing techniques which are not used in industry, so immediate incorporation of these methods is not yet feasible. However, there is no fundamental issue which would prevent this utilization.

Large-area molecular junctions have shown the possibility for integration while high reproducibility and reliability are maintained. On a single 150 mm wafer discrete molecular junctions are fabricated but also strings of molecular junctions [41]. In these strings, multiple interconnects are electronically connected in series, as shown in Figure 6.7. This enables the simultaneous measurement of multiple devices, namely 20, 40, 100 and 200 devices in a single string. The integration of the switchable monolayer devices demonstrates that the switching functionality incorporated in the discrete junctions is highly reliable towards integration of the devices in electronic circuits.

In an electronic circuit with a number of resistors connected in series, the current through every individual resistor is constant. When n identical resistors are connected the potential drop over each resistor is identical as well, resulting in a voltage drop over a single resistor $V = V_{applied} / n$. This offers a method to determine whether a number of fabricated devices are electronically identical. Measuring the characteristics of a single

device and measuring a complete string of devices in series results in this contingency to extract the reproducibility of the devices, since the characteristics of the string should match the single devices at the respective divided voltages. Similarly, the strings of devices can be measured to higher applied voltages such that the potential drop over a single device in the string is equal to the voltages applied in the measurement of single devices. This scaling should be present in measurements of strings of different length.

Figure 6.8 shows representative measurements on the open-ring, low conducting state of the molecular switch assembled in the interconnects of strings of 20 devices and 100 devices, measured to 15 V and 75 V, respectively. Clearly, the resistances in both strings are homogeneous distributed in these series since the *I*–*V* characteristics, plotted on the respective voltage scale, are identical. The non-linearity of the *I*–*V* curves is still visible, although this has decreased slightly in the longer strings. The scaling holds for all string lengths from 20 devices to 200 devices and shows that the electronic behavior of the individual molecular devices in these series is identical.

The scaling of the currents with the number of devices means that the currents can be scaled back to the voltage applied to single devices and compared with the currents of individually measured discrete devices. Figure 6.9 shows that the *J*–*V* characteristics of the devices in the strings correspond adequately to the single devices with the open-ring isomer assembled. The resulting average current density through the strings is a bit higher compared to the single devices, which could indicate that a slightly higher potential is dropped over the separate junctions due to short-circuiting of some interconnects.

To verify that the devices in the strings still retain their functionality, measurements were performed after UV illumination of the strings. UV illumination converts the open ring isomer of the molecular switch to the closed, conjugated state. Figure 6.9 demonstrates that after UV illumination of the strings, the current density has indeed increased. The data obtained for the single devices and the strings of devices match perfectly. This correspondence of the data confirms that every single device behaves identical and has retained its switching functionality. The data shows that over 1250 junctions, processed simultaneously in a single fabrication process, exhibit the desired functionality.

The practically identical curves after UV irradiation also shed light on the somewhat higher currents obtained in the strings before illumination when compared to the single device. Since the strings reproduce the UV irradiated data of the measured single devices, another possible explanation for the higher currents through the low conducting isomer before UV illumination could very well be an increased processing time, and, consequently, an increased exposure to UV light. The fabrication of the strings is a more elaborate process with a number of extra processing steps. These steps were not performed in the fabrication of discrete devices. In the discrete devices, contacts were thermally evaporated through

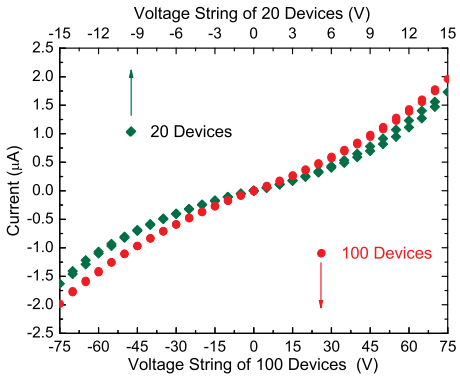

Figure 6.8: *I–V* characteristics of different string lengths of devices with the photochromic diarylethenes as active component. The strings are measured to different applied voltages in a ratio equal to the ratio of the number of devices in the strings. The currents through the strings are identical for the corresponding voltages.

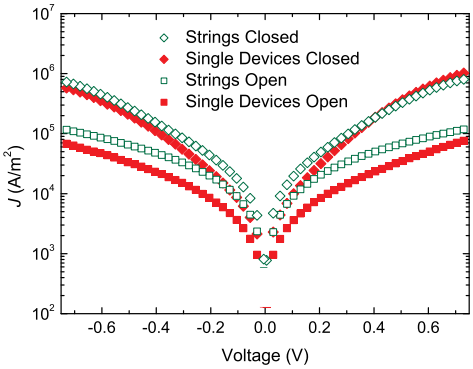

Figure 6.9: Comparison of the *J–V* characteristics of the as-assembled and UV irradiated strings and discrete devices. The strings show the same switching properties as the discrete devices. For the strings, the voltage is calculated back to a single device in the string. The data is averaged over at least 35 discrete devices and at least 14 strings of lengths ranging from 20 – 200 devices in series, resulting in a measurement of over 1250 molecular junctions that were fabricated in a single batch.

a shadow mask instead of structured by UV lithography. The SAMs in the strings have therefore been exposed somewhat longer to ambient and UV light, although this undesired effect has been minimized. Since the transformation to the closed-ring isomer has a higher quantum efficiency than the reverse reaction [18] , a number of molecules in the monolayer could be converted already, resulting in a somewhat more conducting layer.

Nevertheless, it is demonstrated that large-area molecular junctions are reliable with respect to both reproducible fabrication and functionality. Strings of up to 200 devices in series exhibit identical switchable electronic properties as discrete devices. This successful step towards integration of these switchable, monolayer-based electronic devices offers a bright future for the incorporation of molecular electronics in applications. Although large efforts are still needed, no insurmountable fundamental constraints are present to prevent the reliable and reproducible use of nanometer-sized functional molecules.

6.6 Theoretical Basis of Conductance Switching

The most basic understanding of the conductance switching in molecular junctions is based on the tunneling picture. Electrons from the contacts experience an energy barrier dependent on the molecular orbitals of the molecules. This barrier will be larger for saturated compounds and smaller for conjugated compounds. In the molecular switches, switching of the conjugation leads effectively to switching of the HOMO – LUMO gap, thus switching of the barrier for electrons. Additional understanding can however be obtained using more elaborate theoretical frameworks.

The basic photochromic switching core and its conducting properties have been investigated using a combined theoretical framework of non-equilibrium Green's function formalism (NEGF) and density functional theory (DFT) [42]. The geometry of the photochromic core is optimized using DFT leading to parameters as torsion angles, orbital energies and HOMO – LUMO gap. Next, the equilibrium geometries are coupled with semi-infinite gold electrodes. The system is characterized using a NEGF/DFT combined theoretical framework and allows for the extraction of transmission probabilities for electrons as a function of energy. These transmissions can be directly converted in current through the junctions. Projection of the important energy levels in the complete system onto the isolated molecule case yields information on the responsible molecular orbitals. The approach furthermore allows for the application of a bias over the molecule, changing the transmission of various orbitals dramatically.

Results from the calculations show that the specific substitution pattern around the photochromic core essentially does not influence the geometry of the molecules, the HOMO – LUMO gaps and the transmission of the orbitals. As expected, the closed isomers

are more planar and exhibit more delocalized orbitals compared to the open isomers, resulting in a smaller HOMO – LUMO gap. When connected to gold, the electronic orbitals of the different molecules align in a similar fashion resulting in similar offsets from the Fermi level of gold. For both isomers the HOMO level of the molecules is identified as the conducting orbital by energetic alignment closely above (closed) and below (open) the Fermi level. The size of the transmission peaks are determined by the delocalization of the orbital throughout the whole molecule, rationalizing the ON/OFF ratio of the molecular switch.

Due to the application of an electric field over the molecular junctions, the molecular orbitals polarize. This polarization reduces the weight of a molecular orbital on one side of the molecule while increasing the weight on the other side. The polarization leads to a loss of conjugation and thus lower transmission of electrons through the orbitals. It is found that more localized orbitals polarize more easily. The open isomer exhibits more localized orbitals. More polarization leads to an even more decreased conductivity.

By converting the orbital transmission into current through the junctions, the ON/OFF ratio of the photochromic core can be assessed. Computed ON/OFF ratios yield values in the range 6 – 40, dependent on the voltage applied to the junction. This is in reasonable accordance with the measured ratio of 16 at 0.75 V bias. Theoretically, decoupling of the photochromic core from the contacts, however, even leads to an increased ratio up to ~ 300. While a *meta*-coupled phenyl ring is used in the large-area molecular junctions to decouple the photochromic core, such a high ratio is not observed.

6.7 Conclusions

The realization and integration of switchable molecular devices has been demonstrated. The conductance of the molecular devices can be switched reversible between a high conducting (ON) and and low-conducting (OFF) state, based on switching of the delocalization of the HOMO levels of the open and closed isomer. Devices are reliable with respect to fabrication and functionality, as shown by the integration of devices in strings. The molecular devices can operate as an electronic ON/OFF switch and as a reprogrammable data storage moiety that can be optically written and electronically read. Dynamics of switching is understood to be slow, because of the inherent structure of large-area molecular junctions together with quenching of the photo-excited states by the electrical contacts. The present results offer exciting prospects toward tailoring existing molecules and incorporation of novel molecular switches, thereby providing a range of improved functional molecular devices. The current results are a clear leap towards functional molecular electronics.

References

[1] A. Aviram and M. A. Ratner. Chem. Phys. Lett. **29**, 277–283 (1974).

[2] B. A. Mantooth and P. S. Weiss. Proc. IEEE **91**, 1785–1802 (2003).

[3] H. B. Akkerman and B. de Boer. J. Phys. Condens. Matter **20**, 013001 (2008).

[4] K. W. Hipps. Science **294**, 536–537 (2001).

[5] A. Salomon, D. Cahen, S. Lindsay, J. Tomfohr, V. B. Engelkes and C. D. Frisbie. Adv. Mat. **15**, 1881–1890 (2003).

[6] S. M. Lindsay and M. A. Ratner. Adv. Mat. **19**, 23–31 (2007).

[7] M. Elbing, R. Ochs, M. Koentopp, M. Fischer, C. von Hänisch, F. Weigend, F. Evers, H. B. Weber and M. Mayor. Proc. Natl. Acad. Sci. USA **102**, 8815–8820 (2005).

[8] C. P. Collier, G. Mattersteig, E. W. Wong, Y. Luo, K. Beverly, J. Sampaio, F. M. Raymo, J. F. Stoddart and J. R. Heath. Science **289**, 1172–1175 (2000).

[9] M. Delvalle, R. Guitiérrez, C. Tejedor and G. Cuniberti. Nature Nanotechnology **2**, 176–179 (2007).

[10] J. E. Green, J. W. Choi, A. Boukai, Y. Bunimovich, E. Johnston-Halperin, E. Delonno, Y. Luo, B. A. Sheriff, K. Xu, Y. S. Shin, H. Tsjeng, J. F. Stoddart and J. R. Heath. Nature **445**, 414–417 (2007).

[11] J. G. Kushmerick, C. M. Whitaker, S. K. Pollack, T. L. Schull and R. Shashidar. Nanotechnology **15**, 489–493 (2004).

[12] B. de Boer, M. M. Frank, Y. J. Chabal, W. Jiang, E. Garfunkel and Z. Bao. Langmuir **20**, 1539–1542 (2004).

[13] C. N. Lau, D. R. Stewart, R. S. Williams and M. Bockrath. Nano Lett. **4**, 569–572 (2004).

[14] D. Dulic, S. J. van der Molen, T. Kudernac, H. T. Jonkman, J. J. D. de Jong, T. N. Bowden, J. van Esch, B. L. Feringa and B. J. van Wees. Phys. Rev. Lett. **91**, 207402 (2003).

[15] N. Katsonis, T. Kudernac, M. Walko, S. J. van der Molen, B. J. van Wees and B. L. Feringa. Adv. Mat. **18**, 1397–1400 (2006).

[16] J. Li, G. Speyer and O. F. Sankey. Phys. Rev. Lett. **93**, 248302 (2004).

[17] A. Staykov, D. Nozaki and K. Yoshizawa. J. Phys. Chem. C **111**, 3517–3521 (2007).

[18] M. Irie. Chem. Rev. **100**, 1685–1716 (2000).

[19] J. J. D. de Jong, L. N. Lucas, R. M. Kellog, J. H. van Esch and B. L. Feringa. Science **304**, 278–281 (2004).

[20] S. Kobatake, S. Takami, H. Muto, T. Ishikawa and M. Irie. Nature **446**, 778–781 (2007).

[21] T. Kudernac, J. J. D. de Jong, J. van Esch, B. L. Feringa, D. Dulic, S. J. van der Molen and B. J. van Wees. Mol. Cryst. Liq. Cryst. **430**, 205–210 (2005).

[22] T. Kudernac, S. J. van der Molen, B. J. van Wees and B. L. Feringa. Chem. Comm. 3597–3599 (2006).

[23] J. He, F. Chen, P. A. Liddel, J. Andréasson, S. D. Straight, D. Gust, T. A. Moore, A. L. Moore, J. Li, O. F. Sankey and S. M. Lindsay. Nanotechnology **16**, 695–702 (2005).

[24] A. C. Whalley, M. L. Steigerwald, X. Guo and C. Nuckolls. J. Am. Chem. Soc. **129**, 12590–12591 (2007).

[25] M. Ikeda, N. Tanifuji, H. Yamaguchi, M. Irie and K. Matsuda. Chem. Comm. 1355–1357 (2007).

[26] S. J. van der Molen, J. Liao, T. Kudernac, J. S. Agustsson, L. Bernard, M. Calame, B. J. van Wees, B. L. Feringa and C. Schönenberger. Nano Lett. **9**, 76–80 (2009).

[27] J. M. Tour, L. Jones II, D. L. Pearson, J. J. S. Lamba, T. P. Burgin, G. M. Whitesides, D. L. Allara, A. N. Parikh and S. V. Atre. J. Am. Chem. Soc. **117**, 9529–9534 (1995).

[28] C. van der Marel, M. Yildirim and H. R. Stapert. J. Vac. Sci. Technol. A **23**, 1456–1470 (2005).

[29] J. C. Love, L. E. Estroff, J. K. Kriebel, R. G. Nuzzo and G. M. Whitesides. Chem. Rev. **105**, 1103–1169 (2005).

[30] B. de Boer, H. Meng, D. Perepichka, J. Zheng, M. M. Frank, Y. J. Chabal and Z. Bao. Langmuir **19**, 4272–4284 (2003).

[31] A. H. Flood, J. F. Stoddart, D. W. Steuerman and J. R. Heath. Science **306**, 2055–2056 (2004).

[32] H. B. Akkerman, P. W. M. Blom, D. M. de Leeuw and B. de Boer. Nature **441**, 69–72 (2006).

[33] W. R. Browne, J. J. D. de Jong, T. Kudernac, M. Walko, L. N. Lucas, K. Uchida, J. H. van Esch and B. L. Feringa. Chem. Eur. J. **11**, 6414–6429 (2005).

[34] T. W. Kim, G. Wang, H. Lee and T. Lee. Nanotechnology **18**, 315204 (2007).

[35] C. Zhou, M. R. Deshpande, M. A. Reed, L. Jones II and J. M. Tour. Appl. Phys. Lett. **71**, 611–613 (1997).

[36] N. Majumbar, N. Gergel, D. Routenberg, J. C. Bean, L. R. Harriott, B. Li, L. Pu, Y. Yao and J. M. Tour. J. Vac. Sci. Technol. B **23**, 1417–1421 (2005).

[37] G. J. Hwang, P. R. Jeng, C. Lien, C. S. Chen, Y. S. Tsao, H. S. Hwang, S. Q. Xu, T. M. Hong and Y. C. Chou. Appl. Phys. Lett. **89**, 133120 (2006).

[38] K. T. Shimizu, J. D. Fabbri, J. J. Jelincic and N. A. Melosh. Adv. Mat. **18**, 1499–1504 (2006).

[39] A. Vilan and D. Cahen. Adv. Funct. Mat. **12**, 795–807 (2002).

[40] Y. L. Loo, D. V. Lang, J. A. Rogers and W. P. H. Hsu. Nano Lett. **3**, 913–917 (2003).

[41] P. A. van Hal, E. C. P. Smits, T. C. T. Geuns, H. B. Akkerman, B. C. de Brito, S. Perissinotto, G. Lanzani, A. J. Kronemeijer, V. Geskin, J. Cornil, P. W. M. Blom, B. de Boer and D. M. de Leeuw. Nature Nanotechnology **3**, 749–754 (2008).

[42] C. van Dyck, V. Geskin and J. Cornil. Preliminary Results.

Chapter 7

Conclusions and Implications

This thesis has described the electronic transport in large-area molecular junctions. Both fundamental aspects and molecular function have been addressed. The conclusions can be categorized by both aspects and lead to implications for the future of the field of *Molecular Electronics*.

The primary goal of *Molecular Electronics* is the fabrication of functional electronic devices based on single molecules or assemblies of molecules. Realization of a functional component using large-area molecular junctions has been demonstrated in this thesis. The switching is illumination-based, giving rise to the possibility to perform reference measurements to rule out extrinsic effects as basis for the conductance switching. The results have shown that a single molecular layer of ~ 2 nm thick can be used to perform electronic functions. Furthermore, integration of switchable junctions has demonstrated the reliability of the process and, moreover, a previously unrealized essential combination of functionality and technological integration.

From a more fundamental point of view the importance and influence of electrical contacts to molecules has been covered. At the time of fabrication of the first large-area molecular junctions, the testbed was regarded as an versatile method to screen series of molecules, both from a fundamental and functional point of view. PEDOT:PSS, the key ingredient of the junctions, was considered to be a non-interacting metallic electrode. This thesis has shown that this hypothesis is invalid. Large-area molecular junctions exhibit a spectrum of electronic aspects related to both molecular structure and PEDOT:PSS. An exponential dependence of the resistance on molecular length is observed pointing to tunneling as dominant transport mechanism, while temperature and voltage dependent characteristics have been observed derived from PEDOT:PSS. For all molecular junctions and for PEDOT:PSS junctions, replotting the scaled current density $J/T^{1+\alpha}$ as a function of eV/kT yielded a single smooth universal curve spanning over orders of magnitude. Furthermore, the complete J–V characteristics could be quantitatively described by a single equation with two fit parameters. By analysis of the fit parameters the conductivity of

PEDOT:PSS was shown to have a dominant contribution to the electrical characteristics of the large-area molecular junctions, only offset by a molecular contribution. Consequently, in a multi-barrier tunneling model the factorization with PEDOT:PSS had to be explicitly included. The dominant role of the PEDOT:PSS contact explained the absolute value of the junction resistance and its relation to processing conditions. For the future contributions of large-area molecular junctions to the field of *Molecular Electronics* it is necessary to use a strictly constant fabrication protocol. Then clear signatures of the molecular structure can be observed.

As an additional sidestep while investigating transport in large-area molecular junctions, the understanding of transport by organic compounds over larger length scales has been covered in the study of the fundamental electronic properties of PEDOT:PSS. The temperature and voltage dependent electrical characteristics have been shown to constitute a single universal measurement curve. Although this has been related with one-dimensional electronic systems, this explanation has been ruled out by the three-dimensional nature of the morphology of PEDOT:PSS thin films. Other transport mechanisms resulting in scaling are based on dissipative tunneling or Coulomb blockade effects. None of these mechanism have previously been related with transport in organic thin films. A definite choice between mechanisms could, however, not be made. Nevertheless, new functional and fundamental aspects of molecular transport, on different length scales, have been uncovered and keep on challenging the understanding of electronic transport by soft organic matter.

A general outlook on the initial promise of *Molecular Electronics* to replace silicon technology can be given based on the current results on functional large-area molecular junctions and on the parallel developments in the silicon industry. While functionality can thus be incorporated in molecules and while functional molecular junctions can be integrated into more elaborate structures, the silicon industry has kept up with miniaturization of its technology to feature sizes comparable to the size of molecules. Therefore, it can be expected that *Molecular Electronics* will not replace silicon CMOS technology. Nevertheless, there are certain niche applications where a technology based on *Molecular Electronics* can deliver. For application where speed and energy consumption *i.e.* chip size, are not important and production costs are essential, self-assembly of electronic components might pave a path forward. *Molecular Electronics* still exhibits the promise to make considerable contributions into this direction.

Summary

The clock frequency of electronic integrated circuits is inversely proportional to the minimum feature size of electronic components. When electronic components are smaller, an integrated circuit contains more of these components in a unit area. More components effectively yield more computation power. An additional advantage is that smaller circuits will consume less energy.

The electronics industry is a well-developed industry with over 50 years of experience in research. Since around 1960, the minimum feature size of electronic components has decreased every two years by a factor of two. Alternatively, the number of components in an integrated circuit has doubled every two years. This observation is known as Moore's Law. It is expected that miniaturization of electronic components will reach a fundamental limit and Moore's Law will not be obeyed. There is ongoing debate about exactly when the limit is reached, but it is clear that in the future current technologies will not be able to create smaller, less energy-consuming and faster electronic components. Solutions for future electronic devices are therefore being investigated, keeping a worldwide multibillion industry on track.

Molecular Electronics was proposed in 1974 as a possible technology capable of solving the miniaturization problem to extend Moore's Law. At that time the minimum feature size was $\sim 5\ \mu$m. The main concept of *Molecular Electronics* is the use of a single molecule as individual electronic component in circuitry. Organic molecules are the size of a couple of nanometers, leading to a minimum feature size in the nanometer range. The initiation of the field started with a theoretical paper in 1974 by A. Aviram and M. A. Ratner describing a single molecule rectifier Aviram. Interest was sparked in the substitution of electronic components by functional molecules. However, progress was slow due to limited experimental possibilities.

An inherent problem for the experimental field was the fabrication of an electric contact to molecules. A number of different junction geometries were devised based on single molecules or assemblies of molecules. Most of the junctions, however, were fabricated with low yield and reproducibility. A combined effort of the University of Groningen and Philips Research Eindhoven lead to the fabrication of so-called large-area molecular junctions. Molecular junctions were fabricated with conventional processing techniques with high yield, reproducibility and stability. The junctions are based on a highly doped conducting

polymer electrode (PEDOT:PSS) on top of a self-assembled monolayer (SAM) of molecules on a gold bottom contact. The conducting polymer chains are too big to penetrate through the SAM under investigation and therefore yield molecular junctions with over 95 % yield. The molecular junctions were benchmarked using linear carbon chains (alkanes) and yielded experimental results that were in accordance with previous reported studies on molecular transport.

In this thesis the electrical transport in large-area molecular junctions is studied into greater depth. An expansion of investigated molecules in large-area molecular junctions together with a better understanding of transport in PEDOT:PSS leads to a broader understanding of many experimental aspects of the junctions. Furthermore, molecular functionality is introduced in the molecular junctions. The fabrication of the molecular junctions and experimental data on alkanes are summarized in Chapter 2. For these alkanes, an exponential dependence of the junction resistance on molecular length is observed in accordance with literature studies. However, the origin of the absolute values of the resistance in the junctions remains an issue. The value depends on the specific formulation of PEDOT:PSS used and the morphology of the spincoated layer, while PEDOT:PSS was originally intended to behave as a non-interacting metallic electrode. To obtain better understanding of the origin of the absolute resistance in large-area molecular junctions, the work in this thesis starts out with an investigation into the transport properties of PEDOT:PSS only.

Chapter 3 outlines temperature-dependent J–V characteristics down to 25 K of the conducting polymer PEDOT:PSS. Transport in polymer semiconductors generally shows exponentially activated thermal behavior, but a power-law temperature dependence $J \propto T^{\alpha}$ is observed for PEDOT:PSS with $\alpha = 1.25$. In order to more deeply understand the behavior, a pulse measurement technique is used to reduce electrolysis in PEDOT:PSS and facilitates measurements up to higher biases of 3 V. At higher bias the J–V characteristics exhibit a power-law dependence $J \propto V^{\beta}$ as well. Furthermore, the temperature and voltage powers are related, $\beta = \alpha + 1$. A single universal measurement curve, based on plotting $J/T^{1+\alpha}$ versus eV/kT, is constructed from all J–V characteristics at all temperatures. The curve is fitted with a single equation using two independent fit parameters and the measured α. The equation is originally derived for one-dimensional metallic systems. However, the morphology of PEDOT:PSS rules out this origin. Other possible mechanisms are based on dissipative tunneling and Coulomb blockade mechanisms, but no conclusive decision is made which mechanism dominates in PEDOT:PSS. While the current results are obtained within the context of large-area molecular junctions, they also offer new insights in the transport properties of (doped) polymeric semiconductors and can have implications for the implementation of *Organic Electronics*.

Before diving into the influence of the transport characteristics of PEDOT:PSS on the electrical transport of the junctions, Chapter 4 introduces the characterization of π – conjugated compounds using large-area molecular junctions. These measurements expand the molecular scope of large-area molecular junctions by adding to the existing electrical data of alkanes. Length-dependent electrical characteristics are determined for *para*-phenylene oligomers, both monothiol and dithiol derivatives. The resistance of the molecular junctions depends exponentially on the length of the molecules, $R \propto exp^{\beta L}$. The tunneling decay coefficients β equal 0.26 ± 0.04 $Å^{-1}$ and 0.20 ± 0.06 $Å^{-1}$ for dithiols and monothiols, respectively. The values are lower than compared to literature but are consistent within the large-area molecular junction geometry. The tunneling decay coefficients for alkanes equal 0.66 $Å^{-1}$ and 0.73 $Å^{-1}$ for dithiols and monothiols, respectively. Lower coefficients are expected for π – conjugated compounds because of their smaller HOMO – LUMO gap. The small disagreement with literature is explained by the forced planar geometry of the molecules inside the monolayers. The absolute resistances of the conjugated molecular junctions are, however, higher than alkanes in large-area molecular junctions. The compounds are expected to be less resistive because of delocalization of electrons over the π – conjugated system. This fact is not observed in large-area molecular junctions and leads to a necessary deeper discussion of the absolute value of resistance in large-area molecular junctions.

The transport mechanism in large-area molecular junctions is discussed in Chapter 5. Temperature-dependent measurements of molecular junctions are performed. In the simple metal-molecule-metal tunneling picture, based on the exponential length-dependences observed for all molecular series, the molecular junctions should exhibit temperature-independent transport characteristics. However, for both the saturated and conjugated series, a dependence on temperature is observed. While all molecular junctions show the influence of the molecules in the junctions, all molecular junctions show universal scaling behavior of the *J*–*V* characteristics as a function of temperature and voltage as well. The complete electrical characteristics of the molecular junctions can be fitted using a single formula with two independent fit parameters. In Chapter 3 it has been shown that PEDOT:PSS exhibits identical scaling behavior and therefore the scaling in the molecular junctions is likely to stem from the conducting polymer electrode. It is demonstrated that the absolute resistance of large-area molecular junctions is intimately related with the conductivity of the PEDOT:PSS layer, only offset by a molecular contribution. Consequently, in a multi-barrier tunneling model, the factorization with PEDOT:PSS needs to be taken into account explicitly. The dominant role of the PEDOT:PSS contact explains the absolute value of the resistance of the junctions and the relation of the value with processing conditions.

Finally, the realization of functional molecular junctions is covered in Chapter 6. While the electrical characteristics of large-area molecular junctions are determined by molecular transport properties and PEDOT:PSS, observation of molecular functionality is possible when the fabrication protocol is strictly kept constant. It is furthermore necessary to be cautious about the influence of extrinsic effects on the desired functionality. The characterization of large-area molecular junctions with switchable conductance based on molecular switches is described. It is experimentally verified that switching is based solely on the incorporated ~ 2 nm thick functional monolayer. Assembly of molecular switches exclusively in the low- or high-conductance state inside the molecular junctions yields the maximum achievable ON/OFF ratio. Switching in between these states together with the fact that reference devices do not exhibit switching demonstrates that the molecular switches are responsible for the observed behavior. The quantum yields of the switching processes in the junctions show that the time dependence of the switching is dominated by the low amount of photons arriving properly on the molecular layer due to the device geometry. Reliability and reproducibility of the functional junctions is demonstrated by integration of functional molecular devices in strings of devices connected in series.

Chapter 7 summarizes the main conclusions from the current work which hold that functional molecular electronic junctions can be fabricated and integrated using large-area molecular junctions, while PEDOT:PSS cannot be regarded as a non-interacting metallic contact to self-assembled monolayers. The electrical characteristics of large-area molecular junctions are determined by the electronic properties of the molecules in the self-assembled monolayer *and* the electronic properties of PEDOT:PSS. Nevertheless, when the properties of PEDOT:PSS are critically kept constant, molecular structure and function can be studied with high reproducibility and reliability.

The field of *Molecular Electronics* can thus deliver reliable integrated functional components. Nevertheless, the original promise to decrease the minimum feature size of components has to be revisited. Parallel to developments in *Molecular Electronics*, the silicon industry shrunk single components to sizes comparable to molecules. Therefore, the initial reason to develop *Molecular Electronics* has largely disappeared and it might never replace silicon CMOS technology. The emphasis of the community has therefore shifted towards self-assembled electronic components. Realization of such components could provide low-cost electronics.

Samenvatting

De kloksnelheid van moderne geïntegreerde elektronische circuits is omgekeerd evenredig met de kritieke dimensie van de individuele componenten. De kritieke dimensie is de minimale grootte van de individuele componenten. Als de individuele componenten kleiner zijn passen er meer componenten in een geïntegreerd circuit van dezelfde afmetingen. Meer componenten leidt tot meer rekenkracht. Een bijkomend voordeel is dat kleinere circuits minder energie gebruiken.

De elektronica-industrie heeft meer dan 50 jaar ervaring in onderzoek in de onderliggende silicium-technologie. Sinds 1960 is de kritieke dimensie van elektronische componenten om de twee jaar verkleind met een factor twee. Dit houdt in dat het aantal componenten op een chip om de twee jaar verdubbeld is. Deze observatie wordt ook wel de wet van Moore genoemd. Echter, het wordt voorspeld dat de kritieke dimensie van elektronische componenten een fundamentele limiet zal bereiken en dat de wet van Moore niet langer op zal gaan. Er is een debat gaande wanneer precies deze limiet bereikt zal worden, maar het is wel duidelijk dat de huidige technologieën in de toekomst geen kleinere, energie-zuinigere en snellere elektronische componenten zullen kunnen verwezenlijken. Verschillende mogelijke oplossingen worden daarom onderzocht.

Moleculaire Elektronica werd in 1974 voorgesteld als mogelijke technologie die een oplossing zou kunnen bieden voor het verkleinen van elektronische componenten. De kritieke dimensie van elektronische componenten was toen ~ 5 μm. *Moleculaire Elektronica* probeert moleculen als afzonderlijke elektronische componenten te gebruiken in geïntegreerde circuits. Organische moleculen kunnen een nanometer groot zijn, wat tot een kritieke dimensie van enkele nanometers kan leiden. Het onderzoeksveld werd gestart door een theoretisch artikel van A. Aviram en M. A. Ratner dat beschreef dat een enkel molecuul als diode zou kunnen functioneren. Er was meteen interesse in het vervangen van elektronische componenten met organische moleculen. Progressie in het onderzoek was echter gelimiteerd door beperkte experimentele mogelijkheden.

Een inherent probleem was het maken van elektrisch contact met moleculen. Verscheidene geometrieën werden ontwikkeld om moleculaire juncties te maken op basis van moleculen, maar de meeste juncties werden gefabriceerd met een lage opbrengst of waren niet reproduceerbaar. Een gezamenlijke poging van de Rijksuniversiteit Groningen en Philips Research Eindhoven om dit op te lossen heeft geleid tot de fabricage van

moleculaire juncties met een groot oppervlak. De moleculaire juncties werden gemaakt door conventionele fabricage methoden te gebruiken. Hoge opbrengst, reproduceerbaarheid en stabiliteit werden behaald. De juncties zijn gebaseerd op een elektrode van het hoog gedoteerde geleidende polymeer PEDOT:PSS boven op een zelf-geassembleerde monolaag (SAM) van moleculen op een gouden ondercontact. De ketens van het geleidende polymeer zijn te groot om door de SAM te penetreren. Dit leidt tot een opbrengst van werkende juncties van meer dan 95 %. De elektrische eigenschappen van de juncties werden vergeleken met de literatuur door lineaire ketens van koolstof (alkanen) door te meten. De experimentele resultaten kwamen goed overeen met eerder gerapporteerde studies aan alkanen.

In dit proefschrift wordt het elektrisch transport door dit type moleculaire juncties diepgaand onderzocht. Een uitbreiding van het type moleculen dat gekarakteriseerd is, samen met een beter begrip van het transport in PEDOT:PSS, leidt tot een breder begrip van het gedrag van de juncties. Tevens wordt functionaliteit ingebouwd in de juncties. De fabricage en initiële metingen aan alkanen worden samengevat in Hoofdstuk 2. Voor alkanen werd een exponentiële afhankelijkheid van de weerstand van de juncties als functie van de lengte van de moleculen geobserveerd. Echter, de oorsprong van de absolute waarde van de weerstand werd niet begrepen. De absolute waarde is afhankelijk van de specifieke samenstelling en de morfologie van de PEDOT:PSS, hoewel de laag als uitgangspunt bedoeld was als metallische elektrode die geen invloed heeft op de eigenschappen van de juncties. Om de oorsprong van de absolute waarde van de weerstand beter te begrijpen, begint het experimentele werk in dit proefschrift met een analyse van de geleidende eigenschappen van PEDOT:PSS.

Hoofdstuk 3 beschrijft temperatuur-afhankelijke stroom-dichtheid versus voltage (J–V) metingen van het geleidende polymeer PEDOT:PSS. Elektrisch transport in polymeren toont meestal exponentieel geactiveerd thermisch gedrag. Desondanks wordt een machtswet $J \propto T^{\alpha}$ gemeten voor PEDOT:PSS met $\alpha = 1.25$. Om meer inzicht te verkrijgen worden metingen gedaan met zeer korte voltage pulsen. Hierdoor wordt elektrolyse in PEDOT:PSS verminderd en het voltagebereik van de metingen verhoogd tot 3 V. Bij hogere voltages volgen de J–V karakteristieken ook een machtswet $J \propto V^{\beta}$. De temperatuur en voltage machten zijn aan elkaar gerelateerd, $\beta = \alpha + 1$. Een universele curve kan geconstrueerd worden uit alle temperatuur-afhankelijke J–V curves, gebaseerd op het plotten van $J/T^{1+\alpha}$ versus eV/kT. De curve kan worden beschreven door een vergelijking met twee onafhankelijke fit parameters en de gemeten waarde van α. De vergelijking is van origine afgeleid voor een-dimensionale metallische systemen. De morfologie van PEDOT:PSS sluit deze oorsprong uit. Andere theorieën die tot hetzelfde gedrag leiden zijn gebaseerd op dissipatieve tunnelling of Coulomb blokkade mechanismen. Er kan helaas geen definitieve keuze gemaakt worden welk mechanisme domineert. Hoewel de huidige experimentele ob-

servaties zijn gemaakt in de context van moleculaire juncties, geven de metingen ook nieuw inzicht in het elektrisch transport van (gedoteerde) polymere halfgeleiders en kunnen ze implicaties hebben voor de implementatie van *Organische Elektronica*.

Voordat de invloed van de karakteristieken van PEDOT:PSS op het elektrisch transport van de juncties wordt beschreven, introduceert Hoofdstuk 4 de karakterisatie van π – geconjugeerde moleculen. De metingen voegen de bestaande data van alkanen aan. Lengte-afhankelijke karakteristieken van monothiol en dithiol derivaten van *para*-phenylene oligomeren worden bepaald. De weerstand hangt exponentieel af van de lengte van de moleculen, $R \propto exp^{\beta L}$. De β coëfficiënt beschrijft hoe snel de tunnel-stroom afneemt als functie van de lengte. De waarden van deze coëfficiënten β zijn 0.26 ± 0.04 Å^{-1} en 0.20 ± 0.06 Å^{-1} voor dithiol en monothiol derivaten, respectievelijk. Deze waarden zijn lager dan gerapporteerd in de literatuur maar consistent binnen de PEDOT:PSS juncties. De β coëfficiënten voor alkanen in de juncties zijn namelijk 0.66 Å^{-1} en 0.73 Å^{-1} voor dithiol and monothiol derivaten. Lagere waarden voor de coëfficiënten worden verwacht vanwege het kleinere energieverschil tussen de HOMO en LUMO orbitalen van π – geconjugeerde moleculen. Het verschil met de literatuur wordt verklaard door een geforceerde vlakke conformatie van de moleculen in de monolagen. De weerstand van de π – geconjugeerde moleculen is hoger dan de weerstand van alkanen. Het omgekeerde wordt verwacht door delokalisatie van elektronen over het π – systeem. Dit leidt tot een noodzakelijke diepere discussie van de oorsprong van de absolute waarde van de weerstand in de juncties.

Het transport mechanisme in de moleculaire juncties wordt beschreven in Hoofdstuk 5. Temperatuur-afhankelijke metingen worden beschreven van de *moleculaire* juncties. De juncties worden beschouwd als metaal-molecuul-metaal tunnel diodes gebaseerd op de exponentiële afhankelijkheid van de weerstand als functie van de lengte. Tunnel diodes vertonen temperatuur-onafhankelijk gedrag. Voor de moleculaire juncties wordt evenwel temperatuur-afhankelijkheid gemeten. Terwijl alle juncties invloed van de moleculaire eigenschappen ondervinden, tonen de juncties ook universele schaling van de *J*–*V* karakteristieken. De complete temperatuur- en voltage-afhankelijke karakteristieken kunnen worden beschreven met een enkele formule met twee fit parameters. In Hoofdstuk 3 is aangetoond dat PEDOT:PSS identieke schaling vertoond. Daarom wordt dit gedrag in de moleculaire juncties aan de PEDOT:PSS elektrode toegeschreven. Het wordt daarna aangetoond dat de absolute waarde van de weerstand gerelateerd is aan de geleiding van de PEDOT:PSS. De moleculen verschuiven de initiële waarde van PEDOT:PSS. Daardoor moet in een model met (meerdere) tunnel barrières expliciet rekening gehouden worden met de weerstand van PEDOT:PSS. De dominante rol van PEDOT:PSS in de moleculaire juncties verklaard de absolute waarde van de weerstand en de relatie van de weerstand met de fabricage condities van de juncties.

Als laatste beschrijft Hoofdstuk 6 de realisatie van functionele moleculaire juncties. Hoewel de elektrische eigenschappen van de juncties worden bepaald door moleculaire geleiding en door de eigenschappen van PEDOT:PSS, is observatie van functionaliteit mogelijk als het fabricage protocol van de juncties strikt constant wordt gehouden. Het is daarnaast belangrijk om de oorsprong van de functionaliteit goed te achterhalen om extrinsieke effecten uit te sluiten. De karakterisatie van moleculaire juncties met schakelbare weerstand, gebaseerd op moleculaire schakelaars, wordt beschreven. Het wordt experimenteel bevestigd dat het schakelen plaatsvindt middels de ingebouwde ~ 2 nanometer dikke moleculaire laag. Exclusieve assemblage van de moleculaire schakelaars in de AAN en UIT toestand leidt tot de maximale AAN/UIT ratio. Het schakelen van de juncties tussen deze twee toestanden, in combinatie met referentie metingen op niet-schakelbare juncties, levert direct bewijs dat het schakelen gebaseerd is op de monolaag van moleculaire schakelaars. De intrinsieke snelheid van het proces is gedomineerd door het lage aantal lichtdeeltjes dat correct op de monolaag arriveert als resultaat van de geometrie van de juncties. De betrouwbaarheid en reproduceerbaarheid van de functionele juncties wordt gedemonstreerd door tot 200 juncties met elkaar te integreren door ze in serie aan elkaar te koppelen.

Hoofdstuk 7 vat de belangrijkste conclusies van dit proefschrift samen. Functionele moleculaire juncties kunnen worden gerealiseerd en geïntegreerd terwijl PEDOT:PSS niet kan worden beschouwd als een metallisch contact op monolagen dat geen invloed heeft op de eigenschappen van de juncties. De elektrische eigenschappen van de juncties zijn een combinatie van de eigenschappen van de moleculen *en* de eigenschappen van PEDOT:PSS. Desalniettemin, als de eigenschappen van PEDOT:PSS strikt constant worden gehouden, kan de invloed van moleculaire structuur en moleculaire functie worden bestudeerd met hoge reproduceerbaarheid en betrouwbaarheid.

Moleculaire Elektronica kan dus betrouwbare en geïntegreerde functionele componenten realiseren. Echter, het originele idee om de kritieke dimensies van elektronische componenten te verkleinen moet heroverwogen worden. Parallel met de vooruitgang in *Moleculaire Elektronica* heeft onderzoek naar standaard silicium elektronica geleid tot kritieke dimensies in de ordegrootte van het formaat van moleculen. Daardoor is de initiële reden voor *Moleculaire Elektronica* grotendeels verdwenen en zal de technologie misschien wel nooit silicium vervangen. Hierdoor is de nadruk van de meerwaarde van *Moleculaire Elektronica* komen te liggen op zelf-assemblage van elektronische componenten. Realisatie van zelf-geassembleerde componenten zou kunnen resulteren in goedkope elektronica.

List of Publications

Hylke B. Akkerman, Auke J. Kronemeijer, Paul A. van Hal, Dago M. de Leeuw, Paul W. M. Blom and Bert de Boer. *Self-Assembled Monolayer Formation of Long Alkanedithiols in Molecular Junctions.* Small **4**, 100–104 (2008).

Auke J. Kronemeijer, Hylke B. Akkerman, Tibor Kudernac, Bart J. van Wees, Ben L. Feringa, Paul W. M. Blom and Bert de Boer. *Reversible Conductance Switching in Molecular Devices.* Adv. Mat. **20**, 1467–1473 (2008).

Hylke B. Akkerman, Auke J. Kronemeijer, Paul W. M. Blom, Paul A. van Hal, Dago M. de Leeuw and Bert de Boer. *Molecular Electronics with Large-Area Molecular Junctions.* Mat. Res. Soc. Symp. Proc. **1091E**, 1091–AA02–05 (2008).

Paul A. van Hal, Edsger C. P. Smits, Tom C. T. Geuns, Hylke B. Akkerman, Bianca C. de Brito, Stefano Perissinotto, Guglielmo Lanzani, Auke J. Kronemeijer, Victor Geskin, Jérôme Cornil, Paul W. M. Blom, Bert de Boer and Dago M. de Leeuw. *Upscaling, Integration and Electrical Characterization of Molecular Junctions.* Nature Nanotechnology **3**, 749–754 (2008).

Hylke B. Akkerman, Auke J. Kronemeijer, Jan Harkema, Paul A. van Hal, Edsger C. P. Smits, Dago M. de Leeuw and Paul W. M. Blom. *Stability of Large-Area Molecular Junctions.* Org. Electron. **11**, 146–149 (2010).

Herman T. Nicolai, Gert-Jan A. H. Wetzelaer, Martijn Kuik, Auke J. Kronemeijer, Bert de Boer and Paul W. M. Blom. *Space-charge-limited Hole Current in Poly(9,9-dioctylfluorene) Diodes.* Appl. Phys. Lett. **96**, 172107 (2010).

Girish Lakhwani, Roel F. H. Roijmans, Auke J. Kronemeijer, Jan Gilot, René A. J. Janssen and Stefan C. J. Meskers. *Probing Charge Carrier Density in a Layer of Photodoped ZnO Nanoparticles by Spectroscopic Ellipsometry.* J. Phys. Chem. C **114**, 14804–14810 (2010).

Auke J. Kronemeijer, Eek H. Huisman, Ilias Katsouras, Paul A. van Hal, Tom C. T. Geuns, Paul W. M. Blom, Sense J. van der Molen and Dago M. de Leeuw. *Universal Scaling in Highly Doped Conducting Polymer Films.* Phys. Rev. Lett. **105**, 156604 (2010).

Auke J. Kronemeijer, Eek H. Huisman, Hylke B. Akkerman, Stijn M. Goossens, Ilias Katsouras, Paul A. van Hal, Tom C. T. Geuns, Sense J. van der Molen, Paul W. M. Blom and Dago M. de Leeuw. *Electrical Characteristics of Conjugated Self-Assembled Monolayers in Large-Area Molecular Junctions.* Appl. Phys. Lett. **97**, 173302 (2010).

Ilias Katsouras, Victor Geskin, Auke J. Kronemeijer, Paul W. M. Blom and Dago M. de Leeuw. *Binary Self-Assembled Monolayers: Apparent Exponential Dependence of Resistance on Average Molecular Length.* Org. Electron. **12**, 857–864 (2011).

Auke J. Kronemeijer, Ilias Katsouras, Eek H. Huisman, Paul A. van Hal, Tom C. T. Geuns, Paul W. M. Blom and Dago M. de Leeuw. *Universal Scaling of the Charge Transport in Large-Area Molecular Junctions.* Small, Accepted (2011).

Acknowledgements

The scientific work most of you readers have just skipped to get to this page would not have been realized without the help and support of many people. Overall, my time in Groningen has been one of great joy and fun. I feel privileged to have worked in such a stimulating environment as the MEPOS group. Nevertheless, we have experienced great loss as well and this made it difficult for me to choose with whom to begin. My PhD research can be divided into two periods in which I had the honor to work with two different direct supervisors. Initially Bert de Boer supervised me. After he sadly passed away Dago de Leeuw took over the supervision.

Based on the chronology I start with Bert de Boer. I owe Bert a great deal. First of all, he has convinced me to start a PhD in the group. Afterwards, he has shown me how to combine dedication and fun in research. Bert was driven by success but always managed to combine this with a fun side to take the pressure off at the right moment. I will never forget the early coffees with him when I still started early in the morning together with him. Bert turned into a mentor and a friend. He has taught me a lot. After he passed away I (and I think the whole group) fell into a deep black hole. We still miss him a lot.

After the passing away of Bert the whole group had to re-adjust. This meant that the Molecular Electronics project would be supervised by Dago de Leeuw. Dago, thank you very much for all the effort you have put into the project. I admire the countless times you have driven from Eindhoven to come to Groningen. You tackle scientific problems in another way than I was used to before and have shown me how to be effective. I thank you for your easy and direct way of communicating. I enjoyed the writing days with you when we just sat down for a whole day and put all the matter on paper. I am grateful for the opportunity to come and work partially at Philips. Also I enjoyed the drives to Mons and the times we had a drink or diner. Furthermore, I will never ever forget that you smoke literally everywhere.

Essential for the completion of this thesis as well is Paul Blom. Paul, you might have been on the background in the later stages of my PhD but I surely know you have had significant input in the project. Whether it was the times that I would pop into your office or that you would discuss all the findings in the car back to Eindhoven with Dago. I also admire the effort that you still come to Groningen. Furthermore, you were the one who started up the whole lab in Groningen. Look what is has grown out to be. People ought to show their respect for such effort.

I owe a lot to all people who have worked on the large-area molecular junctions project:

Hylke, you were the first to start with the large-area molecular junctions. I started as a master student under your supervision and ended up performing research together with you. I have learned a lot from your experimental knowledge, your general interests in nearly everything and your clubbing experience (Club Fame!). It was a wonderful time working with you. Scientifically and socially. During coffee or in the bar. I enjoyed all the trips to various destinations in the Netherlands and abroad. Even long after you left the group we ended up doing some research together. I am happy that you wanted to be my paranymph.

Paul van Hal, Tom Geuns, Edsger Smits and all other people at Philips Research Eindhoven for the major effort of developing the process technology on the 6" wafers. Without your success, this whole thesis would not have been possible. In literally all chapters the Philips process technology is used. Paul, I thank you for supervising me at Philips, for your direct opinion on research and your easy going character. Tom, thank you for the time you have spent in the cleanroom for the project. A further thanks for the development of the MIMIM wafers as well.

Eek, after the departure of Sense Jan you also became a member of the Molecular Electronics cluster. Maybe you had to adjust a little to the way we were used to interact and comment on each others work in the group, but eventually you managed to adapt very well. Thank you for the nice and easy-going collaboration and for all the useful input in the project. Your views from the more mesoscopic perspective were very insightful. I enjoyed working with you a lot.

Ilias, after a slow start we managed to get to know each other somewhat better. It was nice to see you grow into the Molecular Electronics project. Your wafer-breaking method is still amazing. I admire the effort you put in supervising Jolt, who was officially my student, while I was busy finishing up. I know nice results will come out of all the projects you are involved in at the moment.

Jan Harkema, thank you for the outstanding technical support. The chapters with low-temperature measurements would not have been possible without you helping to build and maintain the cryogenic probe station. All the things you do in the lab are indispensable. Furthermore, I think you have become the guardian of the group in the last couple of years. Thank you for that!

All the students, (kleine) Bert, Maarten, Stephan, Stijn, Paul, Yishi and Jolt, who have assisted in the Molecular Electronics project in Groningen. I thank them for their valuable input in the project and the numerous hours they spent in the lab doing all the difficult experiments. Bert, the initial Master's research period we spent together in the basement was amazing.

The MEPOS group is more than only a work-related environment, it is a whole social experience. All the people described above already made the MEPOS-experience a success. However, it would not have been so amazing without the rest of the research/friends group:

Johan, I enjoyed the time we spent in the office with each other a lot. First in the tiny little room upstairs and later when we moved downstairs. I am happy you wanted to be my paranymph as well. I never forget the countless hours we have spent to understand scientific and technological matter that was totally NOT related to our research projects. Unfortunately no chapter in this thesis has come to describe all this knowledge, as was the original idea. There was always enough time for fun in our room. If serious matter should be discussed however, you were always very helpful as well. Also the beers, guitar hero and Steel Panther are things I will never forget!

Halky, Herman, Johan, Kuik, Lenes & René for all the the things we did together, which is too much to write down in a couple of sentences. Without you guys the Molecular Electronics group is/will be not the same anymore. We had some very nice years together. I loved all the days and evenings we spent, at work the coffeebreaks and borrels, outside work just having diner, watching a movie, drinking some or a lot of beer and going to the Negende Cirkel. Hope to see you all again soon.

Kamal, I enjoyed the (shorter) period in the office as well. Although you are still also somewhat a mystery to me, it was a nice time with the jokes back and forth. Furthermore, research-wise we started collaborating on the ferroelectric transistors.

Many thanks to all the other members of the MEPOS group that have made my PhD such a nice time: Afshin, Alex, André, Anne-Marije, Arne, Date, Dorota, Fatemeh, Francesco, Frans, Gert-Jan, Jan Anton, Jan Derk, Jia, Jurjen, Kriszty, Magda, Marianna, Mark-Jan, Milo, Reza, Simon, Steve, Xiaonan and Yuan. A special thanks for Renate for the excellent administrative support.

There are of course also people outside the MEPOS group who have had valuable input. I would like to thank the reading committee, Prof. dr. Ben Feringa, Prof. dr. Bart van Wees and Prof. dr. Harold Zandvliet, for taking the time to critically read the manuscript. Thanks for all the helpful comments. I would also like to thank Victor Geskin for reading the manuscript, although you eventually did not end up in the reading committee.

For the collaboration on the molecular switches I would like to thank Tibor Kudernac, Jetsuda Areephong, Wesley Browne and Prof. Ben Feringa. My thesis is called *Functional Molecular Electronics*. Without the molecular switches there would be no function at all.

For the collaboration on the theoretical understanding, initially of the molecular switches and later of the mixed monolayers, I would like to thank Victor Geskin, Colin van Dyck and Jérôme Cornil from the University of Mons. Thanks for the valuable input. I enjoyed the visits to Mons and the times you came to Groningen.

For the collaboration on the weird scaling behavior I like to thank Sense Jan van der Molen. Sense Jan, you helped us to put some momentum into the understanding of the scaling behavior. Thank you for helping out with the writing of the PRL paper.

For all the times that I have not been at work I would like to thank Bert en Dorinda for the amazing holidays to New Zealand and Costa Rica and all the nice weekends. Also I appreciate the occasional beer with the scheikunde-gang Erik, Erwin, Jochem, Jeroen and Michiel a lot! Anne-Marije, thanks for showing Christa and me the gondelvaart of Oldeboarn!

I would like to specially thank my parents for all the support and love they have always given me throughout my whole life, for all the amazing memories and for making me who I am today. I am also particularly grateful for the love and support of the rest of the close family: Evert & Arijaan, Lieuwe & Deborah, Eppo & Janny and Ellen & Jeroen.

Finally, I like to thank the most amazing person in my life: Christa. You have always been there for me during my whole PhD. You have witnessed all the ups and downs. Thank you for standing by me and bringing so much joy in my life. I feel confident for all the future things to come with you by my side. Thank you for being who you are. I love you.
'Till Monkeys Fly...'

Auke, March 2011